CHARACTERIZATION AND MODELING OF THE THERMOMECHANICAL FATIGUE CRACK GROWTH BEHAVIOR OF INCONEL 718 SUPERALLOY

A Dissertation
Presented to
The Academic Faculty

by

Andrew Thomas Radzicki

In Partial Fulfillment
of the Requirements for the Degree
Doctor of Philosophy in the
George W. Woodruff School of Mechanical Engineering

Georgia Institute of Technology
August 2016

CHARACTERIZATION AND MODELING OF THE THERMOMECHANICAL FATIGUE CRACK GROWTH BEHAVIOR OF INCONEL 718 SUPERALLOY

Approved by:

Dr. W. Steven Johnson, Co-Advisor
George W. Woodruff School of Mechanical Engineering
School of Materials Science and Engineering
Georgia Institute of Technology

Dr. Richard W. Neu, Co-Advisor
George W. Woodruff School of Mechanical Engineering
School of Materials Science and Engineering
Georgia Institute of Technology

Dr. David L. McDowell
George W. Woodruff School of Mechanical Engineering
School of Materials Science and Engineering
Georgia Institute of Technology

Dr. Olivier Pierron
George W. Woodruff School of Mechanical Engineering
Georgia Institute of Technology

Dr. Christopher Muhlstein
School of Materials Science and Engineering
Georgia Institute of Technology

Date Approved: June 16, 2016

The views expressed in this dissertation are those of the author and do not reflect the official policy or position of the United States Air Force, Department of Defense, or the U.S. Government; or the views of any company mentioned herein.

ACKNOWLEDGEMENTS

The successful completion of my studies at Georgia Tech would not have been possible without the support of numerous people. I would specifically like to thank my advisors, Dr. Steven Johnson and Dr. Rick Neu for their guidance, support, and mentoring throughout my PhD studies. Additionally, the dedication and support of my family, specifically my wife Alyssa and my children Teagan, Avery, and Carter, were critical. I would also like to recognize those others whom I had the opportunity to interact and work with, specifically: James Huggins, Ben Adair, Mike Kirka, Ashley Goulding, Kyle Brindley, Brian Clark, Ernesto Estrada, Sanam Gorgan, Anirudh Bhat, and Ben Seitz. Lastly, I would like to thank United Technologies Corporation, Pratt and Whitney Division, for their support of this research and Dr. Andy Rosenberger of AFRL for providing technical insight.

TABLE OF CONTENTS

LIST OF TABLES

LIST OF FIGURES

SUMMARY

Understanding the impact of the complex and harsh thermomechanical environment aircraft turbine engines subject their components to is critical for designers and operators to ensure the safe and efficient operation of the systems they are responsible for. The combined effects of elevated temperatures and high loads on the components of these engines are not fully understood. The purpose of this project was to better understand this complex interaction. This effort consisted of the characterization and modeling of the performance of Nickel-base superalloys, specifically Inconel 718, used in turbine engine disk applications.

Isothermal and thermomechanical tests up to and above the maximum usage temperature for Inconel 718 (650°C) were executed to characterize the impact of time spent at elevated temperature on fatigue crack growth rate. Various spectra were designed to evaluate the impact of tensile and compressive holds at elevated temperature. This included evaluating the sequence within the spectrum where the holds occurred. Tensile holds executed at a spectrum's maximum load or immediately following an increase in load were shown to increase fatigue crack growth rate immediately following the hold. Additionally, a robust series of tests were executed to evaluate the impact of the stress intensity, duration, and temperature of a tensile hold on fatigue crack growth rate. The concept of a thermally affected zone to describe an area ahead of the crack tip weakened by the tensile hold that allows for the crack to propagate faster than expected is discussed. As the stress intensity, duration, or temperature of a tensile hold increase, the temperature affected zone increases in size leading to an increase in fatigue crack growth rate for cycling following the hold.

Observations made during the experimental investigation were used to develop a

thermomechanical fatigue crack growth model that accommodates realistic spectra and accounts for the effects of time spent at elevated temperature. The model provides designers and operators with a more thorough representation of how their components will respond in actual application and allow them to make more informed decisions on the safe and efficient implementation of their systems.

CHAPTER I

INTRODUCTION

1.1 Motivation

Since it's invention in the 1930's, the jet turbine engine has revolutionized the way people and products are moved around the globe. Fundamental to the efficient operation of a jet turbine is the ability to achieve and sustain elevated temperatures in the hot section of the engine. Figure 1.1 shows a schematic of a typical jet turbine engine identifying the cold and hot sections.

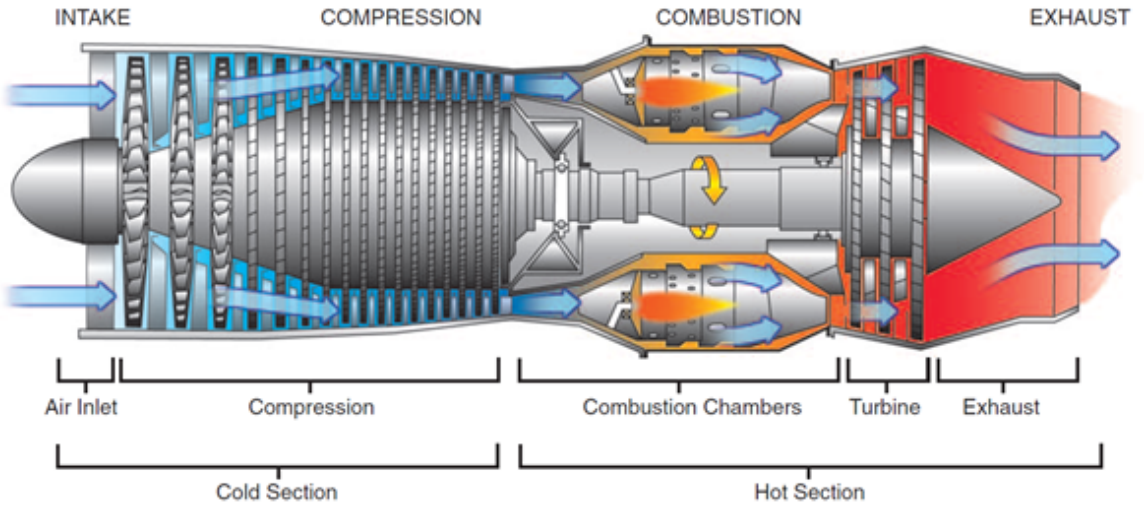

Figure 1.1: Basic layout of a jet turbine engine [1].

In particular, the turbine blades and disks have a unique requirement in the hot section. The materials making up these components need to maintain their integrity for long durations at elevated temperatures while sustaining significant loads from both centripetal forces and thermal gradient induced forces. Additionally, the corrosive environment created by the combustion of fuel also works to break down the alloys used for the hot section. This aggregate of environmental characteristics is particularly harsh.

Additionally, as the use of jet engines is cyclic in nature, in as much as each flight, or for that sake each movement of the throttle, subjects the engine to changing parameters (both load and temperature), fatigue of components is an important consideration for designers and operators. If one considers the turbine entry temperature of a civil aircraft during one flight, Figure 1.2 highlights just how the temperature changes during one flight. This temperature variability is combined with changing loads due to centripetal acceleration and temperature gradients. Combining this with the fact that most engines will be subject to thousands of flight cycles (engine start-up to shut-down) during their lifetime, only further compounds the importance of fatigue considerations. In contrast to vehicle based turbine applications, land-based power generation turbines are typically subject to longer duration operation at a constant temperature and load and are subject to fewer start-up and shut-down cycles.

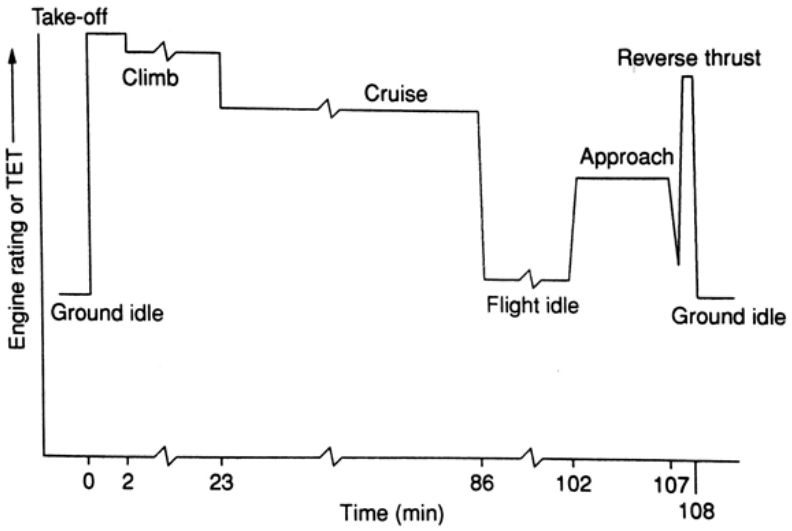

Figure 1.2: Turbine entry temperature (TET) profile for typical civil aircraft flight [2].

One pertinent example of the significance of fatigue and fatigue crack growth in a jet turbine engine occurred on June 2, 2006. During a ground engine run of a Boeing 767-223(ER) by maintenance personnel at Los Angeles International Airport, the number one engine suffered an uncontained engine failure. The high pressure

turbine stage 1 ruptured and broke through the engine casing and cowling. Multiple pieces were ejected that peppered the aircraft and one large piece bounced off of the ground and subsequently severed the left-hand keel beam and partially severed the right-hand keel beam before lodging in the exhaust of the number 2 engine, as Figure 1.3 shows. Another piece was found approximately 2,500 feet away. The high energy discharge of these pieces could have been catastrophic had it occurred in flight. The turbine disk was made of Inconel 718 and analysis of the failure surface indicated a fatigue crack that initiated and grew from a small dent near a blade slot bottom corner. Also, analysis of the fracture surface found primarily intergranular fatigue crack growth with some areas of fatigue striations.

Figure 1.3: Result of uncontained failure of high pressure turbine disk during ground engine run [3].

More recently, on September 8, 2015, a Boeing 777-200ER suffered an engine fire during the takeoff roll at McCarran International Airport in Las Vegas, Nevada. Initial indications show that portions of a high-pressure compressor (HPC) section had failed catastrophically and sent large fragments through the engine case and cowling [4]. The failure appears to have begun in the web of the HPC disk [4].

The National Transportation Safety Board's investigation is ongoing, though the circumstances of this failure show several parallels to the failure mentioned above.

Correct characterization and quantification of the life of aircraft components is of critical importance if accidental failures like those mentioned above are to be avoided. Up until the 1980s, the United States Air Force utilized a safe-life approach to quantifying the useful life of the rotating components of their gas turbine engines. This approach resulted in considerable waste as components were removed from service after a predetermine life had expired, regardless of whether or not the component was still good. The component's life was based on the predicted failure of 1 out of 1000 components, meaning that when the predicted life was reached and the component removed from service, 99.9% of components still had useful life remaining [5]. To save costs on the order of billions of dollars and increase safety, the Air Force implemented the Retirement for Cause (RFC) approach to component life prediction [5]. Under RFC, components are individually evaluated based on their specific characteristics (material, flaws, service history, etc.) and are only removed from service when their is a specific cause to do so. It has proven successful and has since been established as the industry standard for aircraft jet turbine operators.

Thorough and accurate characterization of the fatigue and fatigue crack growth behavior of these components is critical to RFC. More accurate life prediction will result in increased safety and more efficient utilization and management of these components and the systems they make up.

1.2 Research Objectives

The impact of the complex temperature and loading environment on the materials that make up the components of jet turbine engines are not fully understood. This environment subjects these components to thermomechanical fatigue (TMF), where both the temperature and loads are varying with time. This project aimed to help

better understand certain portions of the real-world application spectra for aircraft based turbine engines and their impact on the materials that make up their disks, particularly polycrystalline nickel-base (Ni-base) superalloys. The fatigue crack growth performance of the fine grained polycrystalline Ni-based superalloy, Inconel 718 (IN 718) was characterized and modeled using experimental fatigue crack growth (FCG) tests, failure surface investigation, and finite element analysis (FEA). Specifically, the temperature interaction effects of previous time spent at elevated temperature and its effect on fatigue crack growth rate (FCGR) was investigated. Specific focus areas of this work fell into two categories: characterization and modeling. The areas evaluated included:

1. Characterization

    (a) Isothermal constant amplitude FCG tests, used as a baseline for the model developed with this work.

    (b) Test points to aid in identifying trends in how the specific load of a tensile hold, the temperature during the hold, and the hold duration affect FCGR. This included test spectra of two forms:

        i. Isothermal FCG tests with intermittent tensile holds evaluating the impact of a hold load's relation to the cyclic loading.

        ii. Isothermal constant stress intensity factor FCG tests with intermittent holds of various stress intensities.

    (c) The effect of high temperature compressive holds were evaluated by Out-of-phase (OP) TMF crack growth tests using representative turbine engine disk spectra and simple triangular spectra from 260°C to 650°C.

    (d) Representative turbine engine disk TMF spectra FCG tests to aid in tuning the model developed with this work.

(e) FEA studies conducted to help better understand how the state of stress directly ahead of the crack tip evolved during thermomechanical cycling.

(f) Fractographic investigation of the FCG failure surfaces to better understand and characterize the active first-order mechanisms occurring during crack growth.

2. Modeling

(a) Develop a TMF FCG model able to accurately account for a complex TMF spectra focusing on temperature interaction effect and their impact on FCGR.

1.3 Dissertation Overview

The first chapter of this dissertation lays out the motivation behind the need to better be able to characterize the TMF crack growth response of Ni-base superalloys. A better understanding of a component's response is needed for initial design, to maximize safety, and to minimize programmatic (procurement, operations, and maintenance) costs. Additionally, the overall research objectives are also presented. The second chapter provides a thorough background on the relevant characteristics and response of IN 718 in a high temperature environment. This includes pertinent information on the FCG response of IN 718 at high temperature when subject to various loading scenarios. Additionally, current isothermal and TMF modeling approaches for Ni-base superalloys are discussed. Chapter three includes the material, specimen geometries, and test set-ups and procedures used during this project. Also, stress intensity solutions and FEA model characteristics are presented. The fourth chapter presents the experimental results of the FCG tests. These include identifying trends in the effect of tensile hold stress intensity, hold temperature, and hold duration on FCGR. Findings from fractographic and FEA studies conducted as well as a discussion of the empirical

fits conducted to aid in modeling the temperature interaction effects on FCGR are also presented. A TMF crack growth model able to appropriately account for loading and temperature history is discussed in chapter five. This yield-zone approach model was built off of a previously established model by incorporating the ability to accurately account for temperature interaction effects on FCGR. Chapter six includes the conclusions and recommendations as well as a discussion of the significance of this research.

CHAPTER II

LITERATURE REVIEW AND BACKGROUND

2.1 History of Nickel-base Superalloys

The complex environment of a jet turbine engine, where loads and temperatures are ever changing, presents a challenging environment to material durability. Early jet engines utilized steel alloys for high temperature components [6]. To bring this new invention from the lab to practical use required the development of new alloys that were able to maintain their integrity when subject to the environment of a jet turbine engine [7]. The development of Ni-base superalloys stemmed from the need for an alloy that could: 1) carry load at high temperatures approaching their melting point, 2) be able to sustain that performance for long durations, and 3) not fail in a highly corrosive environment [2]. Nickel-base superalloys are typically found in polycrystalline, directionally solidified, or single crystal form, depending on the application [2]. While directionally solidified and single crystal forms lend themselves well to the highest temperature applications (i.e. turbine blades), the disks of a jet turbine engine operate at lower temperatures and are well suited to a polycrystalline form due to toughness and strength considerations.

2.2 Inconel 718

2.2.1 History

Developed in the late 1950s by the International Nickel Corporation, Inc., Inconel 718 (IN 718) is a nickel-base superalloy that was an early contributer to the effective implementation of jet turbine propulsion and it is still in wide use today [8]. Inconel 718 comes in cast, wrought, or powder metallurgy form and has high strength, weldability, and fabricability [8]. It has been used for a wide range of high temperature

applications ranging from diffuser casings, shafts, blades, fasteners, and as is the case for the current study, turbine engine disks [8].

2.2.2 Microstructure and Composition

Inconel 718 is a precipitate hardened Ni-base superalloy that has a large proportion of iron and is sometimes referred to as a nickel-iron (Ni-Fe) superalloy. Table 2.1 shows the nominal chemical composition of IN 718. It is primarily strengthened by the presence of γ'' (DO_{22} structure) and γ' ($L1_2$ structure) phases occurring in a γ matrix with the γ'' phase considered the main strengthening phase [9]. The γ'' phase causes high coherency strains on the γ matrix which gives IN 718 its strength [10]. The γ'' is disk shaped and the size depends on the heat treatment history but can be found in diameters on the order of 100-400 nm [11]. The γ, γ' and γ'' structure is typical of most Ni-based superalloys. An additional phase is also found in Ni-Fe superalloys, δ, and has an orthorhombic crystal structure (Ni_3Nb) [9]. The γ' and δ phases both evolve from the γ''-phase [9].

Table 2.1: Nominal chemical composition by percent weight of powder metallurgy IN 718 [12].

Ni	Cr	Fe	Nb	Mo	V	Ti	C
Bal.	18.6	18.5	5.0	3.1	0.9	0.4	0.04

Inconel 718 is typically used in applications requiring moderately high temperatures and good crack growth performance. It is usually found in polycrystalline form today and can be had with average grain diameters less than 10 μm. Such a fine grain structure allows for excellent toughness and strength as temperature increases but limits its performance in situations where creep is significant. Figure 2.1 shows a micrograph of fine grained IN 718 with no particular grain orientation. The speckled appearance in the figure shows an intergranular distribution of the δ phase precipitates and several carbides. Additionally, IN 718 was shown to be microstructurally stable

(i.e. no microstructural evolution) when subjected to temperatures up to 600°C for 10,000 hours [13]. Above 649°C however, the main strengthening phase γ'', rapidly coarsens and the alloy weakens [8]. Figure 2.2 shows how IN 718's strength drops off significantly above 650°C.

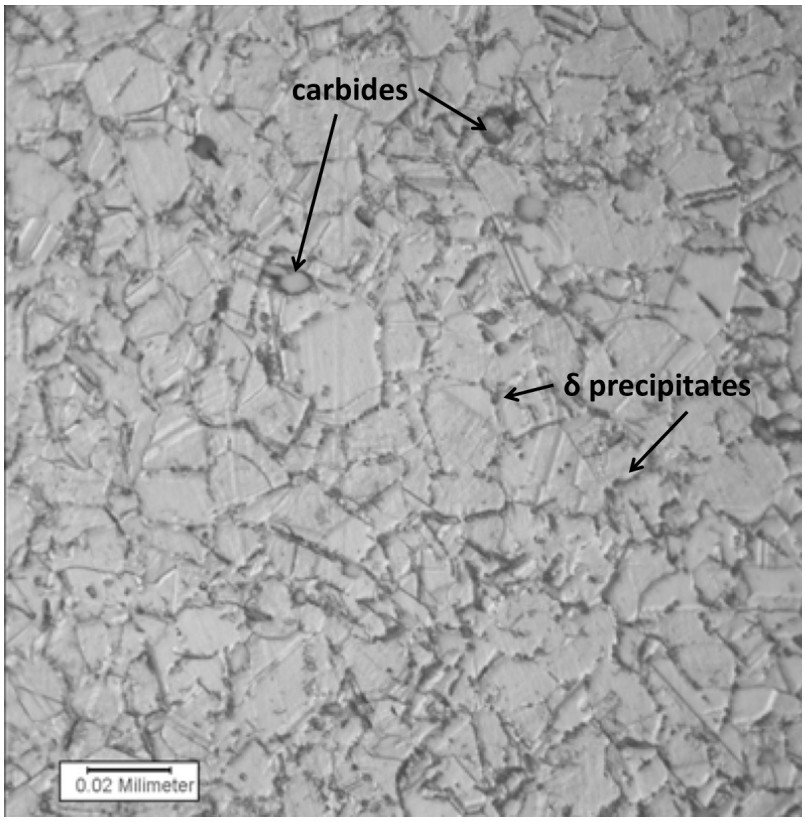

Figure 2.1: Fine grained IN 718 micrograph (approximately ASTM 10 grain size) [14].

In addition to the changes in the strengthening phases that begin to occur at 650°C, creep effects begin to play a larger role. Andersson et al. showed that the dominant creep mechanism for IN 718 below 687°C is dislocation creep [16]. Additionally, IN 718 has a melting temperature range of 1260-1336°C [17]. To avoid loss of strength and to avoid significant creep effects, the maximum usage temperature is typically limited to 650°C, which is a homologous temperature of about 0.5.

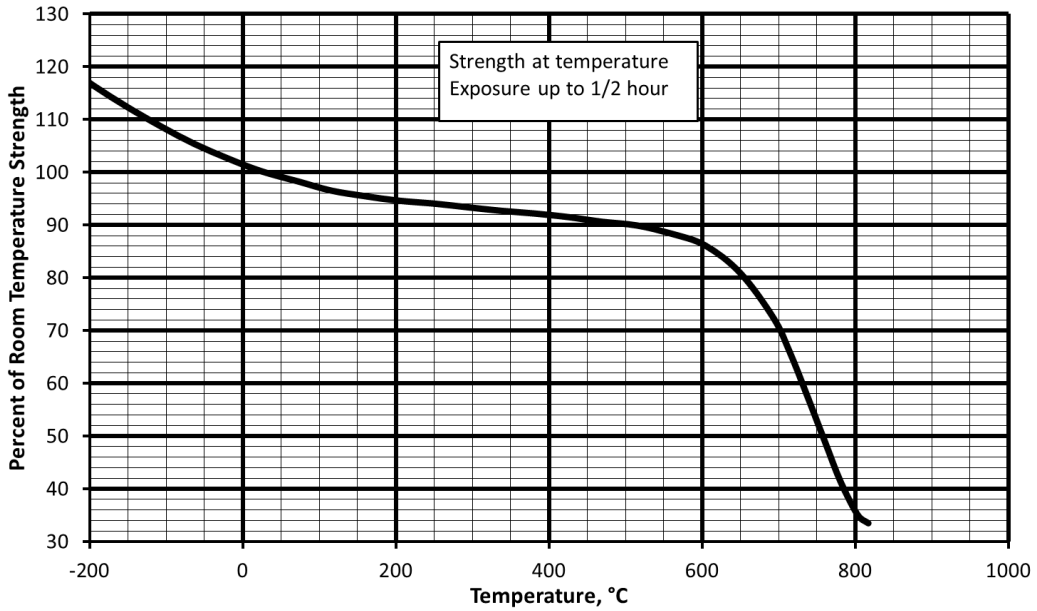

Figure 2.2: Temperature effect on the ultimate tensile strength of IN 718 [15].

2.3 Fatigue Crack Growth in IN 718

2.3.1 Microstructural Effects

Numerous studies have been conducted to characterize the effect of grain size and secondary phase size impacts on the strength and fatigue crack growth behavior of IN 718. Pierragi et al. showed that the fatigue life of IN 718 is improved as grain size is reduced [18]. Conversely, for FCG tests at slow rates (0.33 Hz), Krueger et al. observed an opposite effect of grain size showing that for positive loading ratios at elevated temperatures, a larger grain size will result in a slower FCGR compared to small grains [19]. It was suggested by Pedron et al. that this could be due to the larger grain boundary area for a smaller grained material being subjected to oxidation [20]. This is true for slow loading rates, however at faster rates (shown by Pedron et al. at 20 Hz) no effect of grain size on FCGR was observed [20].

Additionally, although Kreuger et al. showed that the relative size of the γ'' phase will impact strength and fatigue crack growth rate [19], as temperatures increase and creep effects begin to play a larger role, approaching and above 650°C, the δ phase

has a more significant impact on the performance of IN 718 [18]. Specifically, the shape and distribution of the δ phase precipitates are the main factors in this regime. Pierragi et al. showed that globular δ precipitates performed significantly better than acicular δ precipitates in creep rupture tests [18]. Also, intergranular distribution of the globular δ precipitates resulted in an order of magnitude increase in creep rupture life compared to a transgranular distribution [18]. Similarly, for FCG, Pedron et al. showed that the distribution of the δ phase along grain boundaries improved crack growth resistance [20].

2.3.2 Frequency and Temperature Effects

As it has been in use for more than 50 years, numerous studies have been conducted to characterize IN 718's response to different loading and temperature situations, particularly, its fatigue crack growth behavior at elevated temperature.

At elevated temperature, the loading frequency plays a significant role in the performance of Ni-based superalloys. This is particularly true for IN 718. Based on the work of Weersooriya and co-workers [21–23] and Pineau [24], Ghonem et al. further characterized the three different types of crack growth response modes in IN 718 at high temperature. For high frequency loading, a high degree of slip homogeneity is present and will result in primarily transgranular crack propagation (cycle-dependent) [25]. Pedron showed this at a frequency of 20 Hz [20]. Inconel 718's crack growth response at this higher frequency can be attributed directly to its plastic response [26]. As the frequency of loading decreases, the prevalence of slip line homogeneity is decreased allowing for the intergranular diffusion of oxygen [25]. This results in a mixed mode of crack growth (transgranular with intergranular). When the loading frequency reaches a transition level, the crack growth response is largely dependent on environmental exposure duration (time-dependent) and results in primarily intergranular crack growth [25]. This effect is well documented [20, 25,

27–29]. Figure 2.3 shows these different modes of crack propagation.

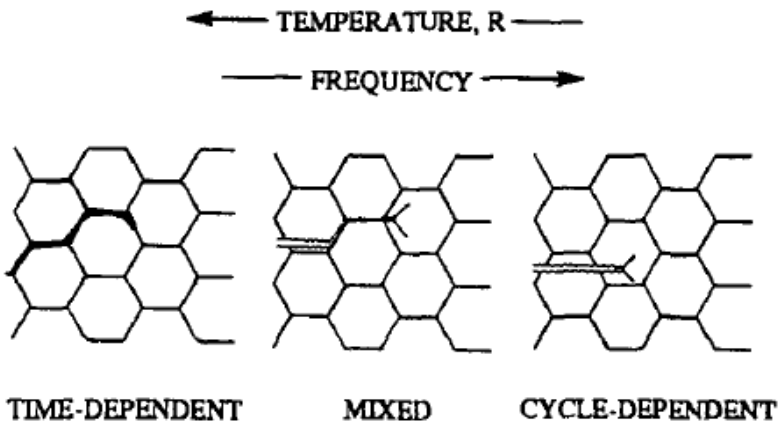

Figure 2.3: Time-dependent, mixed, and cycle-dependent fatigue crack growth modes in air [25].

In addition to loading frequency, the transition from preliminarily cycle-dependent to time-dependent crack response is a factor of ΔK, temperature, and microstructure [21, 24, 30]. As an example, for IN 718 tested at 650°C, a stress intensity range, $\Delta K = 40$ MPa $\sqrt{m}$, and having a grain size of 100 μm, Ghonem et al. showed that the transition frequency was about 0.1 Hz [25]. Figure 2.4 shows the transition from primarily transgranular to intergranular crack growth at various frequencies and temperatures.

Additionally, the fracture surfaces in Figure 2.5 show how the presence of oxygen at elevated temperature for slow frequency loading allowed for a crack to propagate in an intergranular manner. This is evident by the rough appearance of the surface compared to the faster frequency test which shows a primarily smooth, transgranular surface. Conversely, in an environment without oxygen (inert gas or vacuum), a primarily transgranular crack growth surface is observed for slow frequency loading.

The combined effect of loading frequency and a high temperature air environment leading to intergranular and therefore faster fatigue crack growth is termed an oxidation assisted crack growth mechanism. Its effects are shown in Figure 2.6 where the FCG performance in air and vacuum for several different loading frequencies are

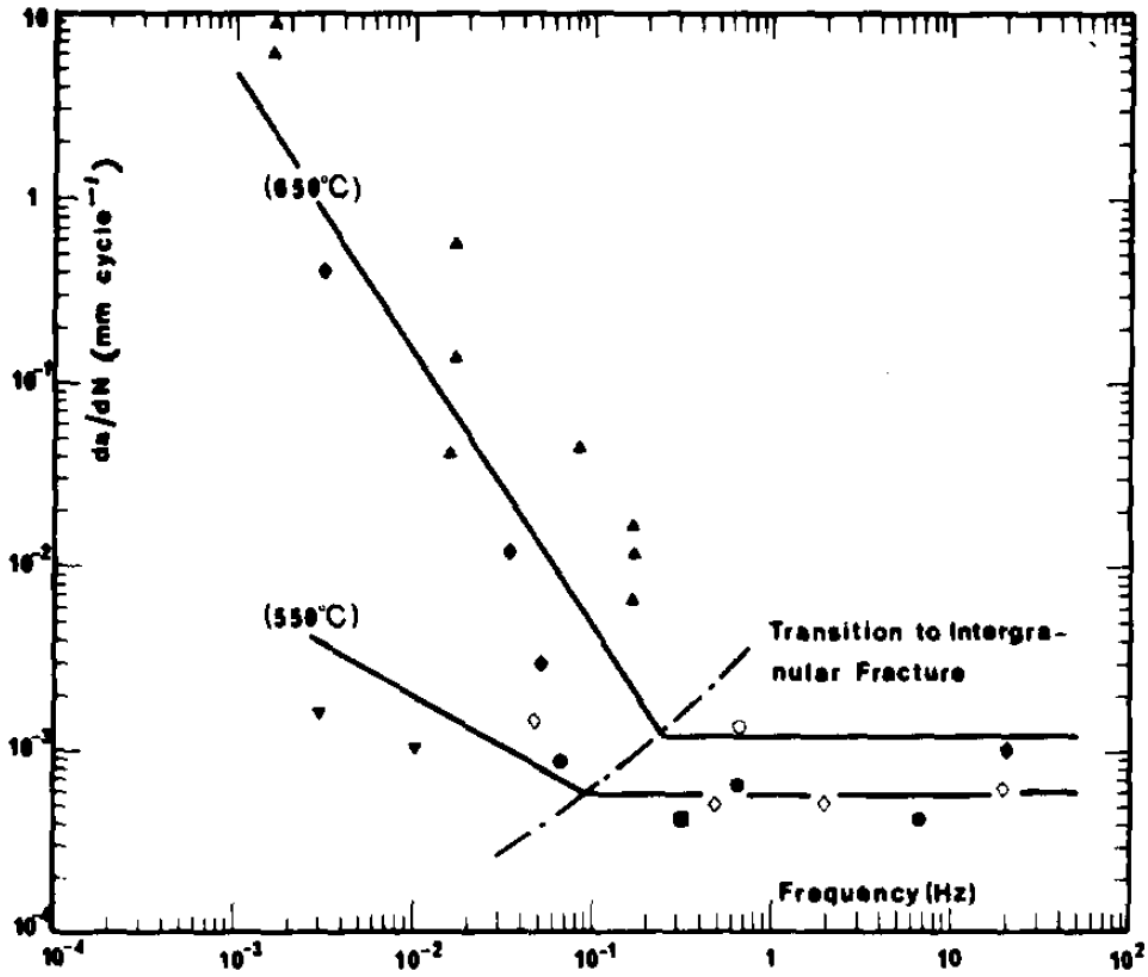

Figure 2.4: Effect of test frequency and temperature on crack propagation mode for IN 718 loaded to $\Delta K = 40$ MPa $\sqrt{m}$ at 650°C and 550°C [20].

compared. This mechanism has typically been evaluated with regard to small scale yielding occurring at a crack tip, and as such is critical to understand for FCG performance. However, for large scale plastic deformation, Zheng et al. showed that the low frequency crack growth rate in IN 718 at elevated temperature was reduced due to increased slip band density [31].

The impact of loading waveform shape on the oxidation assisted crack growth mechanism was evaluated by Ghonem et al. [25]. They showed for a given frequency (below transition frequency) at 650°C, variations in the loading and unloading durations had no impact on the fatigue crack growth rate. This indicated that the effective

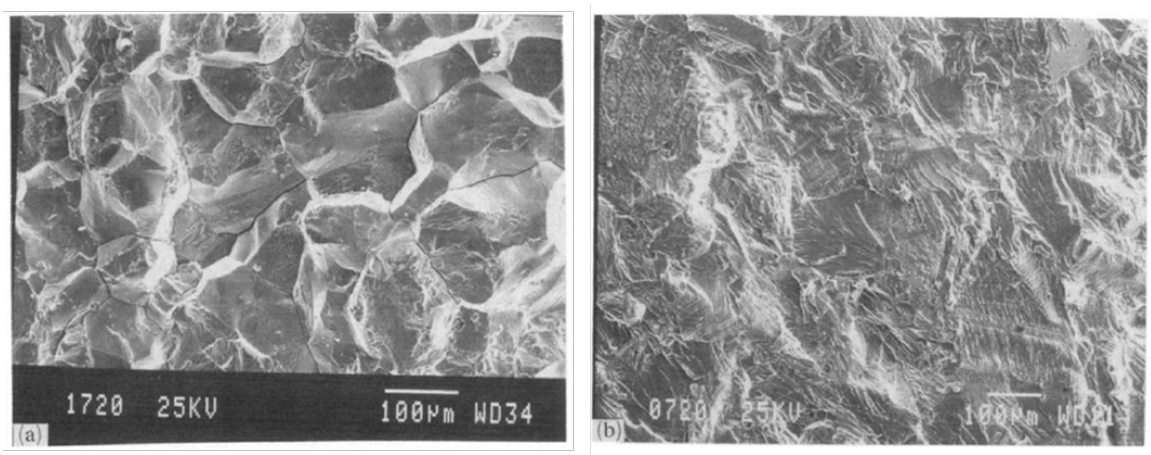

Figure 2.5: IN 718 fracture surface tested at 650°C at 0.05 Hz in (a) air and (b) vacuum [25].

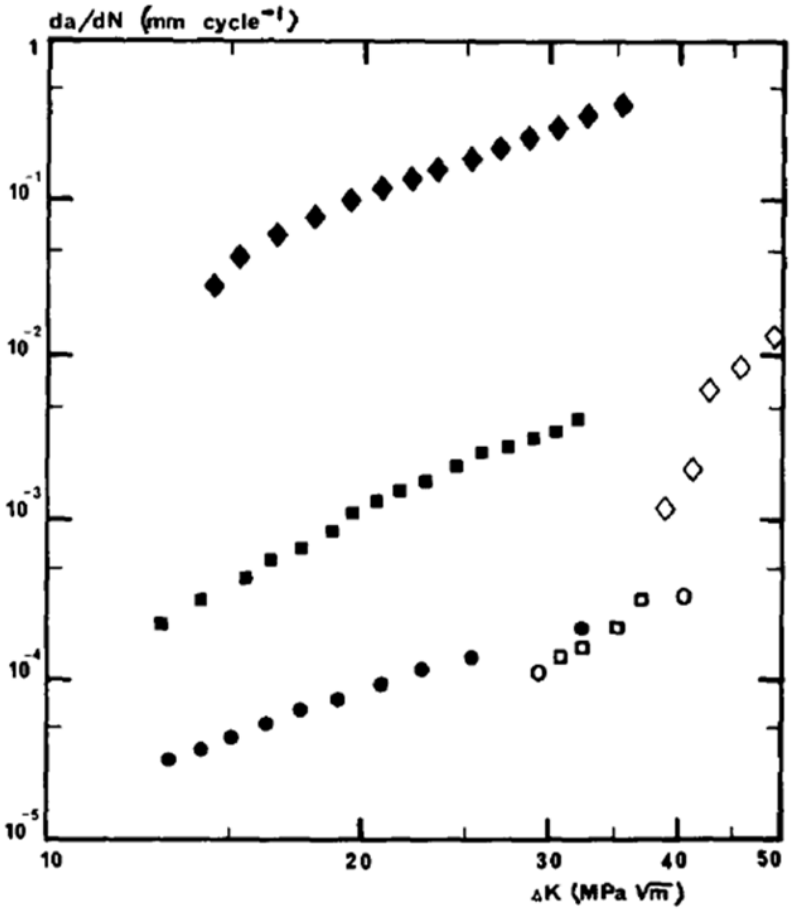

Figure 2.6: Fatigue crack growth rate for IN 718 in air and vacuum subject to various loading rates: open symbols, vacuum; full symbols, air; ◊,♦,10-300-10; □,■,10-10; ○,●, 20 Hz [20].

time for the oxidation to impact crack growth during the cycle was equal to the full duration of the cycle [25]. Weerasooriya et al. came to a similar conclusion for high loading ratio loading (R>0.8) [23].

Along with the presence of oxygen and exposure time, elevated temperature is required for the oxidation assisted mechanism to play a significant role in FCGR in the mixed and time-dependent crack growth modes. The temperature at which oxidation effects begin to play a significant effect on the fatigue crack growth behavior in IN 718 is dependent on the loading frequency [32]. Figure 2.7 shows that as frequency increases, the transition from a transgranular crack growth mode to an intergranular crack growth mode occurs at an increasing temperature. This matches the results of Sadananda and Shahinian who showed that at 425°C the negative effect on FCGR of elevated temperature was no longer present [33]. James et al. showed the negative effect of time spent at elevated temperature was still present at 538°C [34]. This effectively puts the transition temperature for the oxidation assisted mechanism between 425°C and 538°C. The implications of this effect are significant. Ghonem et al. showed that for slow loading rates where oxidation is an important factor, as the temperature rises from 550°C to 650°C, the crack growth rate increases by approximately an order of magnitude [25].

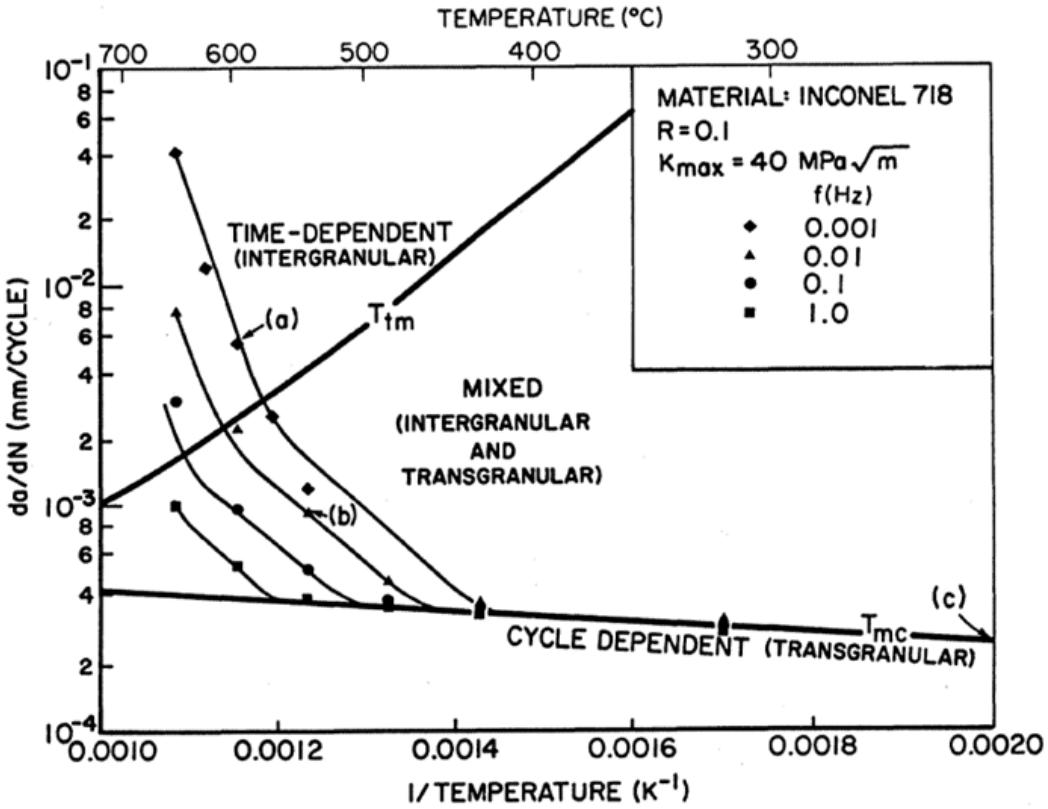

Figure 2.7: Micromechanisms of crack growth in IN 718 with changes in temperature and frequency [32].

2.3.3 Hold Time Effects

The effects of high temperature on fatigue crack growth of IN 718 are compounded when the loading is held constant at high temperatures. This effect is most pronounced when the load is held at the maximum tensile load. However, for isothermal testing at 650°C, Diboine et al. showed that hold times at minimum tensile load for durations as short as 3 seconds significantly increased the FCGR as well [35]. They also showed that this effect saturates after about 1000 seconds [35]. Additionally, Pedron et al. showed this increase in isothermal fatigue crack growth rates occurring down to tensile holds at zero applied load [20]. Ponnelle et al. conducted a study showing a tensile hold following an unloading of at least 20% negated the expected effect of the tensile hold on FCGR [36]. Recent isothermal tests conducted by Gustafsson et al. on fine grained IN 718 up to 650°C showed similar results for

tensile holds at that high temperature [37]. Figure 2.8 shows experimental data for the hold time effect.

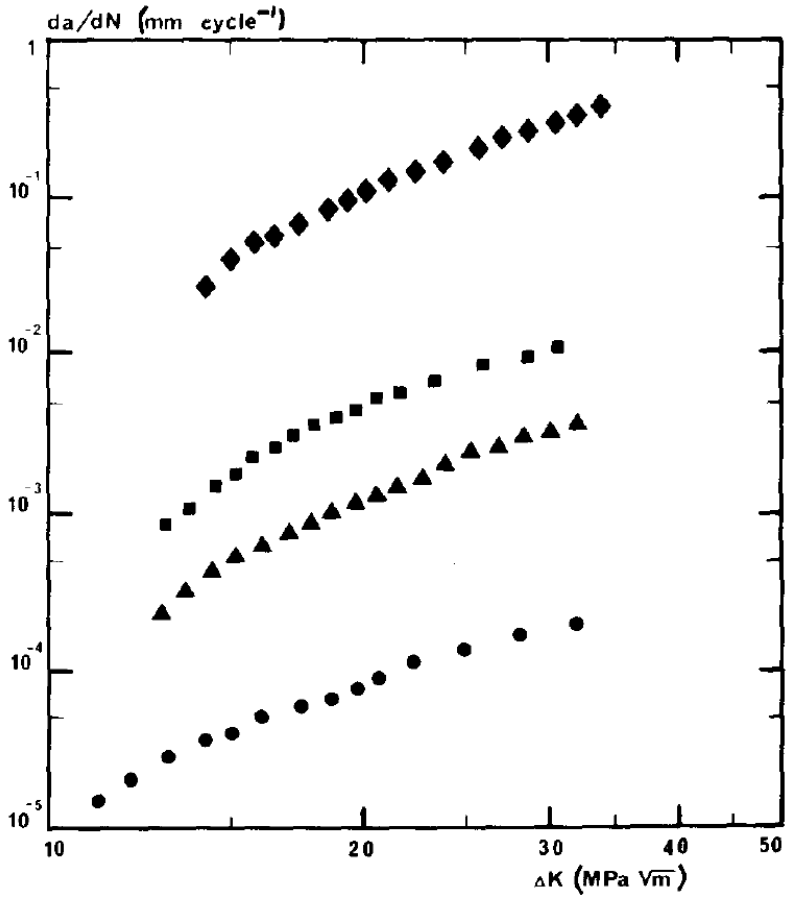

Figure 2.8: Effect of hold time on crack propagation for IN 718 at 650°C for loading waveform: ♦, 10-300-10; ■, 10-10-10; ▲, 10-10; •, 20 Hz [20].

While also observing the impact of a tensile hold on fatigue crack growth rate, Andersson et al. observed that for isothermal tests up to 687°C with tensile hold, no crack growth occurred during the tensile hold portion of the cycle [16]. This shows that the increase in fatigue crack growth rate due to a tensile hold at high temperature is only due to the changes occurring at the crack tip during the tensile hold and its response during subsequent fatigue loading, not time-dependent crack growth. This correlates with other sources indicating that though time-dependent crack growth can be observed in laboratory tests, in the real-world applications, time-dependent crack growth is not considered to be a factor for IN 718 [38, 39].

The effect of tensile holds is significant for a load controlled situation, however for strain controlled tests, Andersson et al. showed that a hold at positive strain did not result in an increased fatigue crack growth rate. This was attributed to crack tip blunting and relaxation of stress at the crack tip [16]. Similarly, it was observed that local homogeneous plastic deformation at the crack tip due to prestraining could also impede oxidation controlled time-dependent cracking [31, 40].

2.3.4 Grain Boundary Weakening Theories

Two theories are typically used to describe the oxidation assisted crack growth mechanism, stress assisted grain boundary oxidation (SAGBO) and dynamic embrittlement [41]. For SAGBO, in an air environment, when oxides form, they tend to favor the grain boundaries as opposed to through the crystal lattice [42]. More specifically, the oxidation is localized on the grain boundaries at the crack tip [25, 43]. This oxidation embrittles the grain boundaries and leads to faster, intergranular crack propagation [25]. Andrieu et al. and Molins et al. stated that the growth of the oxide on the grain boundaries at the crack tip will reduce the effective oxygen partial pressure and slow oxidation, but the cyclic loading will repeatedly break up the oxidation allowing for the crack to propagate and for further oxidation [43, 44]. With dynamic embrittlement, oxygen penetrates along the grain boundaries and embrittles and weakens them [45]. The grain boundaries are thus more susceptible to failure and hence a faster crack growth rate.

2.4 Oxidation of IN 718

The two types of oxides typically found in IN 718 are a niobium oxide followed by a protective chromia layer [43, 46]. Miller et al. showed that the intermetallic γ'' phase oxidized at high concentrations leading to intergranular fracture [47].

The high stress of the crack tip exacerbates oxidation penetration, but not necessarily in a uniform manner. Pfaendtner and McMahon showed that in an oxidizing

environment, certain grain boundaries are more susceptible to embrittlement [45]. The crack will tend to propagate along these embrittled grain boundaries faster than the rest of the crack front. This was corroborated by Viskari et al. [48]. Additionally, Viskari et al. provided a schematic of how uneven oxidation at the crack tip will lead to an uneven crack front, shown in Figure 2.9.

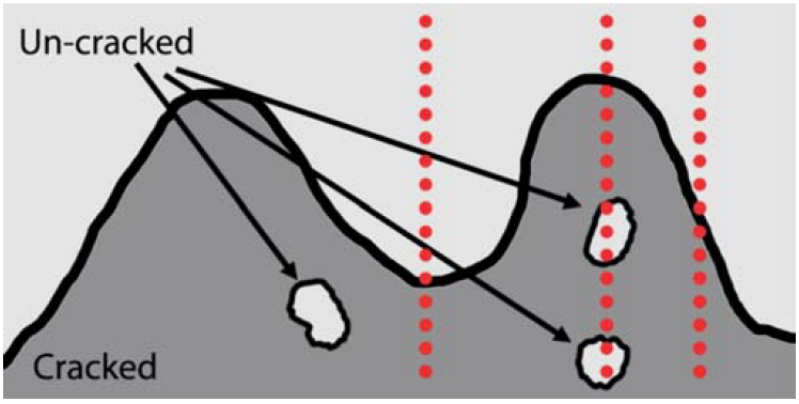

Figure 2.9: Schematic of oxidation penetration at the crack tip leading to an uneven crack front and areas of uncracked material [48].

Work done on the depth of oxidation penetration at the crack tip by Miller et al. characterized how far ahead of the crack tip oxidation penetrated. They conducted a time-dependent crack growth test at 700°C and used X-ray photoelectron spectroscopy to analyze how far ahead of the crack tip oxidation had penetrated and showed an oxidation affected region extending 150μm ahead of the crack tip [47].

In general, the FCG performance is significantly influenced by the environment, specifically exposure to air at elevated temperature. Weakening of the grain boundaries leads to faster intergranular crack growth as exposure duration increases.

2.5 Thermomechanical Fatigue

The harsh environment of jet turbine engines subjects components to ever varying mechanical loads and temperature gradients. Thermomechanical fatigue is typically characterized into two main types: in-phase (IP) where the maximum temperature coincides with the maximum strain/load and out-of-phase (OP) where the maximum

temperature coincides with the minimum strain/load. Figure 2.10 shows a simple representation of IP and OP TMF.

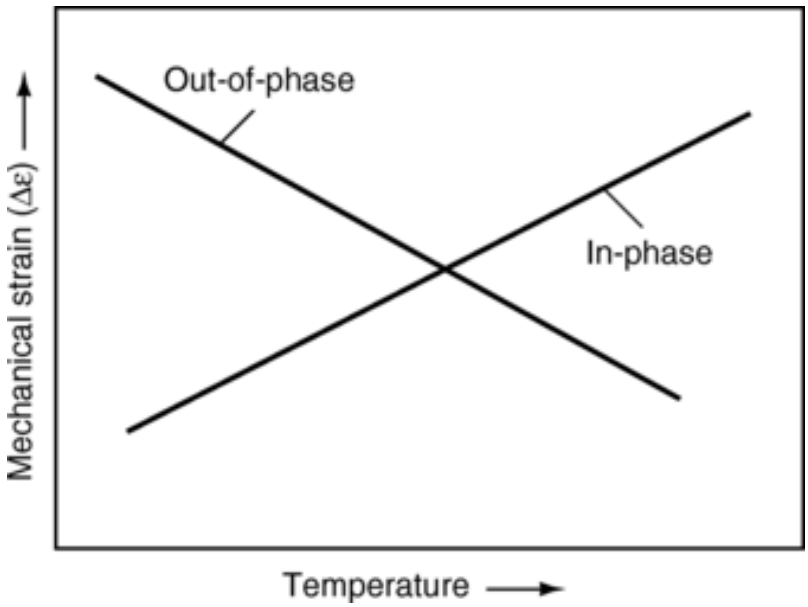

Figure 2.10: Thermomechanical fatigue cycles: in-phase and out-of-phase [49].

For materials where high temperature environmental effects are significant the OP TMF cycle may be more damaging [49]. Oxygen can penetrate the grain boundary and weaken the material even under low strain [49]. Subsequently, the slip lines that develop at low temperature as the strain is increasing break the oxides that formed at high temperature and the damage can propagate further [50]. Conversely for materials where creep effects are more significant, the IP TMF cycle may be more damaging. At high temperature and high strain, creep mechanisms work to weaken the material. As the strain and temperature are reduced, the damage does not propagate further into the material. With repeated IP TMF cycling, the damage done by the creep mechanisms will lead to loss of their ability to sustain further cycling [49].

To better understand IN 718's crack growth performance in a more realistic setting, numerous TMF crack growth studies have been conducted [51–55]. Nicholas et al. showed that for TMF cycling of IN 718 between 427°C and 649°C at a loading

ratio of R= 0.1, in-phase cycles were more damaging than out-of-phase cycles [54]. Additionally, they showed that the crack growth rate for in-phase TMF was slower than for isothermal cycling at the maximum, but the crack growth rate for out-of-phase TMF was comparable to the minimum temperature isothermal crack growth rate.

2.6 The Concept of a Thermally Affected Zone at the Crack Tip

The concept of an area of material ahead of a crack tip, termed "damage zone" or "thermally affected zone," weakened by exposure to time spent at elevated temperature in a FCG situation for IN 718 has been explored by several authors [56–59]. In their work, the specific contributions of the different crack growth mechanisms (oxidation, creep, materials evolution, etc.) are not assigned, only the net result on the FCGR is taken into consideration. It is important to note that though several of these authors use the term "damage zone," to avoid confusion with the concept of fatigue damage or plastically induced damage, the terminology of "temperature affected zone (TAZ)" was utilized for this project. The concept states that while a crack is propagating through this TAZ, an increased FCGR will occur. Once the crack grows through the TAZ, the FCGR will return to the expected FCGR had no exposure to time at elevated temperature occurred. Lundstrom et al. showed that for a specimen subject to fully time-dependent crack growth at 650°C, and then subsequently cycled, an increase in FCGR on the order of three-hundred times as fast is experienced [59]. The results of their test and identified damaged zone is shown in Figure 2.11.

Figure 2.12 shows that this thermally affected zone results in a primarily intergranular failure surface similar to that for a low frequency, high temperature, and air environment situation, as shown in Figure 2.5. This indicates that weakening of the grain boundaries plays a significant role in the effect of the thermally affected zone on

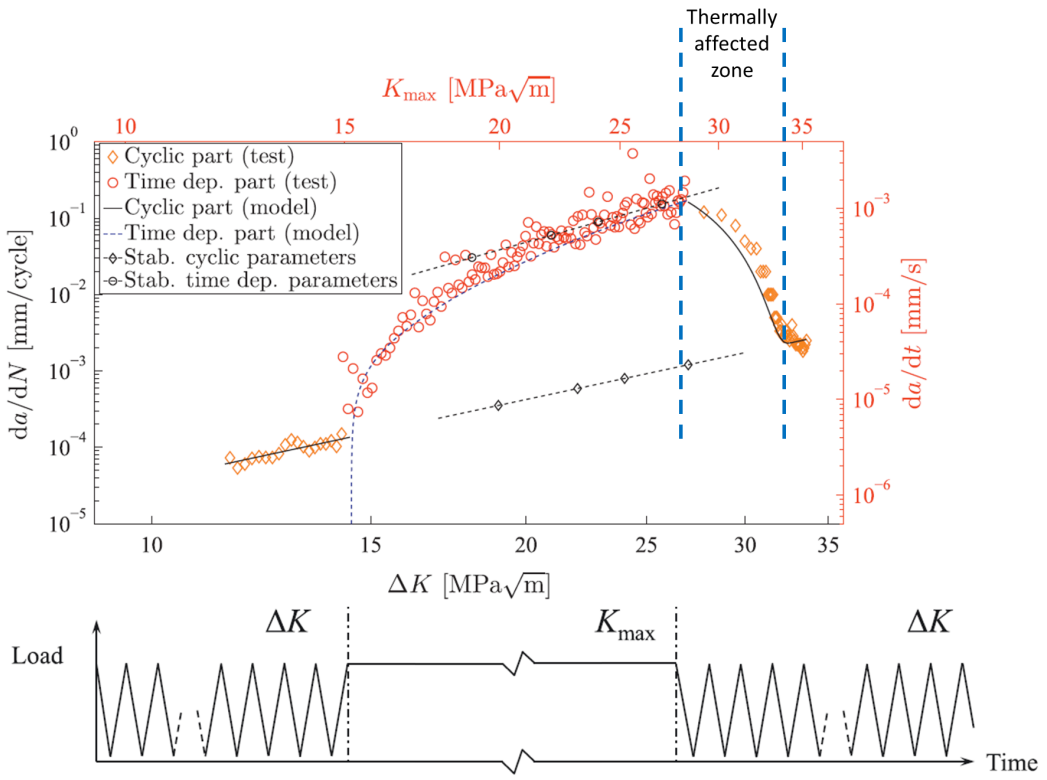

Figure 2.11: The effect of a thermally affected zone at the crack tip on FCGR (test conducted isothermally at 650°C) [59]. Time-dependent crack growth portion of curve utilizes right axis. Thermally affected zone denoted by dashed lines.

FCGR. Along with areas of intergranular failure, areas of transgranular crack propagation are also present indicating that the area ahead of the crack tip is not fully dominated by one mechanism. Areas ahead of the crack tip not significantly weakened by exposure to time at high temperature (transgranular appearance) are left to hold back the crack tip when cycling resumes as the weakened material (intergranular appearance) puts up less resistance.

Also shown in Figure 2.12 is how the effect of a TAZ is more significant away from the surface of the specimen. More significant tensile dilatational forces are found away from the surface of the specimen in the plane strain dominated region. This situation allows for increased oxygen penetration and the enhanced weakening of the grain boundaries characteristic of a TAZ.

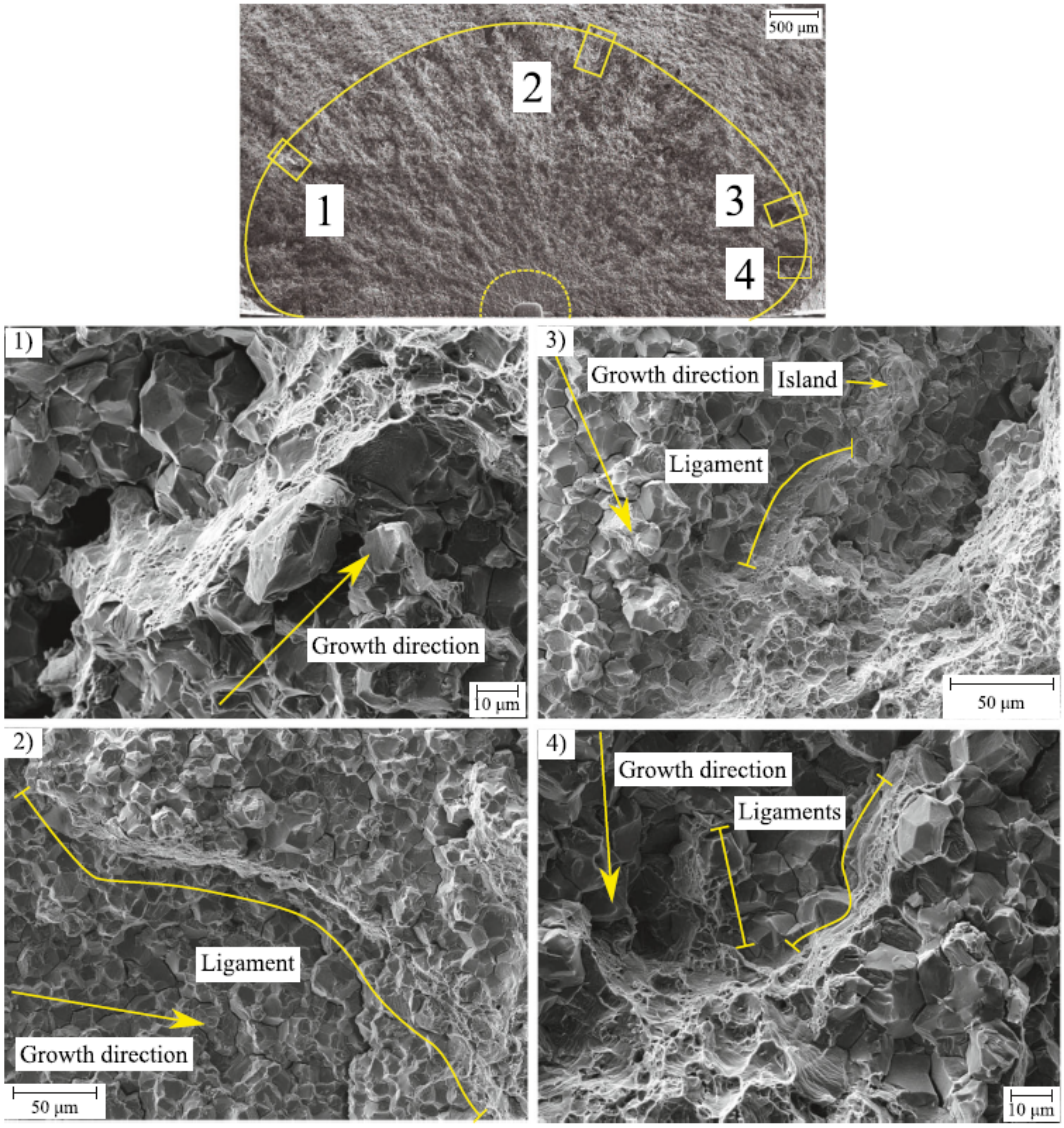

Figure 2.12: Failure surface showing characteristics of the thermally affected zone in images 1), 2), 3), and 4) [60].

Current work on the impact of a thermally affected zone on FCGR typically involves isothermal creation of a steady state thermally affected zone, either through time-dependent or creep-fatigue cycling, and subsequent crack growth through this single temperature affected zone. There are no studies on how a thermally affected zone's creation or its consumption (as the crack grows through it) will be impacted by thermomechanical cycling and what the net result on FCGR is.

2.7 Modeling Fatigue Crack Growth Behavior

2.7.1 Isothermal Fatigue Crack Growth Modeling in IN 718

The low frequency loading of IN 718 at elevated temperatures typically results in a nominally elastic response with a small plastic zone at the crack tip. This supports the use of the stress intensity range, ΔK, parameter for describing creep-fatigue crack growth [20]. Wanhill did a review of literature and came to a similar conclusion [39].

For fatigue at high temperature where time-dependent effects begin to come into play, numerous models for fatigue crack growth in Ni-base superalloys have been proposed that consist of a linear superposition of time-dependent and cycle-dependent crack growth that is of the form:

$$\left(\frac{da}{dN}\right)_{total} = \left(\frac{da}{dN}\right)_{cycle-dependent} + \left(\frac{da}{dN}\right)_{time-dependent} \tag{2.1}$$

The cycle dependent crack growth is typically characterized by some form of Paris law utilizing the stress intensity range, ΔK, whereas the time dependent crack growth is typically characterized by the maximum stress intensity, K_{max} [36, 59, 61].

Although the linear superposition technique has been used to varying levels of success in the past, Hournquist et al. showed that the cycle-dependent prediction is generally under-predicted and the time-dependent portion is grossly over-predicted resulting in a net crack growth that is close to actual (although the individual components are not independently accurate) [61]. This inability to break down superposition to its constitutive components accurately is an important limitation to consider when utilizing this type of model.

In a different approach, Ghonem et al. characterized FCGR utilizing an oxidation penetration model. They hypothesized that the time-dependent portion of crack growth is equal to the intergranular oxygen diffusion depth occurring during the cycle using [25]:

$$X = \alpha \left(D_g t\right)^{1/2} \tag{2.2}$$

where X is the depth of intergranular oxygen diffusion, α is a geometric constant, and D_g is the oxygen diffusivity of grain boundaries.

Utilizing finite element analysis techniques, Zhao et al. [62] also modeled oxide evolution at the crack tip and its impact on crack growth rate in a Ni-based superalloy. They attributed oxide formation to two mechanisms: oxygen diffusivity and deformation-assisted oxygen mobility. Their model showed increased oxygen diffusion for tensile loading compared to limited oxygen diffusion under no load. Their methodology worked well for slow loading situations, but not for fast loading situations. They predicted fatigue crack growth by utilizing the accumulated inelastic strain.

Additionally, Lundstrom et al. developed an isothermal model based on Newman's crack closure model [63] utilizing the thermally affected zone concept [59]. With their model, during a high temperature load hold, time-dependent crack growth occurs and a TAZ is created. The growth of the TAZ was modeled as equal to the rate of time dependent crack growth. During cyclic loading, only cycle-dependent crack growth is occurring (no temperature affected zone is created). The impact of the thermally affected zone on FCGR was implemented as a multiplication factor on the predicted crack growth rate. This factor had a power-law form and was based on the ratio of the current thermally affected zone's size to the maximum expected thermally affected zone size for purely time-dependent crack growth.

2.7.2 Thermomechanical Fatigue Crack Growth Modeling

Most available crack growth data is typically created through simple loading conducted isothermally. However, realistic loading of turbine components can be much more complex. Figure 2.13 shows the complex nature of the operating conditions of

turbine engine disks. To better characterize the FCG response of IN 718 subject to realistic TMF spectra, several models have been developed [54, 58, 64].

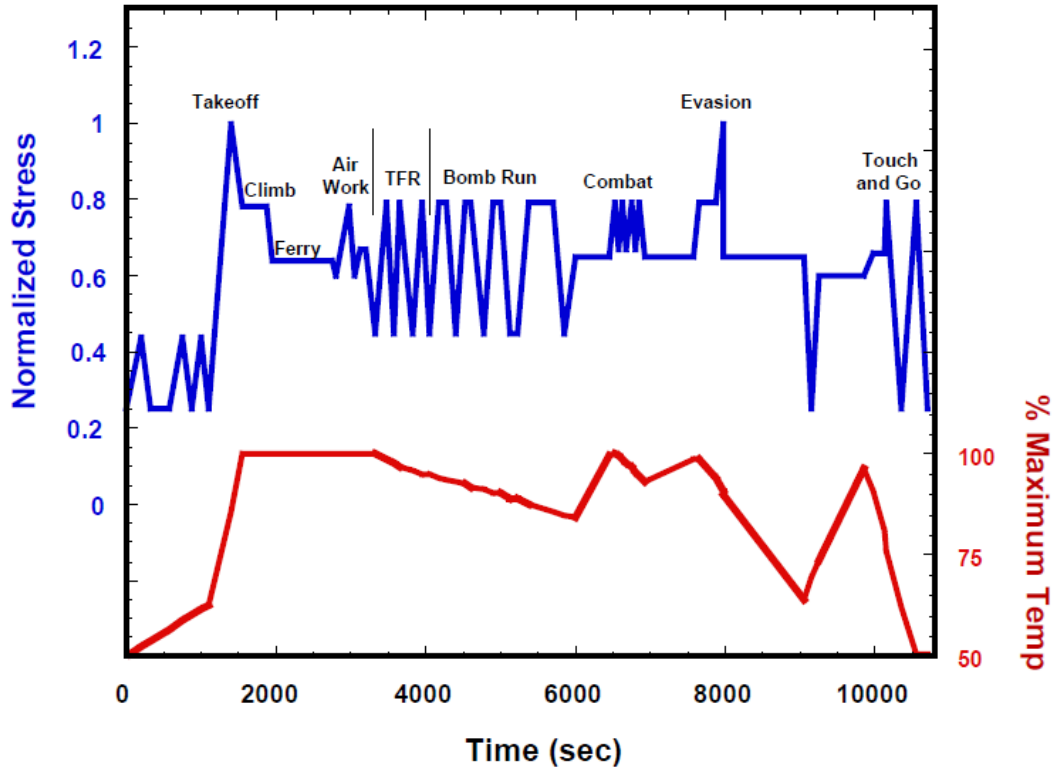

Figure 2.13: Typical mission loading for military turbine engine high temperature rotor components [65].

The model developed by Lundstrom et al. was extended by Storgärds et al. to TMF by interpolating the isothermal model to allow for changes in temperature [64]. Additionally, by leveraging Newman's crack closure model to indicate when the crack tip was open, the development of a temperature affected zone was allowed to occur during cyclic loading when the crack tip was open.

Lundstrom et al. and Storgärds et al. model the rate of development of the thermally affected zone based on the current stress intensity factor without direct reference to the existing size of the thermally affected zone. Since it has been shown that oxidation penetration at the crack tip diminishes as the oxide layer thickens [44], and indications that oxidation at the crack tip contribute to the FCGR effects of the

thermally affected zone, a more robust model should also take into account the size of the current temperature affected zone in those calculations.

2.7.2.1 Multi-Parameter Yield Zone-Thermomechanical Fatigue Model

A phenomenological isothermal load interaction crack growth model was developed by Johnson and identified as the Multi-Parameter Yield Zone model (MPYZ) [66]. It utilized the well established hypothesis that crack growth can be described using linear elastic fracture mechanics. He utilizes a form of the Forman equation:

$$\frac{da}{dN} = \frac{C\Delta K^n}{(1 - R^{eff})^m K_C - \Delta K} \tag{2.3}$$

where m = 1 at R $\geq$ 0, m = 2 at R $<$ 0, K_c is the material's fracture toughness, ΔK is the stress intensity range, and R^{eff} is the effective stress ratio.

His model accounts for crack growth retardation and acceleration due to load interaction effects such as accelerations due to current overloads and decelerations due to previous overloads. He utilizes a residual stress intensity factor, K_R, to account for these accelerations and decelerations. This residual stress intensity was then used to calculate an R^{eff} by:

$$R^{eff} = \frac{K_{min} - K_R}{K_{max} - K_R} = \frac{{K_{min}}^{eff}}{{K_{max}}^{eff}} \tag{2.4}$$

for use in Equation 2.3.

His work was done with a polycrystalline aluminum alloy, but was shown to be effective for Ni-base superalloys [67].

This model was further developed by Barker et al. to account for non-isothermal conditions, identified as the Multi-Parameter Yield Zone - Thermomechanical Fatigue model (MPYZ-TMF) [58, 67]. The MPYZ-TMF model serves as the foundation for the model developed during this project. Barker included a user selected option of a Paris crack growth equation or a Forman crack growth equation in his implementation,

equations 2.5 and 2.6 respectfully.

$$\frac{da}{dN} = C_p \Delta K^{n_p} \tag{2.5}$$

$$\frac{da}{dN} = \frac{C_f \Delta K^{n_f}}{(1 - R_{eff}){K_C}' - \Delta K} \tag{2.6}$$

where C_p, n_p, C_f, n_f, and K_C' are fitting parameters, ΔK is the stress intensity range, and R_{eff} is the effective stress ratio.

The fitting parameters are provided by the user at multiple temperatures within the desired range and a linear interpolation is implemented for intermediate temperatures. Material yield strength variations with temperatures are also treated the same way within MPYZ-TMF. Additionally, the crack growth predictions for MPYZ-TMF utilize the stress intensity solutions for several different common testing geometries, including single edge notched tension, single edge notched bending, center cracked tension, double edge notched tension, and compact tension.

As a crack grows, the stress state at the crack tip transitions from primarily plane strain to primarily plane stress. MPYZ-TMF accounts for the stress state by comparing the crack tip plastic zone size to the width of the specimen and if the plastic zone size is less than $1/6^{th}$ the thickness of the specimen, a state of plane strain is said to exist and α, the stress state, is equal to 3. When the plastic zone size is between $1/6^{th}$ and 1/2 the specimen thickness, a power law is used to transition from plane strain to plane stress where $\alpha = 1$. The transition of α from plane strain to plane stress takes the form:

$$\alpha = \sqrt{\frac{b}{2 * r_p}} \tag{2.7}$$

where b is the specimen thickness and r_p is the plastic zone size.

MPYZ-TMF utilizes the plastic zone size for specific loading conditions to account for interaction effects. The calculation of plastic zone size is based on Irwin's formulation:

$$r_p = \frac{1}{\alpha\pi}\left(\frac{K_I}{\sigma_y}\right)^2 \tag{2.8}$$

and takes into account the maximum applied stress intensity, K_I, yield strength, σ_y, and stress state, α.

Crack growth retardation due to overload is controlled through the use of a residual stress intensity factor that compares the overload plastic zone size to the nominal plastic zone size. This required a re-derivation of Gallagher's residual stress intensity parameter [68] to account for varying temperature:

$$K_R^* = \sigma_y\sqrt{(Z_{OL} - (\Delta a + Z))\pi\alpha} \tag{2.9}$$

where K_R^* is the temperature dependent residual stress intensity and Z is the plastic zone size for the current cycle.

Single overloads that create a large plastic zone relative to the nominal plastic zone have the effect of slowing crack growth while within the region of plastically deformed material from the overload. In a plastic zone model, this effect is accounted for by reducing the mean stress of subsequent cycles. In this manner, an effective stress ratio, R_{eff}, is used to account for the overload effect stress ratio:

$$R_{eff} = C_1\left(\frac{1}{\frac{K_{OL}}{K_{max}} - \frac{B}{A}}\right)K_R^{*C_2} + \frac{K_{min}}{K_{max}} \tag{2.10}$$

where C_1 and C_2 are used to calibrate retardation from experimental data and A and B are the no retardation overload ratio (overload with no effect on crack growth rate) and cut-off overload retardation ratio (overload that causes crack arrest) respectively. The parameter B is determined by a linear function of temperature:

$$B = B_a * T + B_b \tag{2.11}$$

where B_a and B_b are fit to experimental data. A linear interpolation is utilized for partial retardation cases.

Multiple overloads are accounted for by comparing the crack growth during the overload to the the overload zone size and then determining what percentage of uncracked overload zone size remains after a subsequent overload. The crack growth rate is reduced based upon the percentage of the remaining overload zone size down to a material specific saturation value.

Minimum loads that are lower than the nominal minimum loads, including negative loads, termed underloads, have the effect of reducing the effect of previous overloads on crack growth rate. When an underload occurs, the model reduces the overload zone size by a factor proportional to the underload magnitude. The parameter β accounts for this underload effect and is used to calculate a new overload stress intensity factor:

$$\beta = \frac{K_{pr} - K_{UL}}{K_{eff}^{OL} - K_{UL}} \tag{2.12}$$

$$K_{max}^{OL} = \frac{(K_{eff}^{OL} - K_{max})}{(Z - Y)}(Z - \beta) + K_{max} \tag{2.13}$$

where K_{pr} is the minimum stress intensity factor of the cycle that produced the overload, K_{UL} is the stress intensity factor of the underload, and K_{eff}^{OL} is the effective overload ratio. The terms Y and Z are material fitting parameters.

Lastly, a thermally affected zone ahead of the crack tip was utilized to account for time spent at elevated temperature. Upon reduction of temperature, while the crack is still within this thermally affected zone, the crack growth rate remains the same as at the higher temperature. This rate was found to be about four times as fast for the temperature range evaluated (315°C to 649°C) with another Ni-based superalloy, Inconel 100. Once the crack grows out of the thermally affected zone, the crack growth rate will return to the corresponding rate for that temperature. The

size of this thermally affected zone was calculated by:

$$x = \mu\sqrt{t} \tag{2.14}$$

where x is thermally affected zone size, μ is a fitting coefficient similar to the diffusion coefficient, and t is the time spent at the elevated temperature.

The implementation of a thermally affected zone in MPYZ-TMF is limited. The size of the thermally affected zone is only based on time and utilizes a constant fitting coefficient regardless of the temperature. Additionally, the acceleration factor on FCGR if a crack is within the thermally affected zone is set at a constant value. The MPYZ-TMF model did a good job for the specific series of tests conducted, but the approach to model the effect of a thermally affected zone on FCGR is limited.

Lastly, though the MPYZ-TMF model in its current form does a good job accounting for varying temperatures from load cycle to load cycle, its algorithm functions in complete constant amplitude cycles executed isothermally before the next cycle with its own temperature can be executed. As such, it cannot account for a changing temperature within a load cycle so truly IP TMF and OP TMF cannot be modeled. To predict crack growth for a real-world TMF spectrum such as that shown in Figure 2.13, the spectrum must be broken into constant amplitude isothermal cycles by a method such as rainflow counting. This simplification limits the accuracy of the predictions. McClung et al. showed that simple rainflow counting of a complex spectrum resulted in non-conservative predictions [14]. This can be accounted for by the fact that by utilizing the stress rainflow method, sequence and time effects are neglected which are both critical to accurate predictions in TMF situations. To be able to accurately account for real-world TMF spectra, a different approach must be utilized.

CHAPTER III

EXPERIMENTAL METHODS

3.1 Material

The IN 718 material for this study was provided by Pratt and Whitney in the form of a section of forged a turbine engine disk as shown in Figure 3.1. The specific heat treatment history of the provided material was unknown, though it is known that it was given a heat treatment typical of a finished forged disk. The chemical composition of IN 718 is shown in Table 2.1.

Figure 3.1: Section of IN 718 forged disk used for this study: a) front view, b) profile view.

A separate source of IN 718 was also provided by Pratt and Whitney. As with the section of forged turbine disk, the specific heat treatment history of the material was unknown, though it is known that it was given a heat treatment typical of a finished forged disk. A micrographic analysis of the two sources of IN 718 showed that the grain structure (average grain size, grain orientation, distribution of δ-phase, distribution of carbides), as shown in Figure 3.2, were similar and consistent with IN 718 as shown in Figure 2.1.

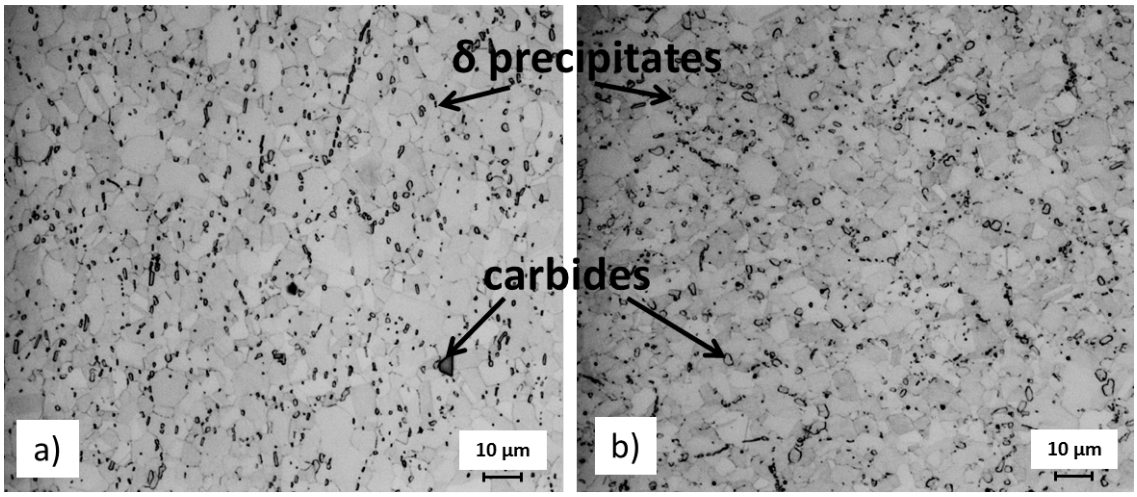

Figure 3.2: Micrographs highlighting grain boundaries of provided IN 718: a) other source material, b) disk material.

3.2 Specimen Geometry

3.2.1 Single Edge Notched Tension

A single edge notched tension (SENT) specimen with overall length of 203.2 mm, width of 38.1 mm, and thickness of 2.54 mm with a starter notch of radius 0.2 mm and length of 7.62 mm was utilized for the load controlled tests. This geometry was utilized due to previous success with it in high temperature fatigue crack growth experiments with Ni-base superalloys [69]. The specimens were cut from a section of forged turbine disk such that the loading direction in the specimen corresponded to the radial direction on the turbine disk. See Figure 3.3 for the specimen geometry and its orientation within the turbine disk section they were cut from.

Specimens were machined by Metcut Research, Inc. in Cincinnati, OH. Four specimens were obtained through the thickness of the disk section (which had a minimum thickness of about 25 mm). A total of 16 specimens were extracted from the disk section. To minimize surface residual stresses on the specimens, the final machining step included low stress grinding. The final surface finish provided by Metcut Research, Inc. on the specimens immediately ahead of the notch in the crack growth path was 8 μm. This area was polished further progressively with 9, 3, and 1μm

diamond suspensions using a Dremel tool with felt wheel to aid in more easily seeing the crack tip.

The flat specimen design allowed for the use of a long focal length traveling microscope to measure crack length without corrections needed for specimen curvature. Additionally, the SENT geometry allowed for the use of water cooled wedge grips for better heat dissipation when compared to the pin loading found on the common single edge notched specimen.

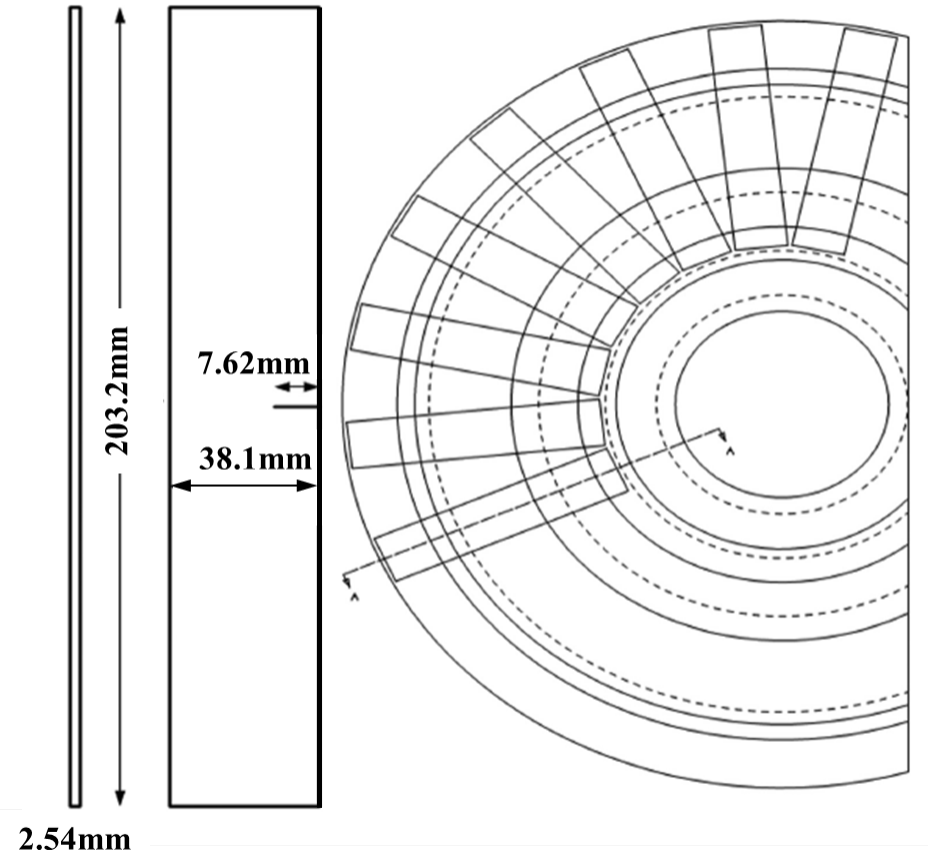

Figure 3.3: Single Edge Notched Tension (SENT) specimen and orientation on disk they were cut from [69]

3.2.1.1 SENT Stress Intensity Solution

Compared to the typical single edge crack tension specimen described in ASTM Standard E647-13 that is eccentrically pin loaded and hence allowed to rotate about the

loading pins, the SENT specimen used for this study was gripped by wedge grips and not allowed to rotate. This unique uniform displacement boundary condition required a non-standard stress intensity solution. The stress intensity solution for the SENT specimen was developed for this specimen by Newman using his FADD2D boundary element code for a previous project [69]:

$$K = S\sqrt{\pi a}\Big[1.126 - 0.504\left(\frac{a}{W}\right) + 10.473\left(\frac{a}{W}\right)^2 - 48.17\left(\frac{a}{W}\right)^3 + 112.87\left(\frac{a}{W}\right)^4 - 124.63\left(\frac{a}{W}\right)^5 + 53.327\left(\frac{a}{W}\right)^6\Big] \tag{3.1}$$

where S is the gross stress, a is the crack length, and W is the width of the specimen.

Previous projects utilized a starter notch of 11.43 mm. This limited the amount of usable crack growth ligament. A finite element analysis (FEA) study utilizing the commercially available software ANSYS (version 15.0) was completed. A 2-D model of the SENT specimen with uniform displacement boundary conditions was constructed to evaluate if the Newman stress intensity solution could be expanded to a shorter starter notch length. A fixed length crack was created using singular elements and the pre-meshed crack feature in ANSYS with 10 solution contours. The average element size of the mesh was 1 mm. The crack length was then varied to calculate the stress intensity solution for different crack lengths. Figure 3.4 shows the geometry and mesh utilized. Good correlation between the Newman stress intensity solution and ANSYS predictions were obtained and are shown in Table 3.1. This allowed the starter notch to be shortened to 7.62 mm.

Table 3.1: SENT specimen stress intensity solution comparison; Newman and ANSYS FEA. Applied stress = 100 MPa.

Total Crack Length (notch + crack) (mm)	**7.62**	**11.43**	**15.0**	**20.0**	**25.0**	**30.0**
K, Newman (MPa $\sqrt{m}$)	18.61	24.01	29.15	37.55	48.08	63.87
K, ANSYS (MPa $\sqrt{m}$)	18.52	23.9	29.1	37.25	47.68	63.26
Percent Difference (%)	0.48	0.46	0.17	0.80	0.83	0.95

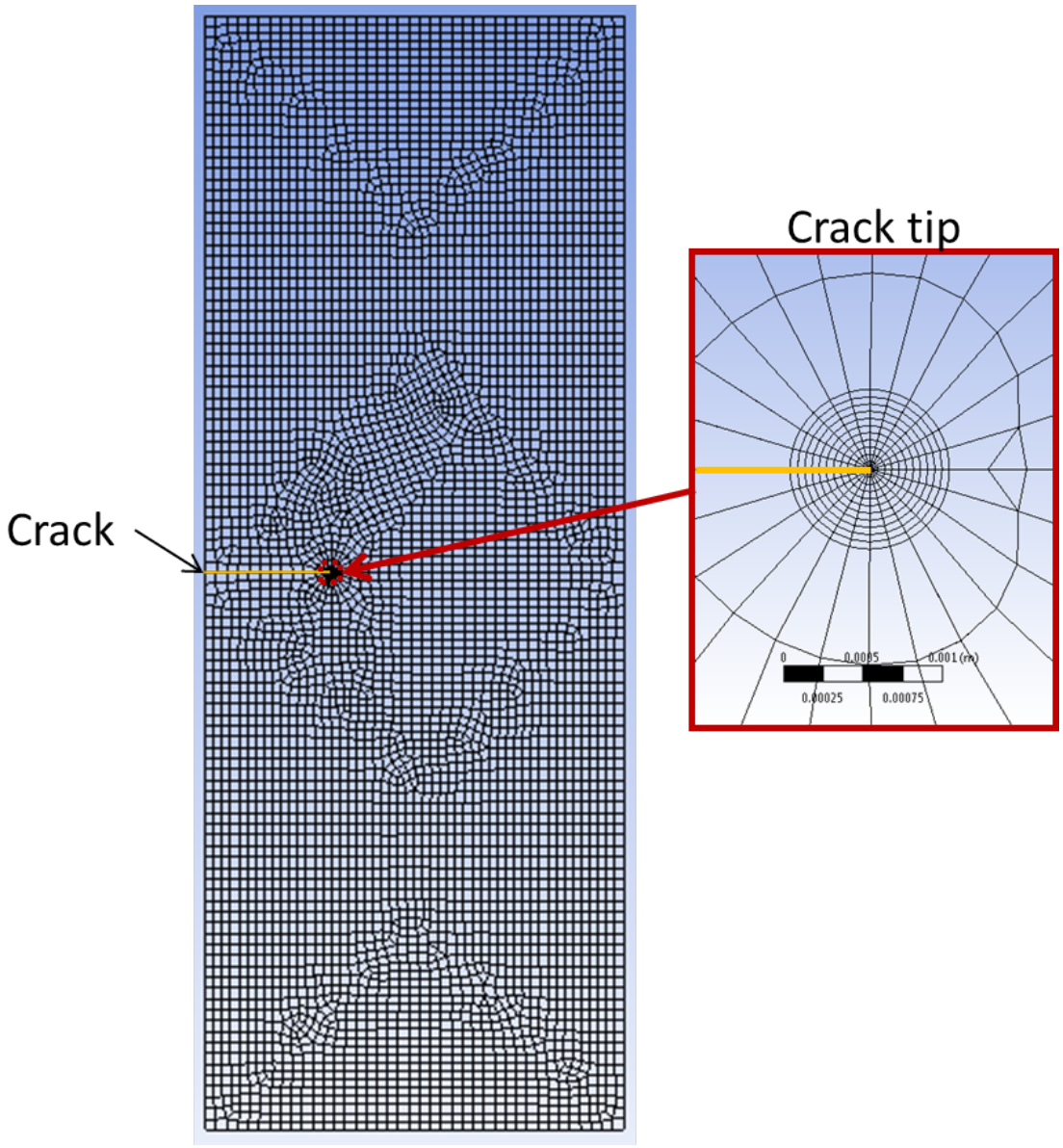

Figure 3.4: SENT specimen FEA geometry and mesh.

3.2.2 MT-41 Specimen

An MT-41 specimen was used for displacement controlled tests. The overall dimensions of these specimens were 108.2 mm in length with a gage diameter of 13.8 mm and a wall thickness of 1.2 mm as shown in Figure 3.5. A single starter hole of 0.254 mm diameter was laser machined for crack initiation.

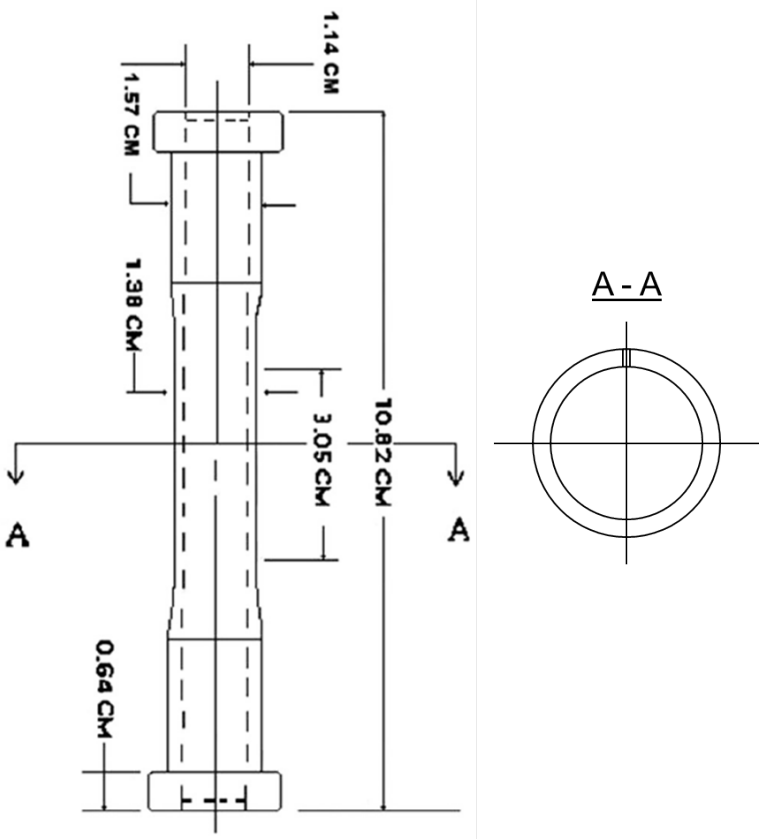

Figure 3.5: Pratt and Whitney provided MT-41 specimen geometry

3.2.2.1 MT-41 Stress Intensity Solution

Pratt and Whitney provided the solution to the stress intensity of the MT-41 specimen in the form of an output of their FRANC3D finite element software. It showed the progression of stress intensity with increasing crack length. Since it was not practical to run a finite element solution for every data point, an analytic solution was sought. The stress intensity solution for a circumferential through crack in a hollow cylinder loaded axially was utilized from Forman et al. and is given by [70]:

$$K_I = \sigma F \sqrt{\pi a} \tag{3.2}$$

where a is the crack length and the geometric correction factor, F, is computed by:

$$F = \left(\frac{I}{2\pi\alpha} \right)^{1/2} \tag{3.3}$$

where the dimensionless energy release rate integral, I, is given by:

$$I = \epsilon^{-1}\alpha^2 \left[g(\alpha) + \pi\lambda^{-1}C^2 - 2\sqrt{2} \right] \tag{3.4}$$

with a shell parameter, ϵ, given by:

$$\epsilon^2 = \left(\frac{h}{R} \right) \left[12 \left(1 - \nu^2 \right) \right]^{-1/2} \tag{3.5}$$

where h is the cylinder wall thickness and R is the outside radius of the specimen. The stress intensity magnification factor, C, is given by:

$$\begin{aligned} C &= 1 + \frac{\pi}{16}\lambda^2 - 0.0293\lambda^3 && \lambda \leq 1 \\ &= \left(\frac{2\sqrt{2}}{\pi}\lambda \right)^{0.5} + \left(\frac{0.179}{\lambda} \right)^{0.885} && \lambda > 1 \end{aligned} \tag{3.6}$$

and g(α) is given by:

$$g(\alpha) = 2\sqrt{2} \left(1 + \frac{1 - \alpha\cot\alpha}{2\alpha\cot\alpha + \sqrt{2}\alpha\cot[(\pi - \alpha)/\sqrt{2}]} \right)^2 \tag{3.7}$$

A shell parameter, λ, is given by:

$$\lambda = \alpha/2\epsilon \tag{3.8}$$

and the half opening angle of the crack, α, is given by:

$$\alpha = \frac{a}{R} \tag{3.9}$$

where a is the crack half length.

A comparison between the FRANC3D data and analytic solution is shown in Figure 3.6.

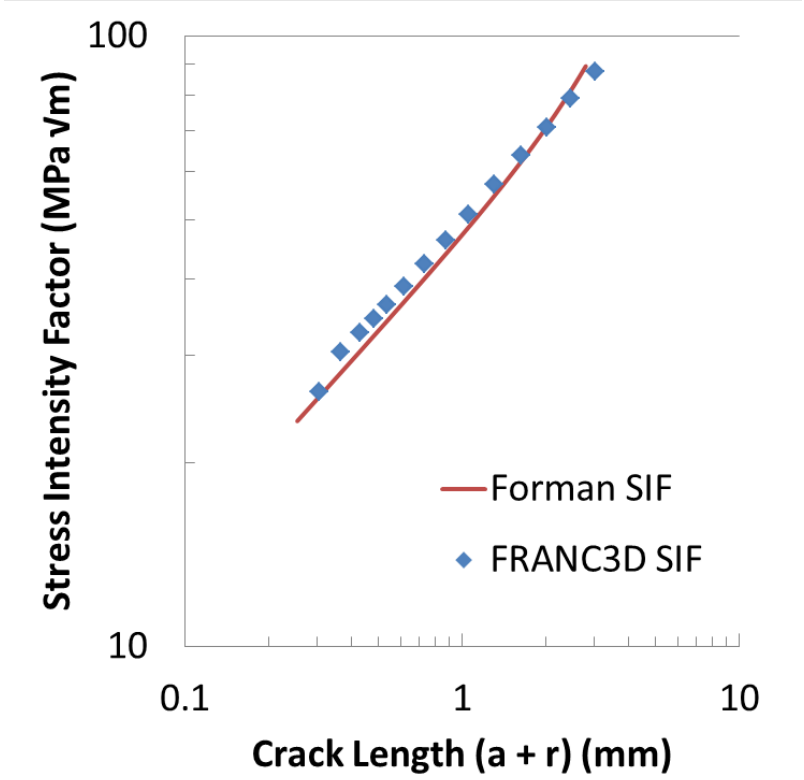

Figure 3.6: MT-41 specimen FRANC3D SIF comparison to Forman et al. SIF solution [70]

3.3 Test Equipment

Load controlled fatigue crack growth testing was accomplished in accordance with ASTM Standard E647-13 [71]. Tests were conducted on a 89kN MTS servo-hydraulic load frame controlled by a MTS TestStar IIs controller in ambient air. The load frame was outfitted with water cooled wedge grips for heat dissipation during thermomechanical cycling. The wedge grips gripped approximately 40 mm on either end of the specimen with a grip pressure of approximately 16,500 kPa.

A 3.5 kW Ambrell Hotshot induction heater with temperature feedback via a single K-type thermocouple was used to maintain test temperatures up to 725°C. The thermocouple was spot welded about 6 mm below the crack plane in the center of the crack growth ligament. In addition to the water cooled wedge grips, cooling was also accomplished by forced air from two fans controlled by an EuroTherm temperature

controller. Temperature in the crack plane was verified with an optical pyrometer and shown to be +/- 5°C across the crack plane [72]. The load frame set-up is shown in Figure 3.7.

Optical crack measurements were taken using a Questar QM-100 long distance microscope mounted on a three-axis Remote Measurement System platform with linear encoders. Crack images were captured at specific intervals to coincide with the maximum tensile load of the test spectrum by an Edmund Optics USB 2.0 CCD camera attached to the Questar microscope. Capturing crack images at the maximum tensile load allowed for the best contrast between the specimen and the crack tip. The Questar images were calibrated using a specimen with reference marks every 0.250 mm. The field of view of the Questar was adjustable using different lenses and spacing away from the specimen to between 2.5 mm and 0.5 mm. Further details on the TMF crack growth test system can be found in [73].

Additionally, several test points were accomplished utilizing a direct current electric potential difference (EPD) system set up according to ASTM Standard E647-13 [71]. Power was supplied by a Sorensen SRL 10-25 power supply at a constant 5 amps for all test points. Sixteen-gage Nickel-Chromium wire was spot welded approximately 45 mm above and below the crack plane for the current leads. Twenty four-gage Nickel-Aluminum wire was spot welded approximately 1 mm above and below the notch for crack tip voltage readings. The voltage signal around the crack tip was amplified with an Omega Omni-Amp III set to 1000X and recorded with the TestStar IIs. Figure 3.8 shows the overall test setup with the EPD and Questar configuration. Due to significant noise induced by the induction heater on the EPD readings, it was only used for crack growth test points with the induction heater off (i.e. at room temperature).

Strain controlled tests of the MT-41 specimen were conducted by Derivation Research Laboratory in Ottawa, Canada. A 97.8 kN MTS load frame with an

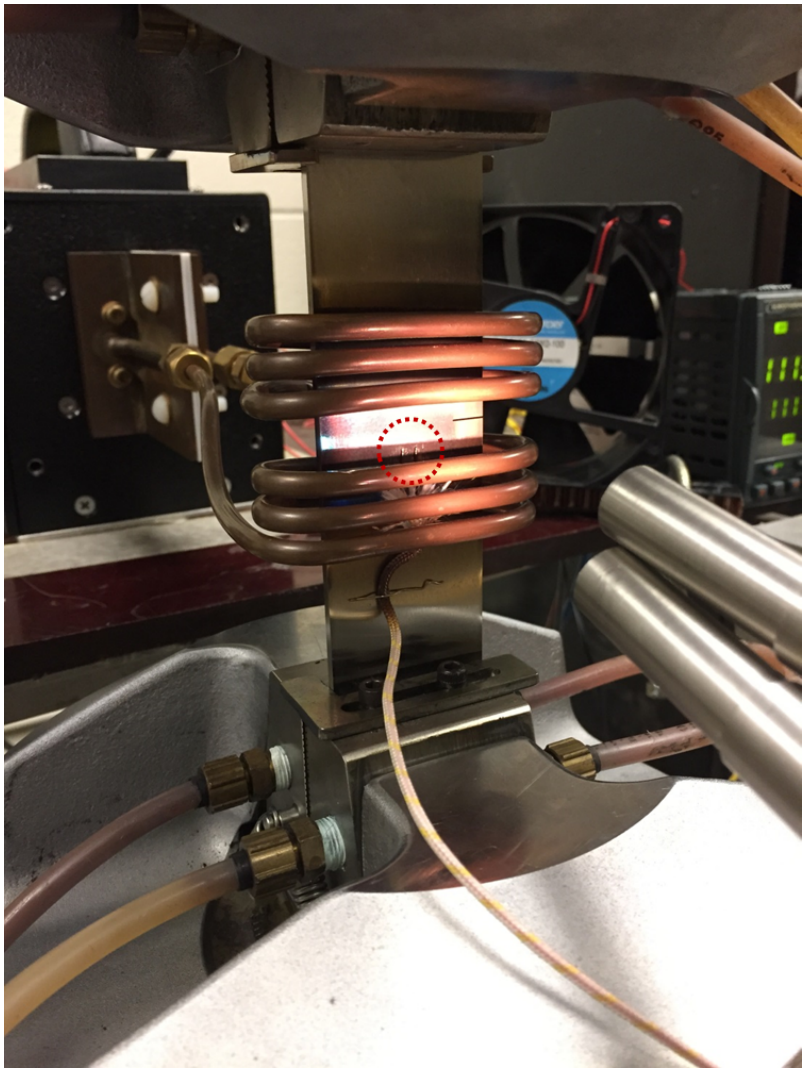

Figure 3.7: TMF crack growth set-up showing induction heating coil, one of the cooling fans, and thermocouple placement (circled)

Ameritherm NovaStar 5 kW induction heater was utilized. An infrared pyrometer was used for temperature feedback control. Additional cooling was provide by forced air both through the center of the specimen and on the outside of the specimen. Crack growth measurements were taken using an infrared camera and a correction for surface curvature was employed to calculate the crack length on the surface of the specimen. Figure 3.9 shows the setup for the strain controlled tests.

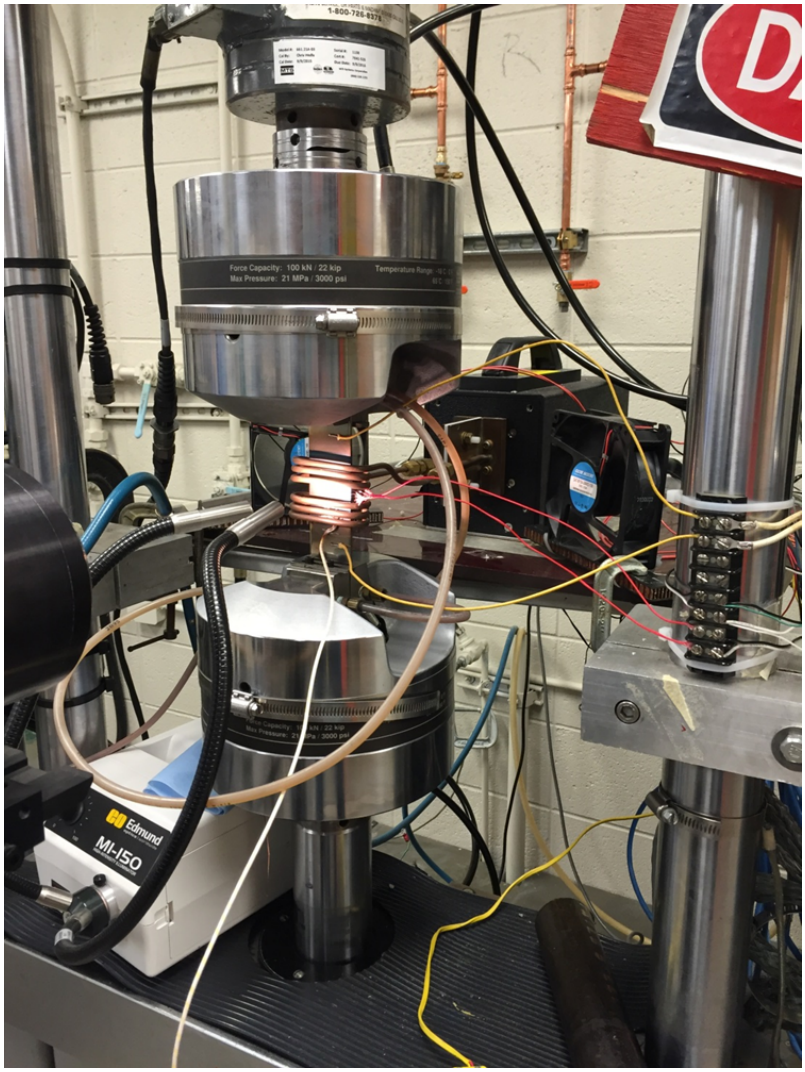

Figure 3.8: TMF crack growth with EPD set-up showing the overall configuration

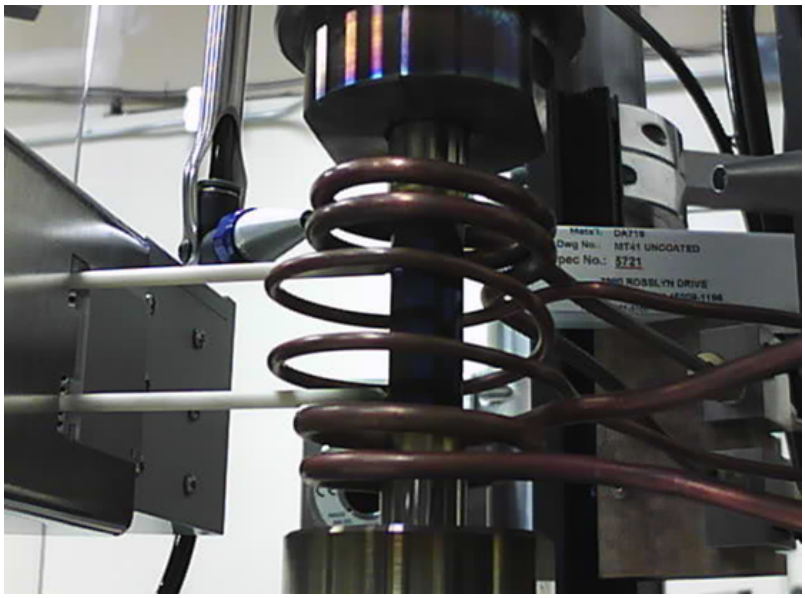

Figure 3.9: Strain controlled TMF crack growth configuration

3.4 Testing Methodology

In order to excite a response in the specimens similar to what the material might see in actual use, multiple different TMF as well as isothermal test spectra were designed and executed. Specifically, spectra were designed to evaluate the material's response to time spent at high temperature when subject to both tensile and compressive applied loads. Additionally, at the location on the disk of greatest concern for failure due to FCG, the outer rim, a general OP TMF spectrum is experienced in actual application due to the forces induced by the spinning disk and those thermally induced. This overall out-of-phase nature was used as a foundation for the design of the spectra used in this project.

3.4.1 Multiple Test Points on a Single Specimen

Due to the limited number of SENT specimens available, several steps were taken to maximize the number of tests points able to be accomplished. First, as mentioned above, the initial notch length was shortened from 11.43 mm to 7.62 mm to allow for more crack growth ligament. Additionally, as the response of the material and specimen were better understood through the initial tests, several test points utilized the same specimen (see Specimen ID 1404 and 1403 in Table 3.5 as an example). Supporting the use of a single specimen for multiple test points were, the small amount of crack front tunneling, less than 0.5 mm in center of specimen compared to the surface, the relatively flat crack plane created during high temperature testing, the microstructural stability of this alloy for the test temperatures, and the limited amount of creep expected at temperatures of 650°C and below. When multiple TMF spectra or isothermal test points were accomplished on a single specimen the general procedure was:

1. Precrack virgin specimen according to ASTM E647-13 at 10 Hz at room temperature.

2. Execute planned spectrum until sufficient crack growth has occurred to capture desired trend.

3. Precrack at least 0.25 mm to grow out of the linear elastic fracture mechanics cyclic plane stress plastic zone from the previous test point.

4. Execute next planned spectrum.

In addition to precracking when leading into a new test point on a specimen, to ensure test points earlier in a specimen did not impact test points later in the specimen the sequence of test points were specifically chosen to minimize temperature and load history effects. Specifically, lower temperature test points were accomplished before higher temperature test points and lower load (and hence crack tip stress intensity) test points were accomplished before higher load test points.

3.4.2 Fundamental Fatigue Crack Growth

Several isothermal fatigue crack growth tests were executed to be used as a baseline for crack growth with no effects of time spent at temperature for the model developed during this project. There were several options to mitigate the effects of time spent at elevated. First, the test could be run in an inert environment such as Argon. Second, the tests could be run in a vacuum chamber. Third, the tests could be run at sufficiently high frequency as shown by Pedron et al. [20]. The third option was utilized as it was an accurate and simple approach. Tests were conducted in accordance with ASTM E647-13 at 10 Hz using a sinusoidal waveform with a loading ratio of R = 0.05 at several temperatures: room temperature, 427°C, and 650°C [71].

3.4.3 High Temperature Tensile Hold

The performance of IN 718 when subject to tensile loads for longer durations of time has been well documented [20, 35, 37]. These types of studies have focused primarily on isothermal characterizations and have utilized either a slow loading frequency or a

creep-fatigue cycle with a high temperature hold imparted every cycle. The spectra designed and executed during this project were undertaken with the specific focus of determining how the FCG response of IN 718 varies as temperature is also varying. There have been limited studies on how this material responds to time at temperature as temperature is changing (i.e. a TMF cycle). An additional focus of this project was to characterize the effect on fatigue crack growth of a single high temperature hold imposed on an otherwise constant amplitude loading waveform. The test described in this section follow this approach.

3.4.3.1 Effect of Tensile Hold at High Temperature: Hold Load Relation to Cyclic Loading

In a typical turbine engine disk spectra, in addition to cyclic loads, holds at high temperature under tensile loading are typically found as shown in Figure 2.13. To best simulate the situation of a tensile hold occurring during a spectra, an isothermal spectra was designed to grow a crack in a SENT specimen under constant amplitude loading and intermittently impose single tensile holds of different durations and at loads of various relation to the maximum cyclic load. Figure 3.10 shows the spectrum for a several test points. The spectra were designed to be executed isothermally with a constant amplitude 0.5 Hz sinusoidal waveform. A loading ratio of R=0.05 was used to remain in tension throughout the duration of the spectra and to mimic other published data [57]. Tests were executed at 650°C. Test frequencies (faster) and temperatures (lower) were selected to ensure a transgranular fracture surface (i.e. no environmentally enhanced FCG effects) so that only the holds would impart the environmental damage.

Hold load relations of 0, 25, 50, 75, and 100% to the cyclic maximum load were executed. Additionally, hold durations of 30, 90, 300, and 3600 seconds were imposed. This test design mimics the work done by Ponnelle et al. with IN 718 where they conducted similar test to characterize the effect of a high temperature load hold

following an unloading of various amounts [36]. Crack length measurements were collected optically. Table 3.2 shows the test matrix.

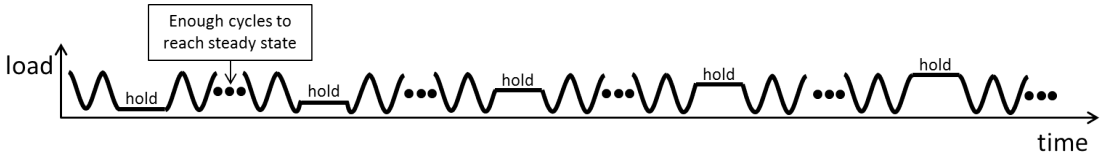

Figure 3.10: Isothermal FCG test spectra with intermittently imposed tensile holds.

Table 3.2: Constant load, tensile hold isothermal FCG tests

Specimen ID	**Temp (°C)**	**Hold load relation to cyclic maximum load (%)**	**Hold Duration (sec)**
1405	650	0,25,50,75,100	90, 300
1408	650	0,25,50,75,100	3600, 30

3.4.3.2 Effect of Tensile Hold at High Temperature: Constant Stress Intensity Factor

Additional tests were designed and executed to characterize the effect on FCGR of time at elevated temperature on FCGR using a constant stress intensity factor approach. The previous tests described in Section 3.4.3.1 were executed under constant amplitude and as such, as the crack length increased, the stress intensity factor at the crack tip increased with subsequent test points. To better characterize the effect of the stress intensity of a tensile hold at high temperature, test spectra were designed to hold the stress intensity factor at the beginning of test point constant. A test matrix including three temperatures: 550°C, 600°C, and 650°C, three stress intensity factors: 25, 35, and 45 MPa $\sqrt{m}$, and five different hold durations: 30, 90, 300, 3600, and 18200 sec was designed to gather sufficient data to identify trends in the effects on FCGR of each of the three variables.

As the temperature drops, the effect of hold time decreases. James et al. showed the negative effect of time spent at elevated temperature still present at 538°C [34]. Sadananda and Shahinian showed that at 425°C the negative effect of elevated temperature was no longer present [33]. The minimum temperature evaluated with this series of tests was 550°C to ensure the effects of time at temperature would still be present.

A total of 36 test points were executed. Table 3.3 shows the test matrix. As described in Section 3.4.1, multiple test points were accomplished on a single SENT specimen and as such, the lower temperature test points were accomplished first. All cycling was accomplished with a sinusoidal waveform and loading ratio of R = 0.05 at either 0.5 Hz (optical crack length measurement only) or 1 Hz (optical and EPD crack length measurement) to allow for the best accuracy.

Table 3.3: Constant stress intensity tensile hold tests (optical crack length measurement)

Stress Intensity of Hold (MPa $\sqrt{m}$)	**Hold Temp (°C)**	**Hold Duration (sec)**
25	550	90, 300, 3600, 18200
	600	30, 90, 300, 3600
	650	30, 90, 300, 3600
35	550	90, 300, 3600,18200
	600	30, 90, 300, 3600
	650	30, 90, 300, 3600
45	550	90, 300, 3600,15675
	600	30, 90, 300, 3600
	650	30, 90, 300, 3600

The specific design of the spectra included cycling the specimen at a lower temperature than the test point (either 260°C (optical measurement only) or room temperature (for the EPD test points)) and a slightly lower stress intensity than the test point. Although previous testing had shown that a damaged area was visible on the failure surface due to high temperature tensile holds, the nature of the cyclic portion

of the crack growth at high temperature made it more difficult to distinguish the damaged area. Therefore cycling at low temperature was chosen to better distinguish the effect of the high temperature hold on the fracture surface since a crack was expected to propagate in a transgranular manner for the lower temperature cycling, while the damage created by the high temperature hold would show a more intergranular appearance.

The loads for the cycling leading into specific test point were selected to minimize the effect of previous loading on the effect of the tensile hold (i.e. did not want any previous overload or underload impacting test point). Specifically, the low temperature cyclic loading leading into a test point was designed to match the its cyclic plane stress plastic zone size to the cyclic plastic zone size if one were to cycle at the test point temperature. This resulted in the stress intensity for the crack growth leading into a test point reduced between 1 and 9 MPa $\sqrt{m}$ depending on the specific test point. Additionally, the crack was allowed to propagate for at least 0.25 mm prior to all test points. The same loading ratio of R = 0.05 was maintained for both the crack growth leading into a test point and the cycling immediately following a tensile hold. The tensile hold at a specific stress intensity factor, temperature, and for a specific duration was then executed. Following completion of the hold, the temperature was reduced to the cycling temperature and the specimen was cycled at a loading ratio of R = 0.05 with the maximum load the same as the load used for the tensile hold. This cycling was continued until the crack had propagated through the expected damaged area based on previous testing. When a test point required a significant reduction in stress intensity factor from a previous test point, additional crack growth was allowed to re-initiate the crack at the lower stress intensity factor before executing the next test point (for example when going from a test point at a stress intensity of 45 MPa $\sqrt{m}$ at 550°C to a test point at a stress intensity of 25 MPa $\sqrt{m}$ at 600°C).

As mentioned in Section 3.4.1, when test points of different temperature were accomplished on a single specimen, the lower temperature test points were accomplished first. Figure 3.11 shows the spectrum for a test point. The overall design of these spectra are very similar to the work done by Liu et al. on characterizing the effect of high temperature tensile holds in IN 718 [56].

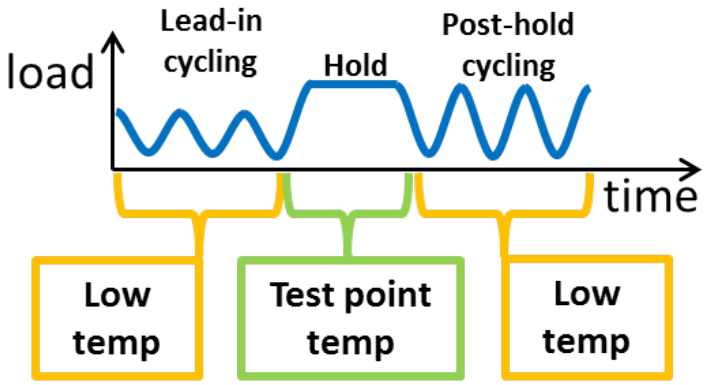

Figure 3.11: Constant stress intensity tensile hold at high temperature test spectrum

The crack length was initially measured optically, however, when the initial tests indicated no effect on FCGR, the EPD system was employed along with the Questar QM-100 to track crack length to accomplish several more test points as shown in Table 3.4. The use of the EPD system required the induction heater to be turned off to minimize noise in the measurement signal, so the cycling temperature was changed from 260°C to room temperature. A simple 1 Hz sinusoidal waveform was used for the EPD test points.

Table 3.4: Constant stress intensity tensile hold tests (optical and EPD crack length measurement)

Stress Intensity of Hold (MPa $\sqrt{m}$)	**Hold Temp (°C)**	**Hold Duration (sec)**
25	650	3600
35	600	3600
45	650	3600

3.4.4 Effect of Compressive Hold on Thermomechanical Fatigue Crack Growth

To evaluate the impact of a high temperature compressive hold on FCGR, two different OP TMF spectra were executed. One was a aircraft engine consortium developed spectrum as shown in Figure 3.12 and was run on both the SENT (load controlled) and MT-41 (strain controlled). This spectrum was run both with and without the compressive hold. The other spectrum utilized was a simpler triangular waveform as shown in Figure 3.13 with 60 seconds for heating, a hold time as applicable, and 60 seconds for cooling and was only run on the SENT specimen. Hold times of 10, 30, and 300 seconds were investigated at a maximum temperature of 650°C. A hold time of 30 seconds was investigated for maximum temperatures above 650°C. The maximum load and a loading ratio of R=-0.2 were the same for both spectra. The temperature range was different between the two spectra with the simple aircraft spectrum temperature range 260°C to 600°C and the triangular waveform temperature range 315°C to 650°C. Additionally, tests were conducted utilizing the triangular waveform where the maximum temperature was incrementally increased from 650°C to 725°C to assess the impact of increasing the maximum temperature above the typical maximum usage temperature for IN 718. Table 3.5 lists the parameters for the tests executed in this area. Crack length measurements were collected optically. A total of five specimens were utilized for the OP TMF testing with test durations

ranging from 337 hours to 473 hours.

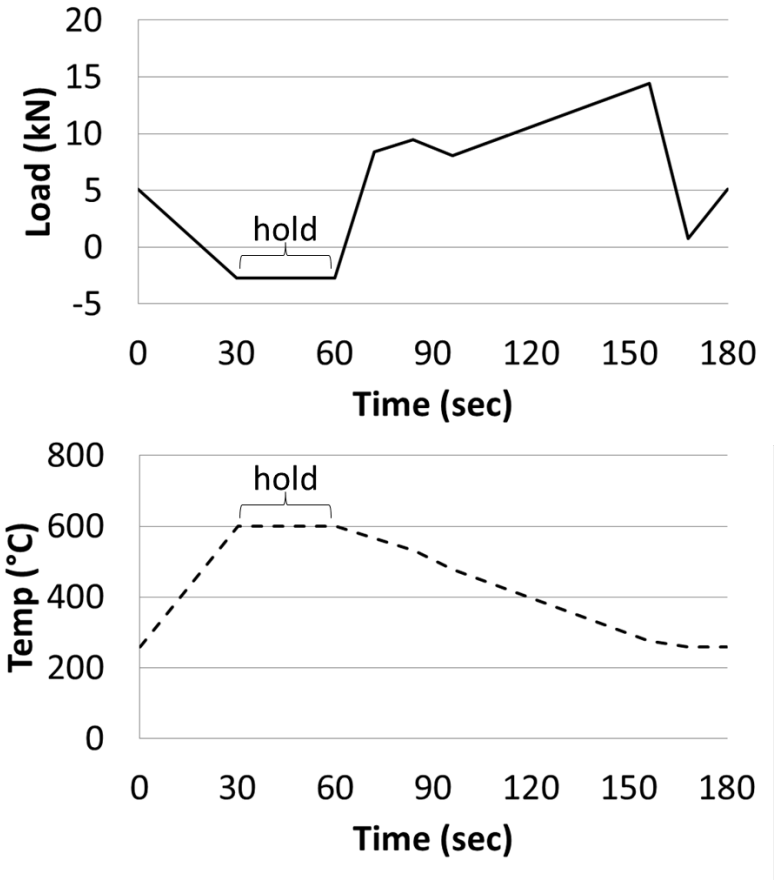

Figure 3.12: Aircraft engine consortium developed out-of-phase aircraft spectrum including compressive hold

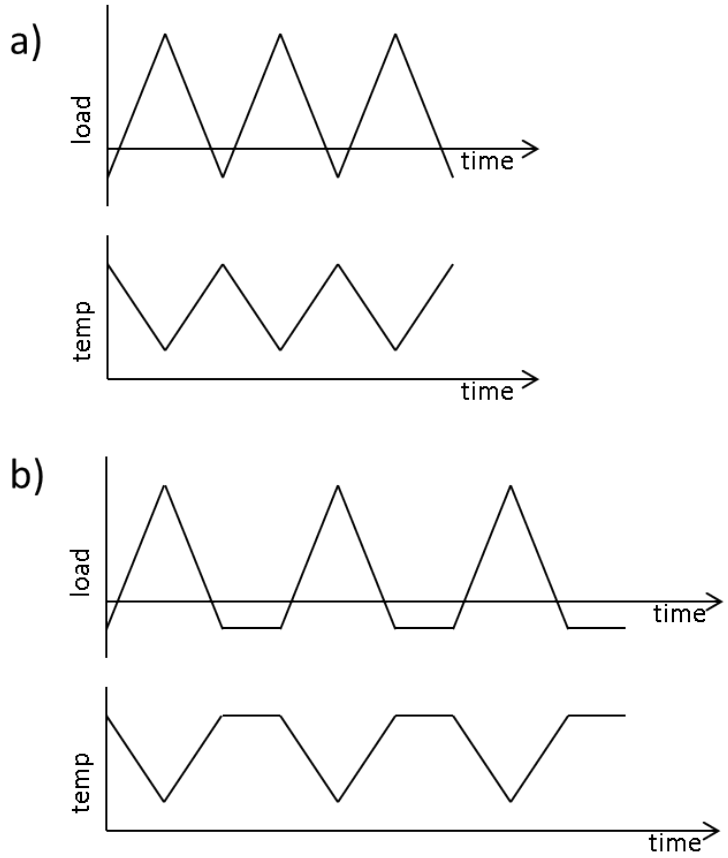

Figure 3.13: Out-of-phase TMF triangular waveform spectrum: a) no hold, b) with hold

Table 3.5: Compressive hold impact on out-of-phase TMF crack growth

Description	**Specimen ID**	**Temp$_{min}$ (°C)**	**Temp$_{max}$ (°C)**	**R**	**Cycle Duration (sec)**	**Hold Duration (sec)**
TMF Turbine Disk Spectra	1401	260	600	-0.2	180	30
	1402	260	600	-0.2	150	None
Triangular Waveform OP TMF	1404	315	650	-0.2	120	Multiple: 0, 10, 30, 300
	1409	315	650	-0.2	120	None
	1403	315	Multiple: 675, 700, 725	-0.2	T_{max} Dependent: 140, 140, 150	Multiple: 0, 30

3.4.5 Tensile Hold Sequence Effects on Out-of-Phase Thermomechanical Fatigue Crack Growth

Along with the TMF spectra tests described in Section 3.4.4, Several TMF spectra were designed and executed to isolate characteristics of realistic spectra and identify the effect of a tensile hold occurring at different points in the spectrum. The triangular waveform OP TMF spectra with no compressive hold (labeled as: Specimen ID: 1409 in Table 3.5) was modified to include a high temperature tensile hold at 50% of the cycle maximum load. As shown in Figure 3.14, this tensile hold was imparted in two different ways: one, on the loading portion of the waveform (labeled as forward), the other, on the unloading portion of the waveform (labeled as backward). The same loading ratio from the simple triangular waveform of R = -0.2 was utilized along with the same rates for load and temperature change.

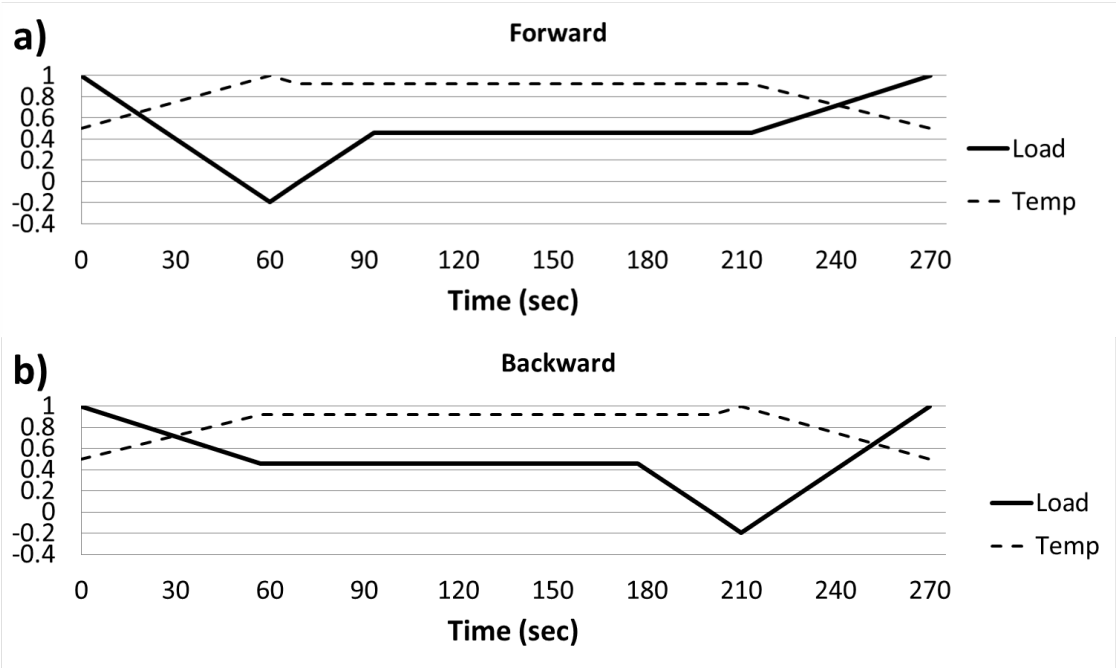

Figure 3.14: OP TMF spectra used evaluate tensile hold sequence effects on FCGR normalized to maximum load and maximum temperature a) forward, b) backward

3.4.6 Representative Turbine Engine Disk Spectrum

Additional TMF spectra were designed and executed to evaluate the impact of tensile subcycles on the FCGR. The spectra maintain the general OP TMF nature as described in the tests in Section 3.4.4 but with an imposed tensile hold both with and without intermediate subcycles. Figure 3.15 shows the spectra executed with subcycles and is more indicate of the fighter aircraft spectra Figure 2.13 shows. Figure 3.16 shows the spectra with only a tensile hold and is more indicative of a transport aircraft spectra. The temperature range for both tests was 315°C to 650°C.

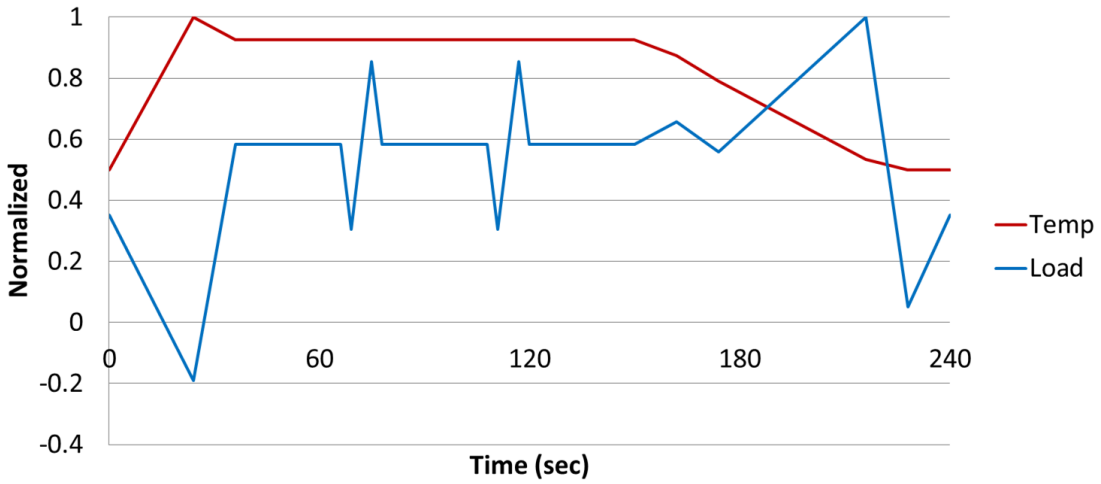

Figure 3.15: Representative fighter aircraft turbine engine disk spectrum

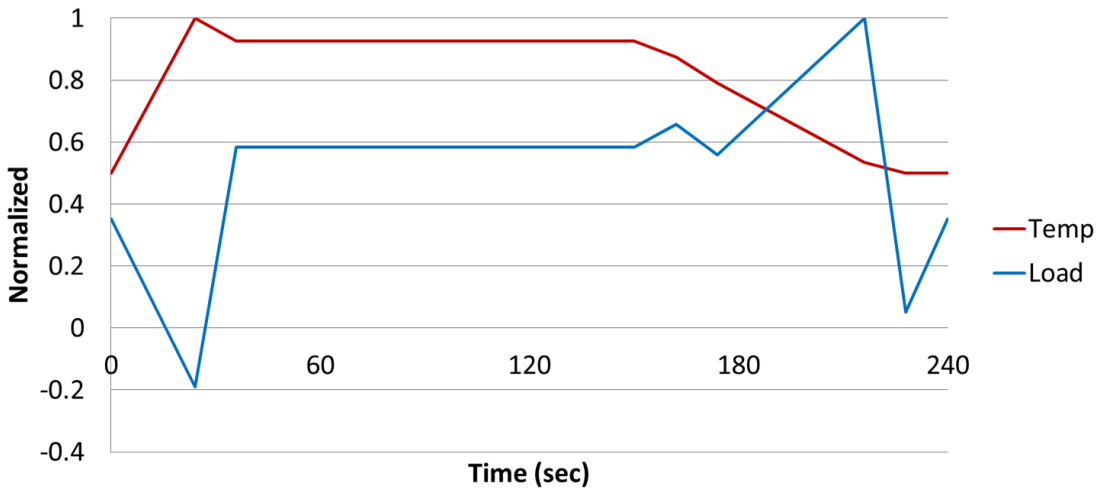

Figure 3.16: Representative transport aircraft turbine engine disk spectrum

3.4.7 Data Reduction

Crack images collected optically were selected at set intervals (on the order of every 200 cycles for TMF spectra tests). Depending on which lenses were used, a fidelity of $\pm 10\mu$m was achieved with the optical crack length measurement system. The crack length was measured and crack growth rate was calculated using an 7-point incremental 2nd order polynomial method in accordance with ASTM E647-13 [71]. The stress intensity range was calculated using the maximum range of the spectrum loading (including if the minimum load was compressive). Though slight tunneling of the crack was observed, the difference in crack length between the center of the specimen and the edge resulted in a calculated ΔK difference of less than the 5% limit specified in ASTM E647-13 and no crack length correction was needed [71].

Due to the noise inherent in any EPD system, the voltage reading was oversampled at 1024 samples per second and an average of the 100 data points nearest the peak tensile load of the cycle (i.e. when the crack tip was most open) were used for that cycle's crack length reading. A MatLab script was created to accomplish this data reduction. The EPD voltage signal was converted to crack length using HH Johnson's equation [74]:

$$a = \frac{W}{\pi} COS^{-1}\left[\frac{COSH\left(\frac{\pi}{W} \times Y_0\right)}{COSH\left[\frac{V}{V_r} \times COSH^{-1}\left[\frac{COSH\left(\frac{\pi}{W} \times Y_0\right)}{COS\left(\frac{\pi}{W} \times a_r\right)}\right]\right]}\right] \quad for\ 0 \leq \frac{2a}{W} \leq 1 \tag{3.10}$$

where a is the crack length, a_r is the reference crack length, W is the specimen width, V is the EPD voltage reading, V_r is the reference voltage, and Y_0 is the voltage spacing from the crack plane. Calibration of the EPD crack length was accomplished by simultaneous tracking of the crack length optically and by post test fracture surface measurements of features induced in the surface by test points. A fidelity of ± 6 μm was achieved with the EPD system.

Failure surfaces were examined using an optical microscope or a Tescan Mira3 scanning electron microscope (SEM). The pertinent settings of the SEM include: images were captured with secondary electrons, a beam voltage of 5 kV, and a beam intensity of 5.0.

CHAPTER IV

EXPERIMENTAL RESULTS

4.1 Fundamental Fatigue Crack Growth

Constant amplitude isothermal FCG tests were conducted to identify the baseline FCGR independent of time at temperature effects across the range of use temperatures for IN 718.

4.1.1 Crack Growth Rate

Figure 4.1 shows the results of the 3 tests run compared to low and high temperature crack growth data reported by McClung et al. for a fine grained IN 718 in a vacuum and crack growth collected in air at 0.67 Hz from the MMPDS [14, 15].

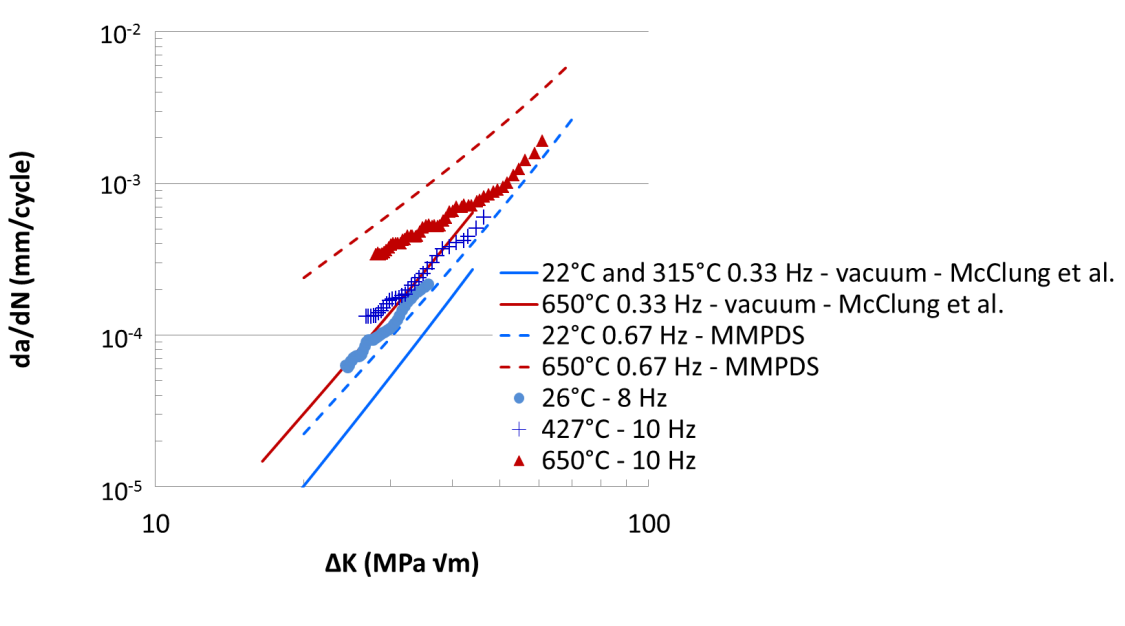

Figure 4.1: Fast frequency FCG data in air compared to published data [14, 15]

Data for the room temperature and 427°C test points had to be truncated as the tortuous nature of the crack growth at these lower temperatures caused the crack

plane to diverge by more than the 20° alloted by ASTM E647-13. Across the lower stress intensity range where most time will be spent, the collected data compares favorably to the published data. The lower temperature (room temperature and 427°C) data collected falls within the scatter of a typical FCG test. The data collected at 650°C falls faster than the published vacuum FCG data but slower than the published slower frequency data. This is to be expected since in a vacuum there is no oxidation present and in air as the frequency decreases the effect of oxidation plays a larger role in increasing FCGR.

Empirical fits to the Paris crack growth equation, Equation 2.5, and Forman crack growth equation, Equation 2.6 were also accomplished from the fast frequency isothermal FCG data collected in this project. The Forman fit is shown in Figure 4.2 and parameters for both the Paris and Forman equations are shown in Table 4.1.

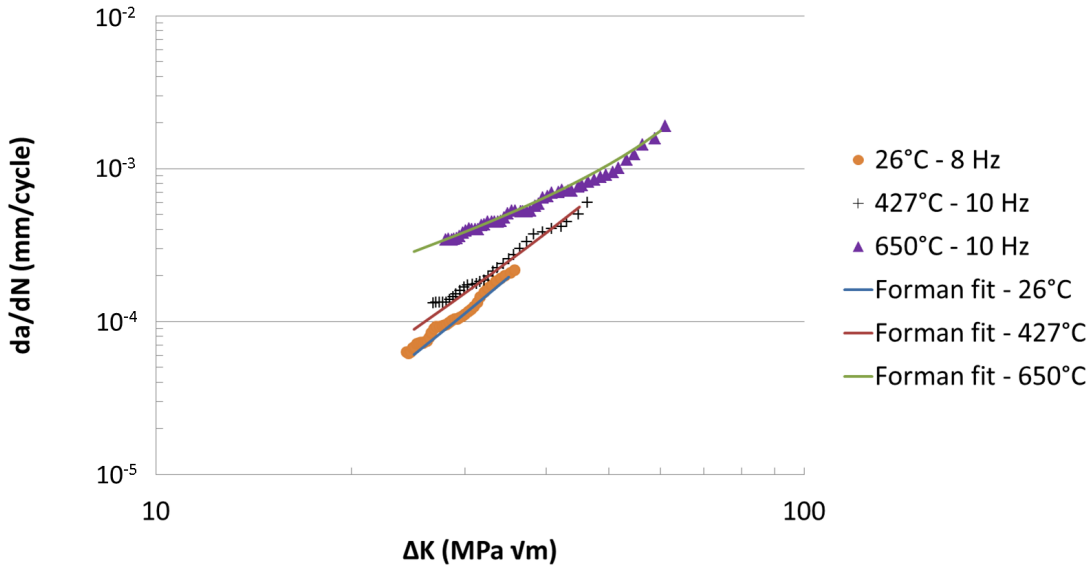

Figure 4.2: Forman crack growth equation fit to experimental data

The critical fracture toughness for these 3 test points were determined and are provided in Table 4.2.

Table 4.1: Crack growth coefficients

Temperature	Paris Coefficients		Forman Coefficients		
°C	C_p	n_p	C_f	n_f	K_C' MPa $\sqrt{m}$
26	1.85 x 10^{-9}	3.26	2.40 x 10^{-7}	3.1	116
427	7.10 x 10^{-9}	2.95	1.31 x 10^{-6}	2.7	119
650	5.32 x 10^{-7}	1.93	3.93 x 10^{-4}	1.2	95

Table 4.2: Critical fracture toughness for fast frequency isothermal FCG tests

Temperature (°C)	K_c MPa $\sqrt{m}$
26	116
427	119
650	96

4.1.2 Fractography

Since the isothermal FCG tests were executed at a fast frequency (greater than 8 Hz), transgranular crack propagation was expected as there was insufficient time for the grain boundaries to be weakened before the crack propagated forward even at the highest temperature of 650°C. From a macroscopic perspective, the isothermal FCG test failure surfaces show two main trends: a more torturous nature of crack propagation for the lower temperature tests and a flatter failure surface for the 650°C test as Figure 4.3 shows.

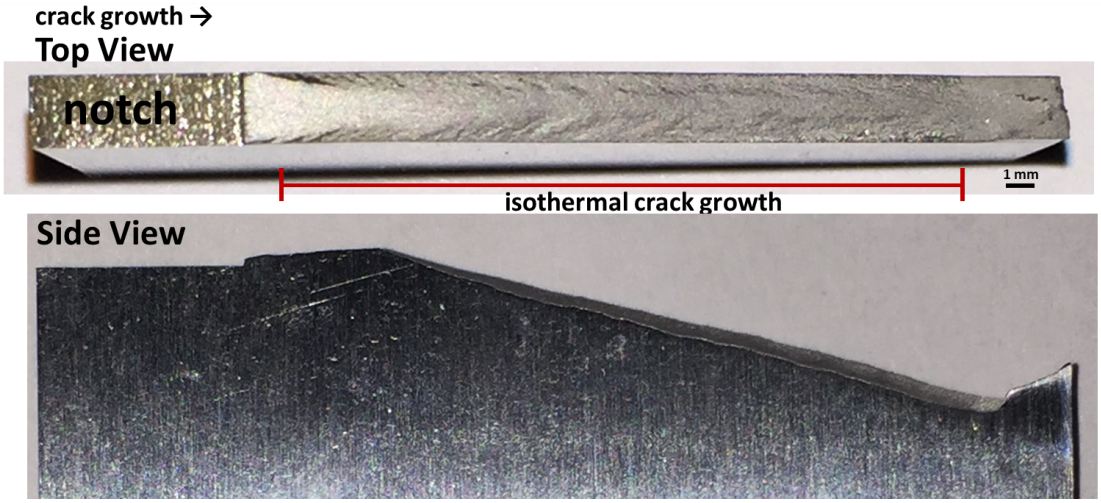

(a) Room temperature isothermal crack growth at 8 Hz failure surface showing chevron like shapes

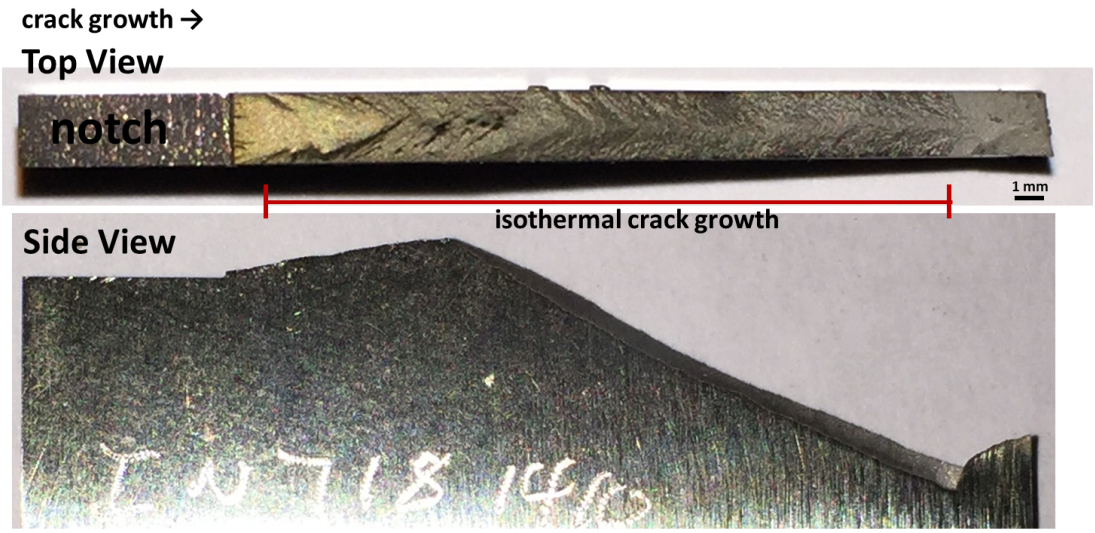

(b) 427°C isothermal crack growth at 10 Hz failure surface showing chevron like shapes

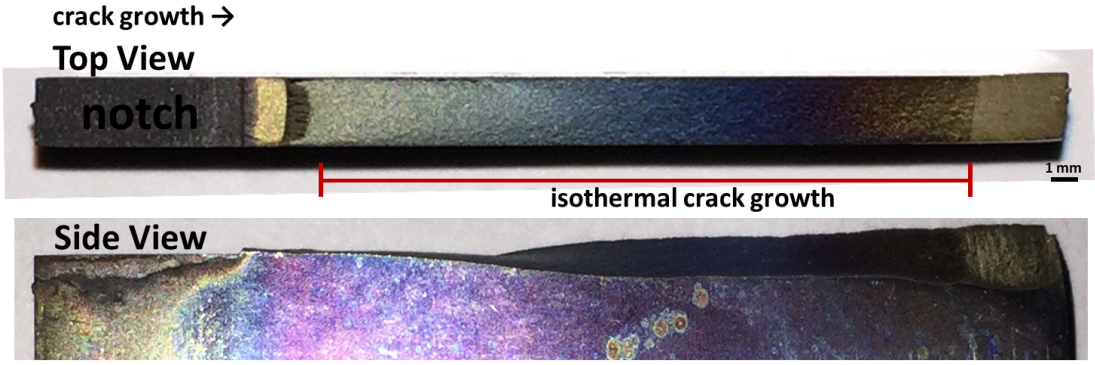

(c) 650°C isothermal crack growth at 10 Hz failure surface showing no chevron shapes

Figure 4.3: Isothermal fracture surfaces

Figures 4.4 and 4.5 show the fracture surfaces under higher magnification. A similar transgranular appearance is observed, however, the highest temperature, 650°C, does show a somewhat spalling-like appearance.

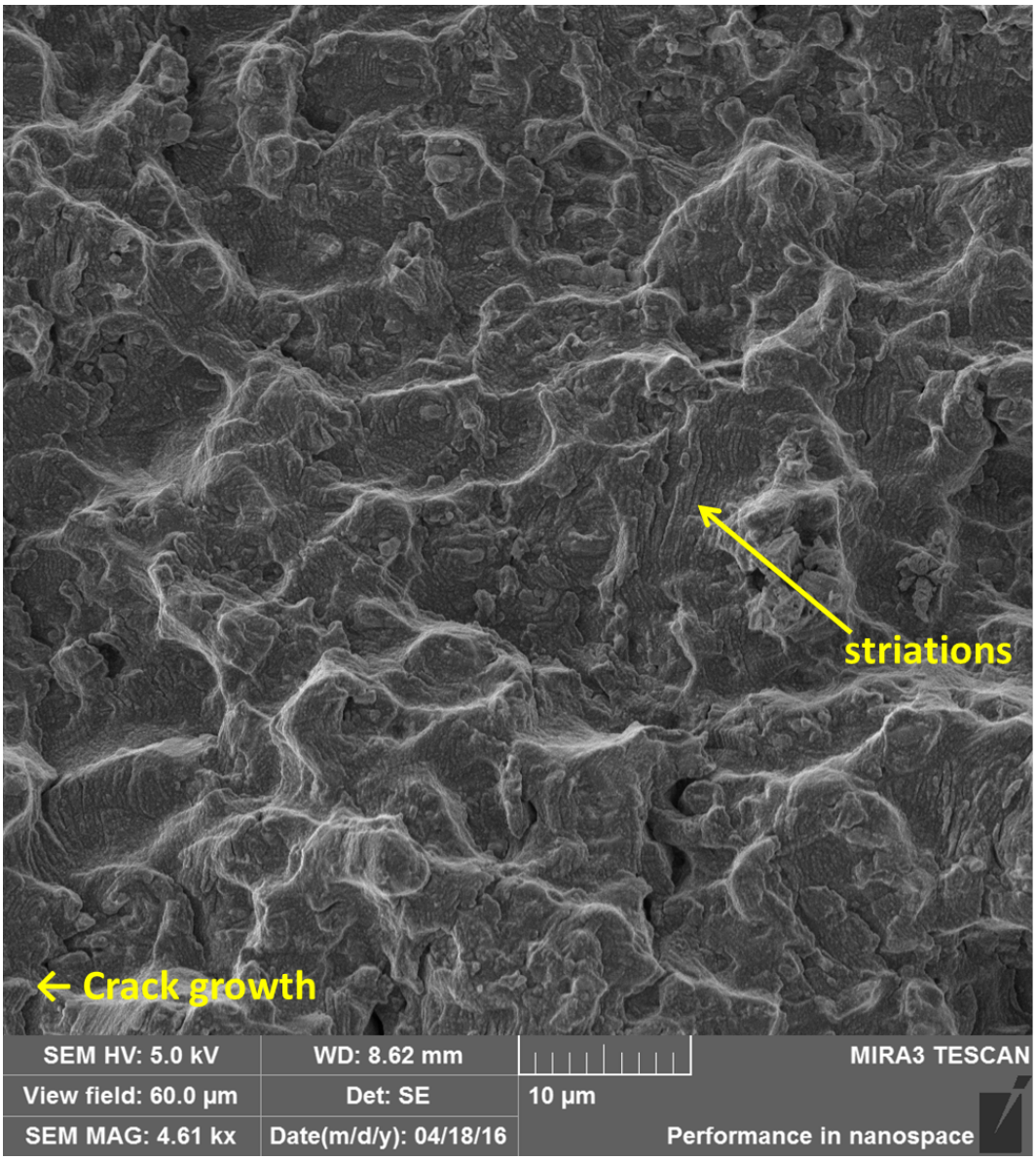

Figure 4.4: Room temperature isothermal crack growth at 8 Hz failure surface showing transgranular crack growth with striations at $\Delta K = 40$ MPa $\sqrt{m}$

The highly tortuous nature of the lower temperature test points appears to be dominated by shear failure since the dominant orientation of the failure surface is out

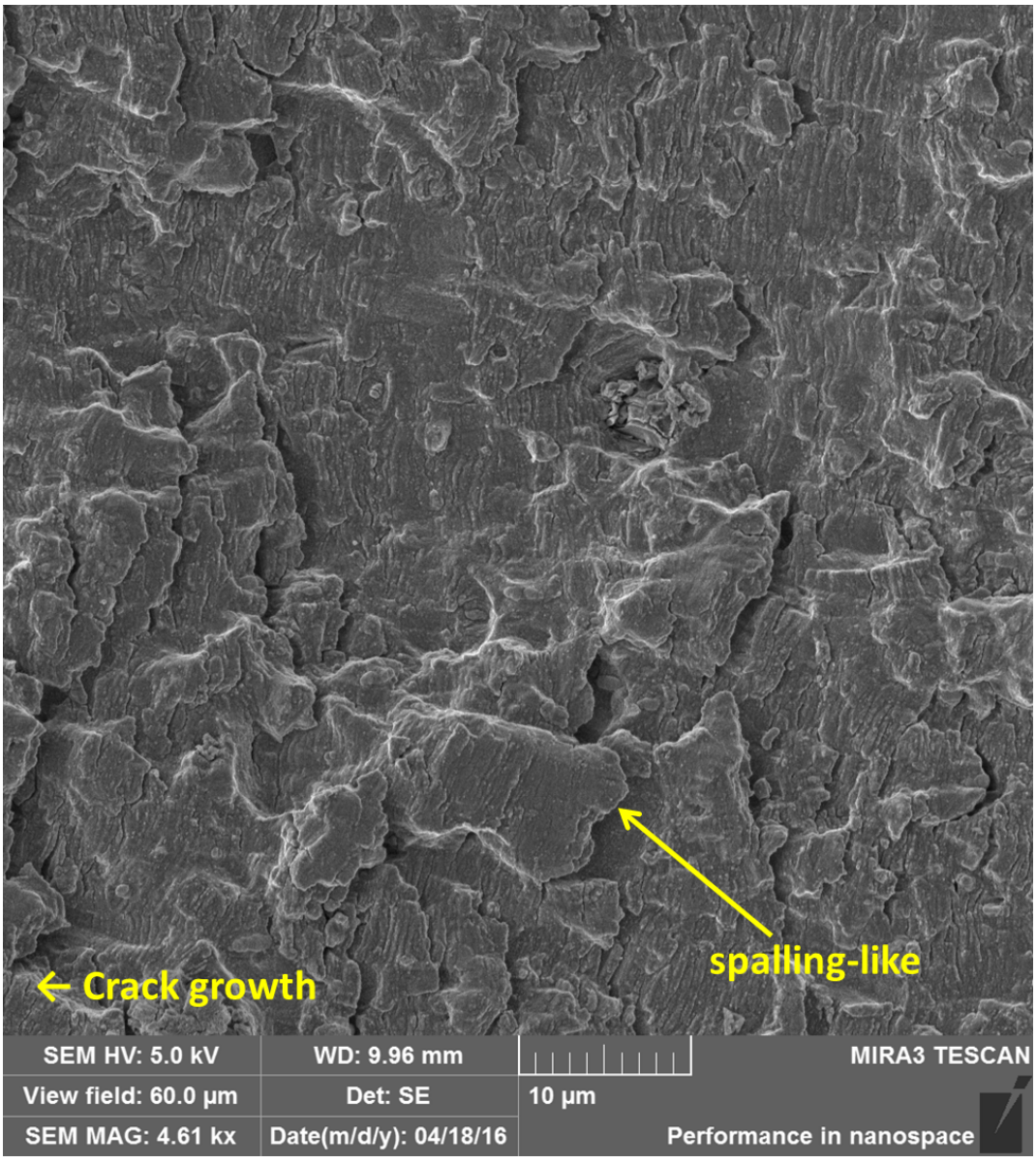

Figure 4.5: 650°C isothermal crack growth at 10 Hz failure surface showing transgranular crack growth with striations and a spalling-like appearance at $\Delta K = 40$ MPa $\sqrt{m}$

of plane and near 45°. This is thought to be a function of the dynamic strain aging performance of IN 718. Fournier et al. showed IN 718 is subject to the Portevin - Le Chatelier effect up to 470°C where serrated flow of dislocations dominate over the continuous plastic flow observed at higher temperatures [75]. This causes a shear dominated failure surface at the lower temperatures.

Figures 4.6 and 4.7 show how the failure surface transitions to include a larger proportion of intergranular crack growth as the frequency slows down to 0.5 Hz and 0.1 Hz, respectively.

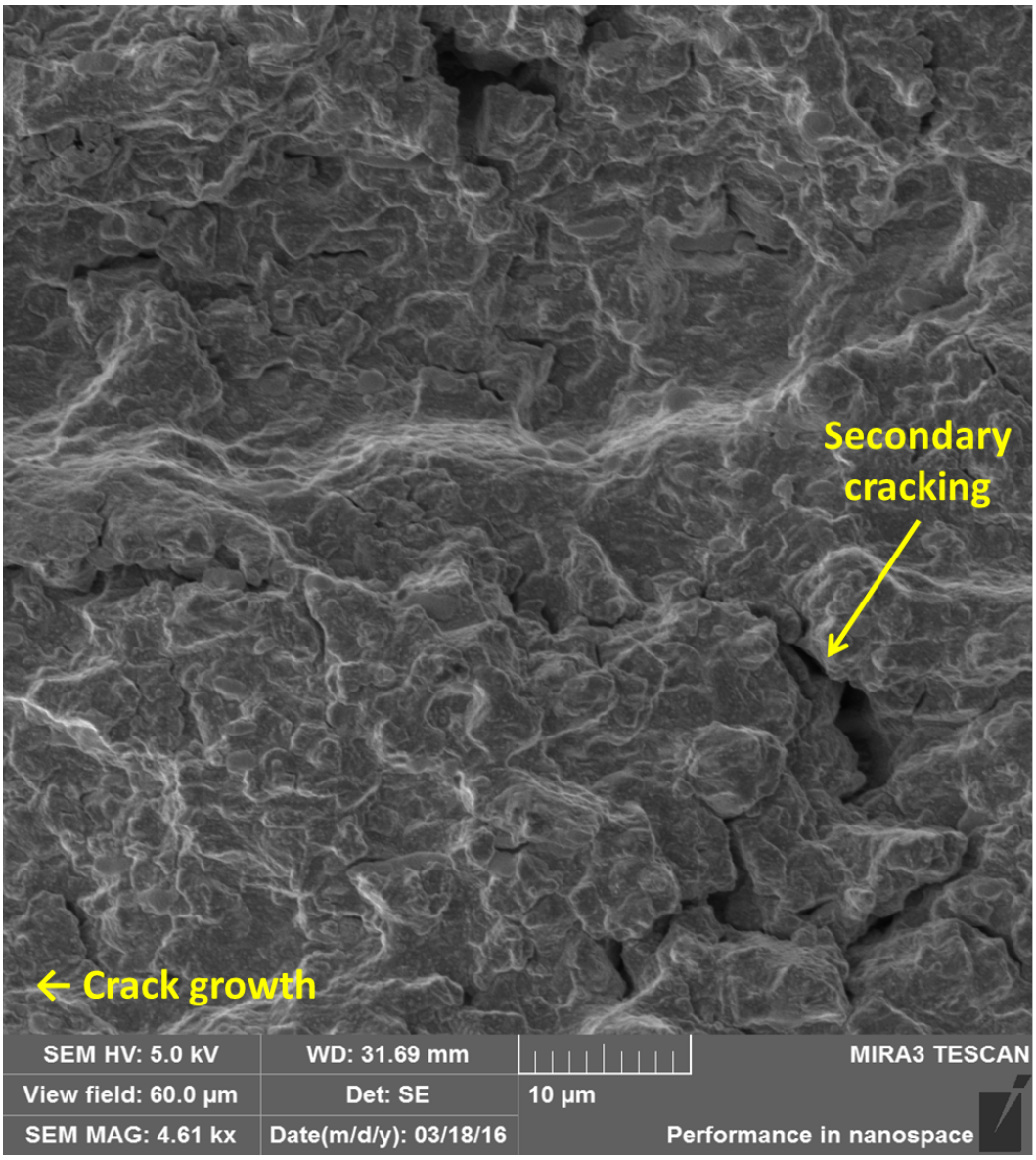

Figure 4.6: 650°C isothermal crack growth at 0.5 Hz failure surface showing transgranular crack growth with striations and some intergranular secondary cracking at $\Delta K = 40$ MPa $\sqrt{m}$

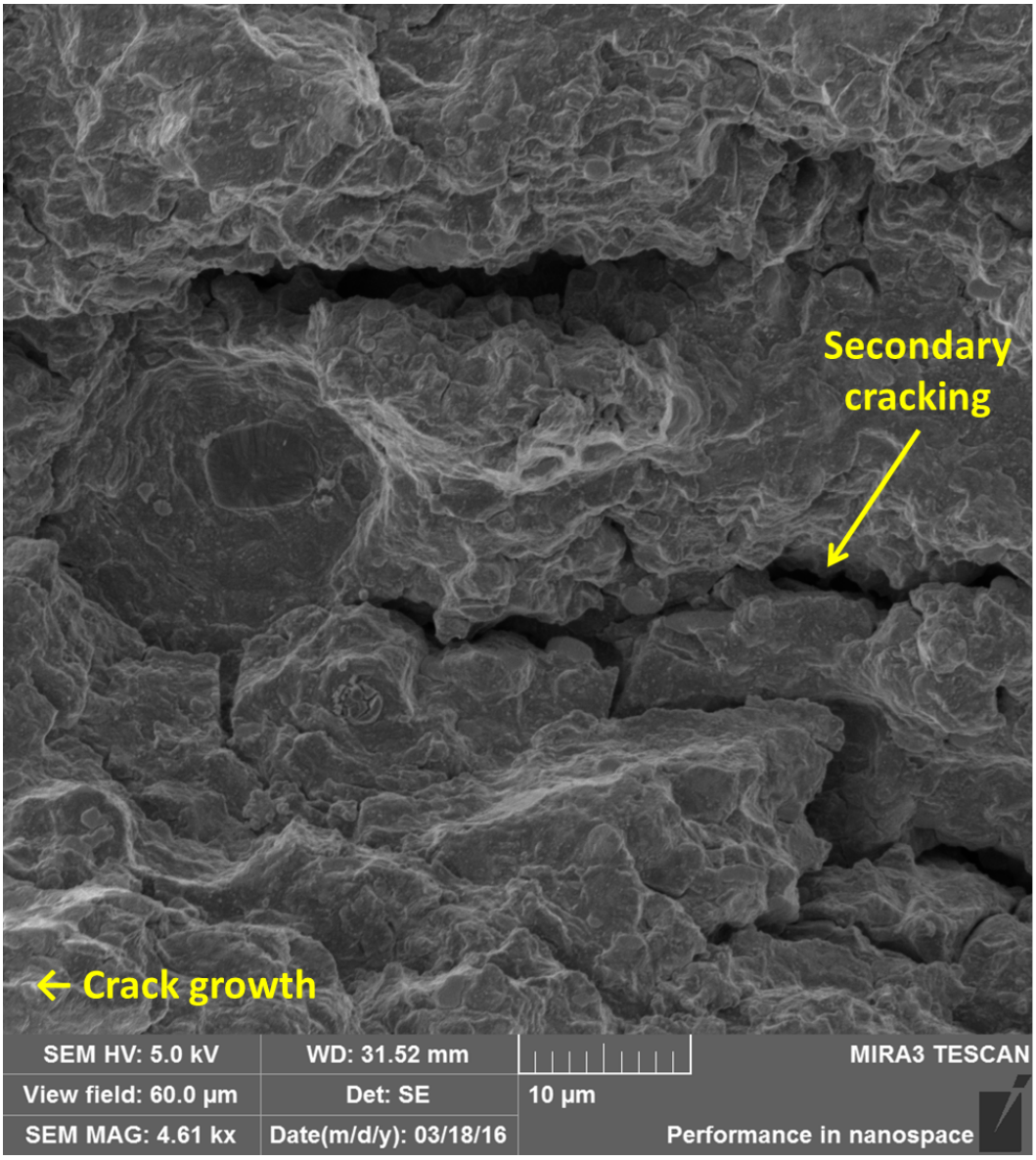

Figure 4.7: 650°C isothermal crack growth at 0.1 Hz failure surface showing transgranular crack growth increased intergranular secondary cracking at $\Delta K = 74$ MPa $\sqrt{m}$

4.1.3 Significant Findings

The isothermal FCG tests conducted in this project was similar to published data. The fast frequency (10 Hz) tests executed at elevated temperature (650°C) reduced but did not completely eliminate the weakening of the material ahead of the crack tip due to time at temperature.

4.2 Effect of Tensile Hold at High Temperature: Hold Load Relation to Cyclic Loading

To best simulate realistic applications where there are complex sequences of cycles and holds, high temperature tensile holds were imposed at various load levels in relation to the cyclic maximum load to evaluate the impact of the tensile hold on subsequent crack growth.

4.2.1 Crack Growth Rate

Crack length measurements for these test points were taken optically. Figure 4.8 shows the crack growth response of these test points. As is evident, no clear impact on FCGR can be discerned from this data.

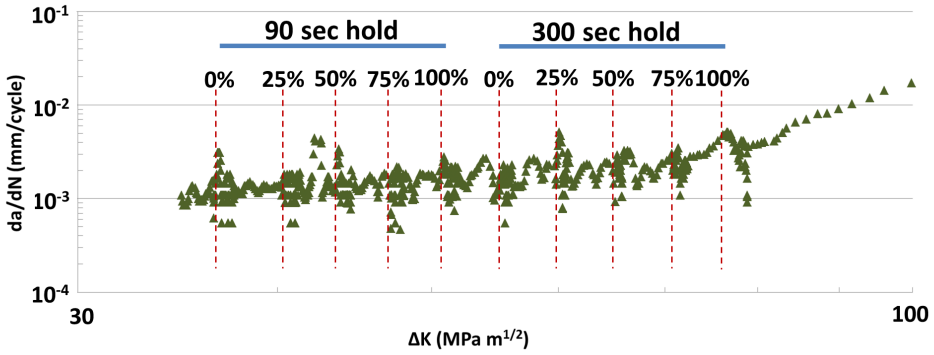

(a) 90 and 300 second tensile hold

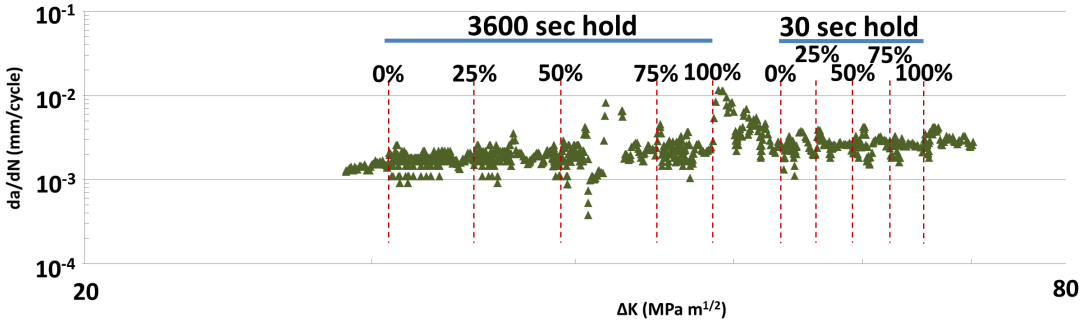

(b) 3600 and 30 sec tensile hold

Figure 4.8: Fatigue crack growth rate results of 650°C isothermal tests with tensile holds of various relation to the cyclic maximum load and where the holds occurred measured using crack length on the surface

There is secondary evidence of the potential acceleration of FCGR due to the holds since the FCG data does appear to show a slightly wavy appearance. This would be indicative of a situation where the crack is allowed to propagate faster in the center of the specimen (as is possibly the case with the TAZ and the failure surfaces discussed later indicates it may be doing), and the outside surface continues at the FCGR had no TAZ been created. As the disparity between the crack length in the center of the specimen and the edge of the specimen gets larger, the FCGR on the outside surface must increase to return to the crack front to a more balanced semi-circular shape as was observed before the tensile hold was executed.

4.2.2 Fractography

During constant amplitude high temperature FCG, imposing a single tensile hold at various percentages of the cyclic maximum load left a change in the failure surface visible to the naked eye as Figure 4.9 shows. These temperature affected zones (TAZ) only occurred when the tensile hold was conducted at 100% of the cyclic maximum load. This was verified by SEM investigation of the failure surface. The beginnings of a TAZ area is visible just prior to the 3600 sec hold test point in Figure 4.9. This TAZ area occurred during a hold at 75% of the cyclic maximum load. This could be an artifact of the testing procedure as when the cycling was stopped to conduct the hold the test machine stopped the load at the mean load (50%) of the cycle and the load was manually ramped to the hold load. Since the hold load was an increase from where the cycling stopped, the effect of loading to the test point may have allowed for some more significant tensile strains to develop at the crack tip for the 75% hold test point for 3600 seconds which would better allow for oxygen penetration to weaken the grain boundaries. This effect was not observed for the shorter duration tests and as such, it is reasoned that in general, a tensile hold would have to exceed 75% of the cyclic maximum load to induce a TAZ.

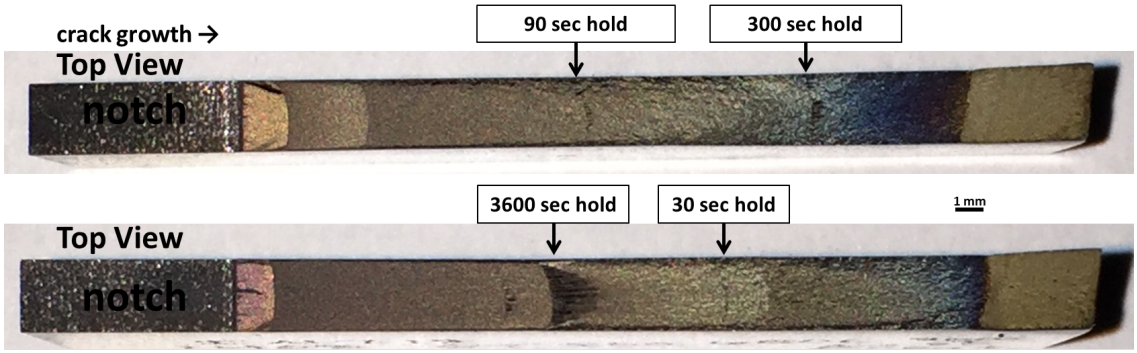

Figure 4.9: Visible TAZ on the failure surface for holds at 100% of the cyclic maximum load for various durations

The width of the TAZ in the crack growth direction (TAZ size) and the TAZ surface morphology varied with changes in the hold duration. As the hold duration increased, the amount of secondary cracking and oxidation visible on the TAZ surface increased. Figure 4.10 shows the extent of the TAZ on the failure surface for the 30 and 3600 second hold test points. The TAZ created during the 30 second hold is not as significant as that created during the 3600 second hold. An additional contributing factor to the TAZ width is the increasing stress intensity of the hold as the crack length increases and its effect will be addressed later.

Also evident in Figure 4.10 is how the TAZ size is largest in the center of the specimen where plane strain effects and tensile dilatational forces are greatest and how the TAZ size reduces as it approaches the surface of the specimen where plane stress effects are greatest and stress redistribution can reduce tensile dilatational forces.

Additionally, Figure 4.11 shows how the 30 second hold resulted in a primarily transgranular crack propagation with some obvious areas of secondary cracking occurring parallel to the crack growth direction.

Figure 4.12 shows how when the hold duration is increased to 3600 seconds, the amount of secondary intergranular cracking occurring parallel to the crack growth direction dominates over the now limited amount of transgranular crack propagation.

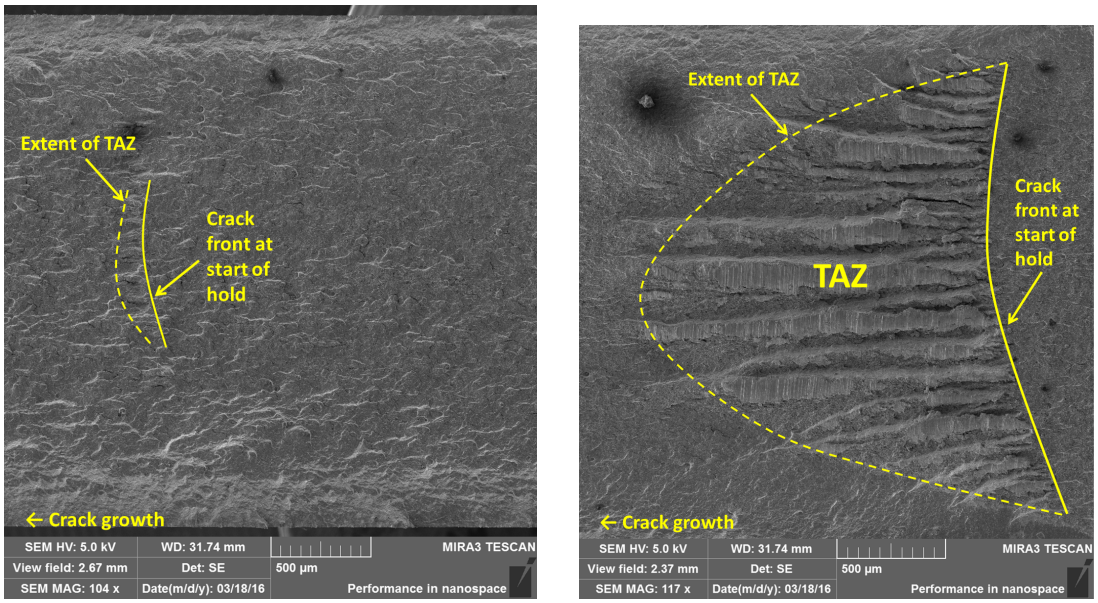

(a) 30 second hold, $K_{hold} = 69$ MPa $\sqrt{m}$ **(b)** 3600 sec hold, $K_{hold} = 51$ MPa $\sqrt{m}$

Figure 4.10: Temperature affected zone on the failure surface for tensile holds of various duration at the cyclic maximum load for 650°C isothermal loading

As the TAZ resulted in an increase in intergranular cracking, one would expect a faster crack growth rate than purely transgranular crack growth. However, utilizing the optical method of crack length measurement did not show any clear FCGR acceleration. It is important to note that all TAZ observed in this project, even the highest temperature and longest hold test points, showed areas of transgranular crack propagation with striations within the TAZ. Figure 4.13 shows an example of this. These striations are relatively disoriented to the crack growth direction which is probably due to the complex state of the material within the TAZ. The spacing of striations in the TAZ were measured to try and capture the FCGR to compare to the optical crack length measurements, but the results were inconclusive, probably due to the relatively disoriented nature of striations within the TAZ. The presence of striations indicates that the TAZ is not traditional time-dependent crack growth, but more likely a weakening of some areas ahead of the crack tip. The remaining areas that are not weakened in the TAZ are left to hold back the crack front when cycling

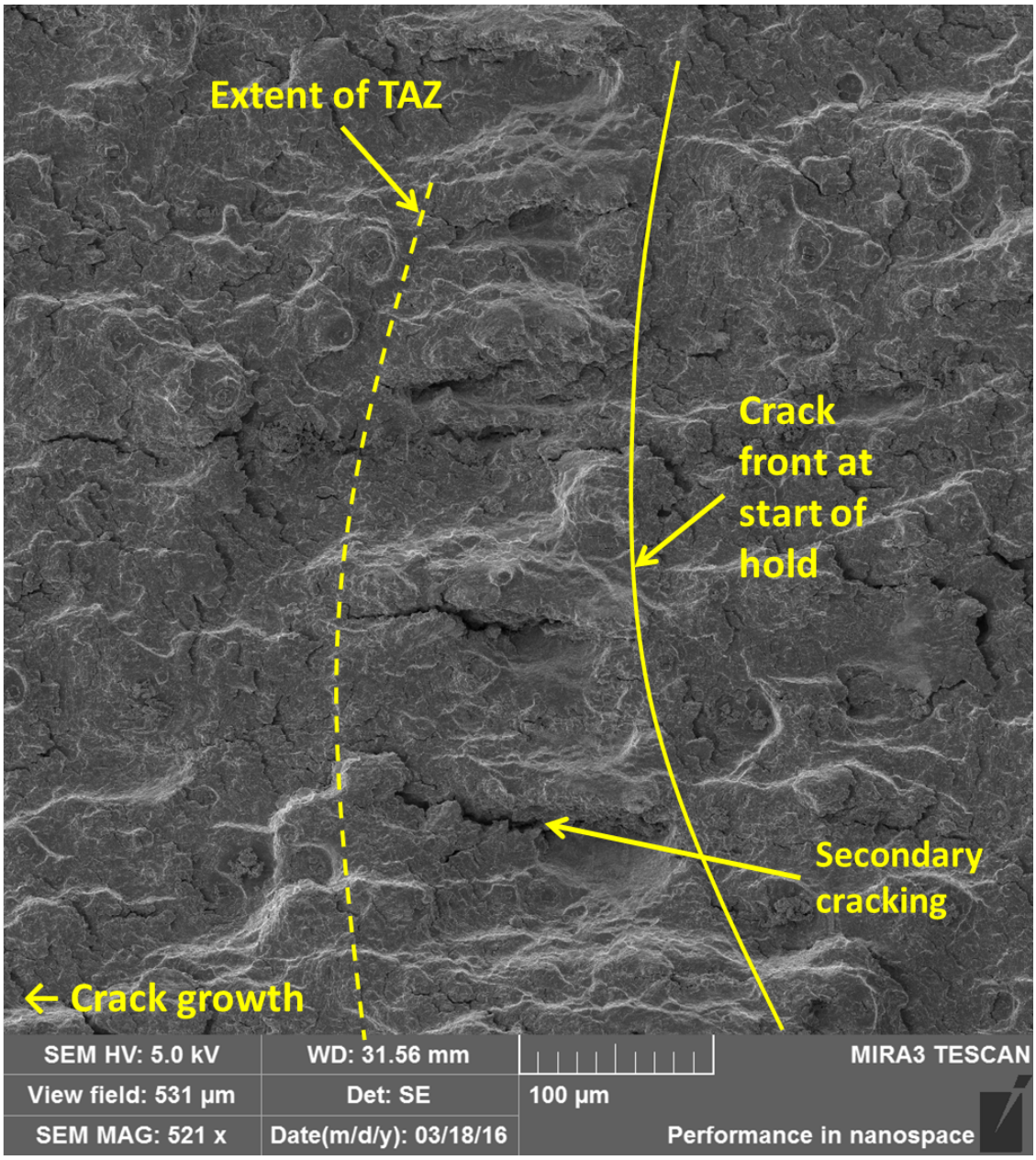

Figure 4.11: Temperature affected zone created by 30 second hold at 650°C at the maximum cyclic load showing a primarily transgranular failure surface with some secondary cracking

is resumed. These "fingers" of weakened material extending ahead of the crack tip coincide with the work of Viskari et al. [48].

The failure surface in Figure 4.12 shows these "fingers" as a repeated pattern of ridges with no secondary cracking and depressions with secondary cracking running

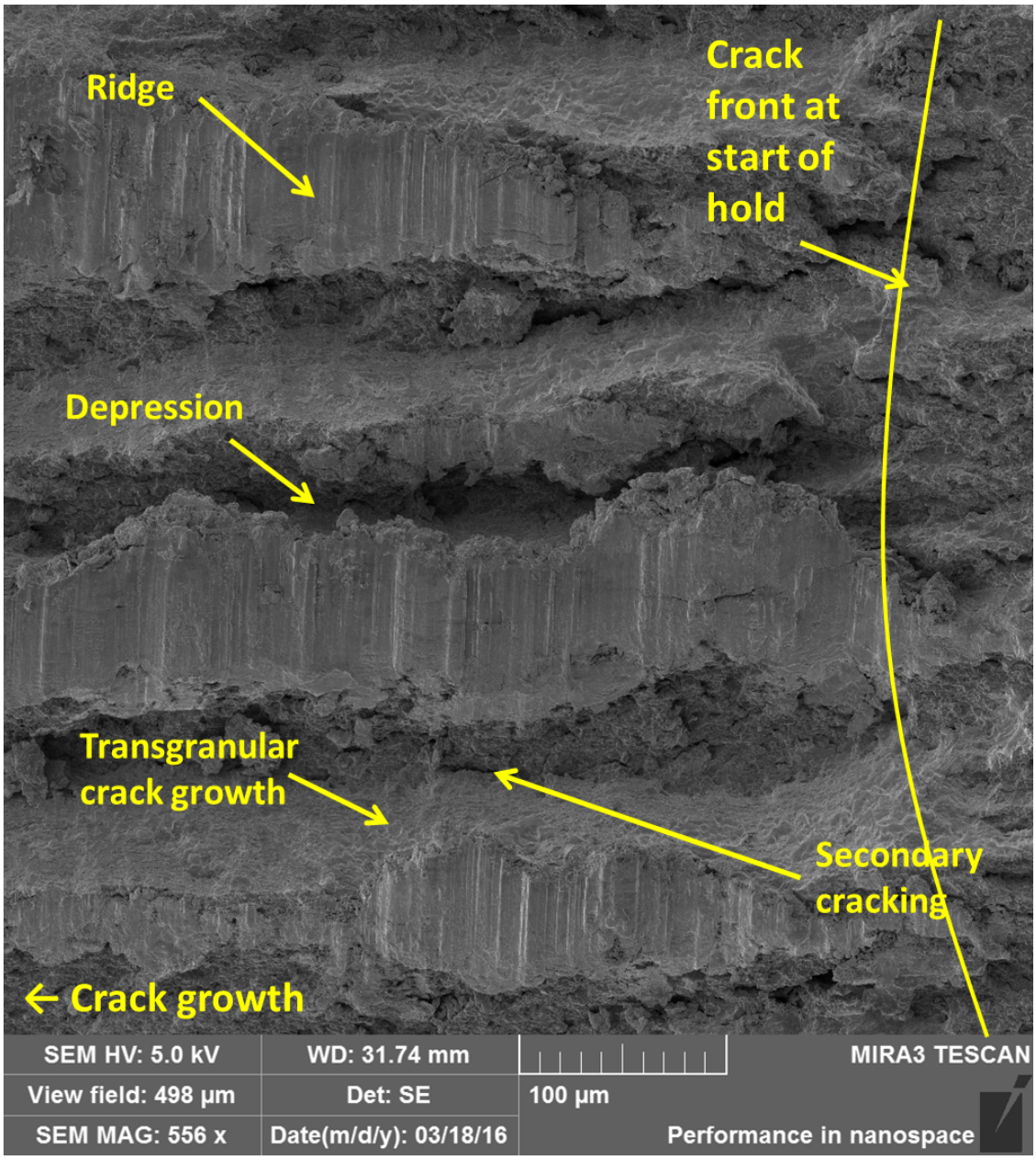

Figure 4.12: Temperature affected zone created by a 3600 second hold at 650°C showing a mix of transgranular and secondary intergranular cracking

parallel to the crack growth. This pattern was seen for all TAZ observed.

Additionally, the ridges observed in Figure 4.12 appear to have markings indicative of the opposite surfaces rubbing against each other as the crack propagates forward. Further investigation of these features was undertaken with a Keyence-VK 3D laser scanning confocal microscope. Figure 4.14 shows how the ridges are not flat but

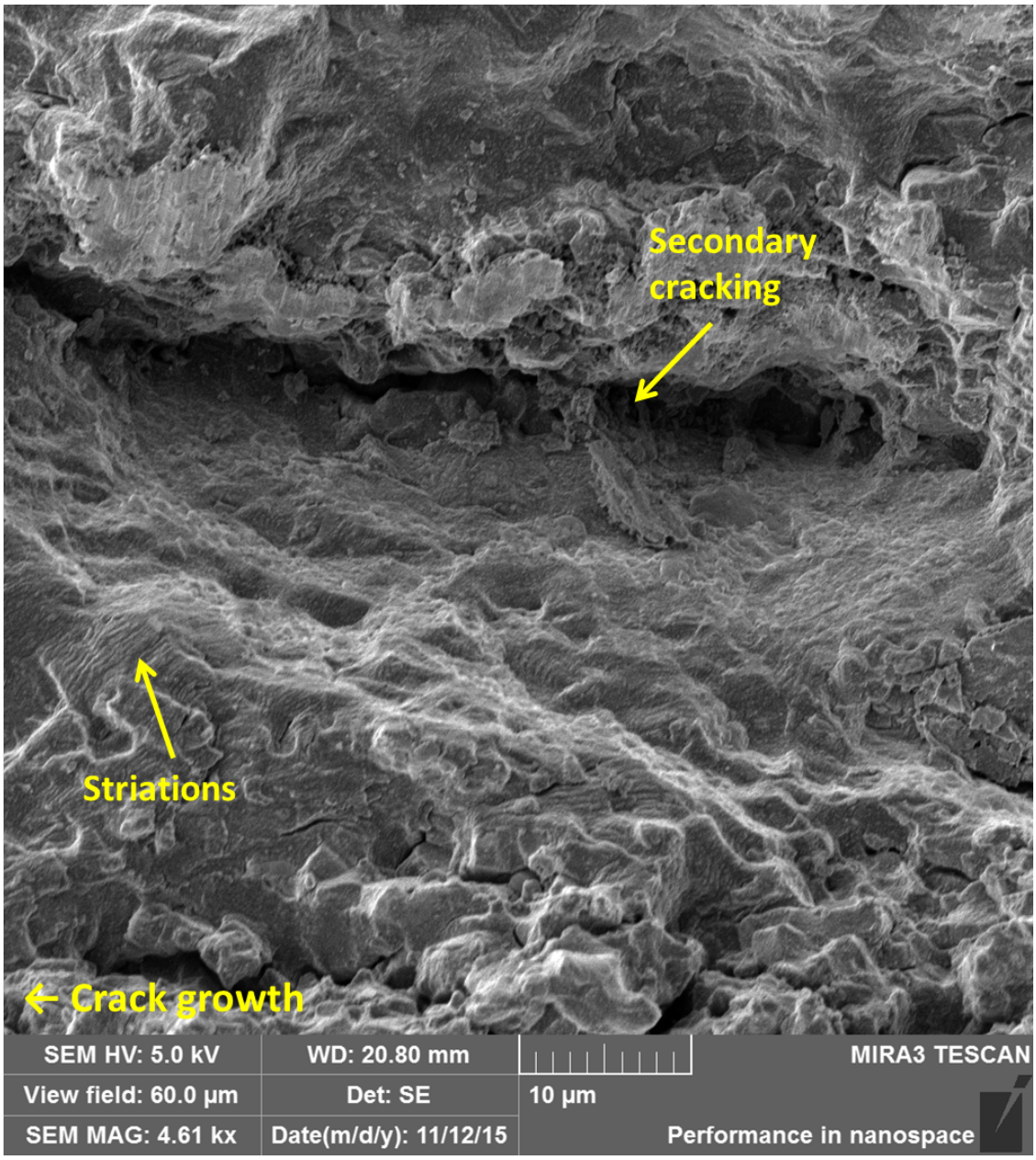

Figure 4.13: Transgranular crack propagation with striations occurring within a TAZ created by a tensile hold with a stress intensity of K_{hold} of 45 MPa $\sqrt{m}$ for 30 seconds at 650°C. Cycling $\Delta K = 43$ MPa $\sqrt{m}$

relatively pointed and probably coincide with a complementary depression on the opposite failure surface.

As the specimens for this project were machined with the longest dimension in the radial direction and the width of the specimens in the same plane as the disk these

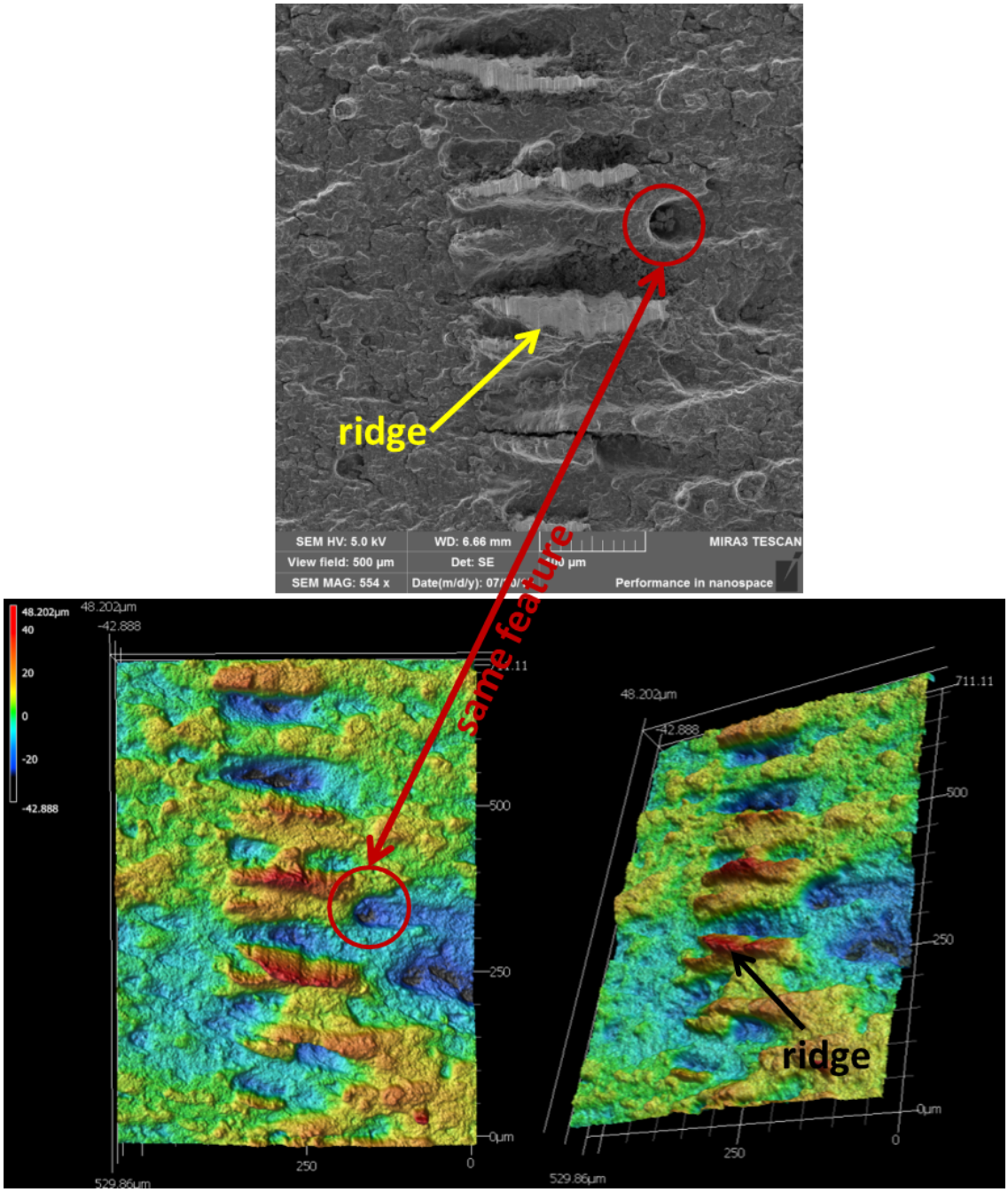

Figure 4.14: Temperature affected zone created by a 90 second hold at 650°C highlighting the 3D surface morphology

ridges and depressions run coplanar to the plane of the disk. The orientation of these features with regard to the forging direction of the disk indicate that preferential channels for the weakening of the grain boundaries ahead of the crack tip may be driven by the residual stresses and strains and changes in the microstructure created

by the forging process though further work is required to confirm this.

4.2.3 Finite Element Analysis

A two-dimensional finite element analysis (FEA) model of the SENT specimen was developed to aid in understanding the response of the material at the crack tip, specifically, why no TAZ developed during holds at 75% of the cyclic maximum load and lower. Care was taken to ensure the uniform displacement boundary conditions of the experiment set-up were modeled correctly. To keep things simple, material models inherently available in ANSYS were utilized. A three term non-linear Chaboche kinematic hardening model was selected because of its good fit to the data and its ability to account for cyclic softening (as IN 718 has been observed to do). Also, to best capture the primary and secondary creep expected at the low homologous temperatures (at or below 0.5) evaluated with this project and based on the form of creep data available, a modified time-hardening model was utilized. The time-dependent model also had a good fit to the data. Additionally, the temperature dependent material properties of elastic modulus, Poisson's ratio, and coefficient of thermal expansion were input. All material data were found in Metallic Materials Properties Development and Standardization (MMPDS-08) [15]. ANSYS's ability to fit material models to data was utilized to determine the fitting coefficients for the three term non-linear Chaboche kinematic hardening model and the modified time-hardening model. A more thorough description of the material models used can be found in Appendix A. Additionally, because of how thin the SENT specimen is, the simulations were executed in plane stress.

The FEA simulation consisted of two loading cycles followed by tensile holds of varying magnitude and the corresponding normal stresses at the beginning of the tensile hold immediately ahead of the crack tip were plotted as shown in Figure 4.15. The stresses immediately ahead of the crack tip do not reach yield stress ($\sigma_y = 836$

MPa [15]) when a tensile hold less than the cyclic maximum load was executed. This indicates that tensile stresses at or exceeding yield strength must be present to allow for the development of a TAZ.

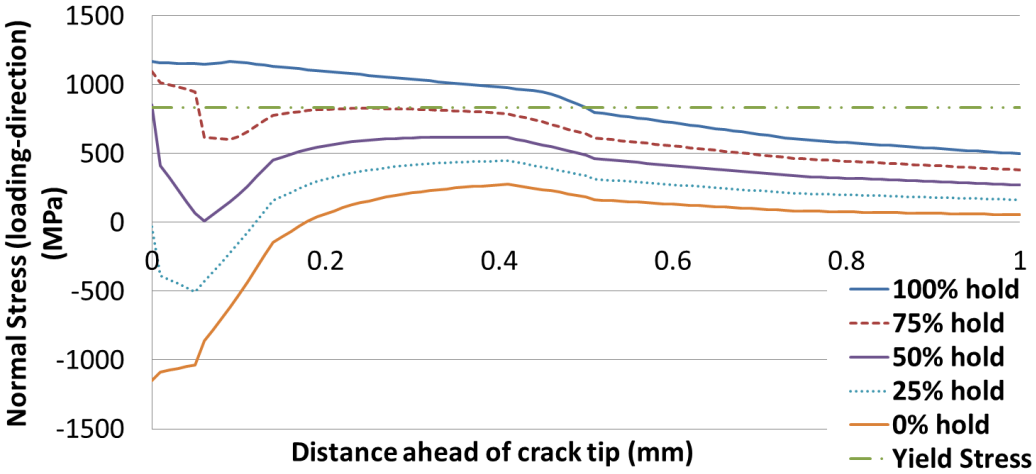

(a) FEA prediction

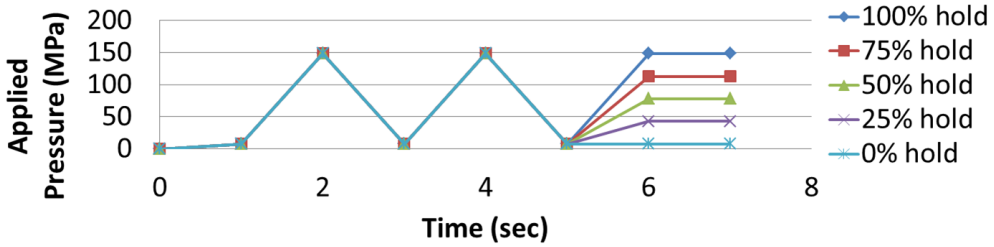

(b) FEA spectra

Figure 4.15: Finite element analysis prediction of the normal stresses in the loading direction ahead of the crack tip for holds of various loads compared to the cyclic maximum load and the 650°C isothermal spectra utilized for the analysis

4.2.4 Significant Findings

Subjecting a specimen to a tensile hold at a load of 75% or less than the cyclic maximum load, no TAZ was observed. For holds at the cyclic maximum load, a TAZ was visible on the failure surface. The failure surface characteristics of a TAZ included increased secondary cracking and oxidation, though regions of transgranular crack propagation with striations were present for all holds. No impact on FCGR was

observed with optical crack length measurement. This corresponds to failure surface observations where the TAZ did not extend to the free surface where crack length measurements were made.

4.3 Effect of Tensile Hold at High Temperature: Constant Stress Intensity Factor

Tensile holds at constant stress intensities for various durations at several temperatures resulted in the creation of TAZs of various sizes. As mentioned in Section 4.2.1, the optical method of crack length measurement was unable to definitively show the extents of a TAZ and its impact on FCGR and therefore the TAZ size was measured on the failure surface at their widest point visible in the direction of crack growth post test as Figure 4.16 shows. Several measurements were taken at the widest point in the TAZ and averaged to come to the values reported in Table 4.3.

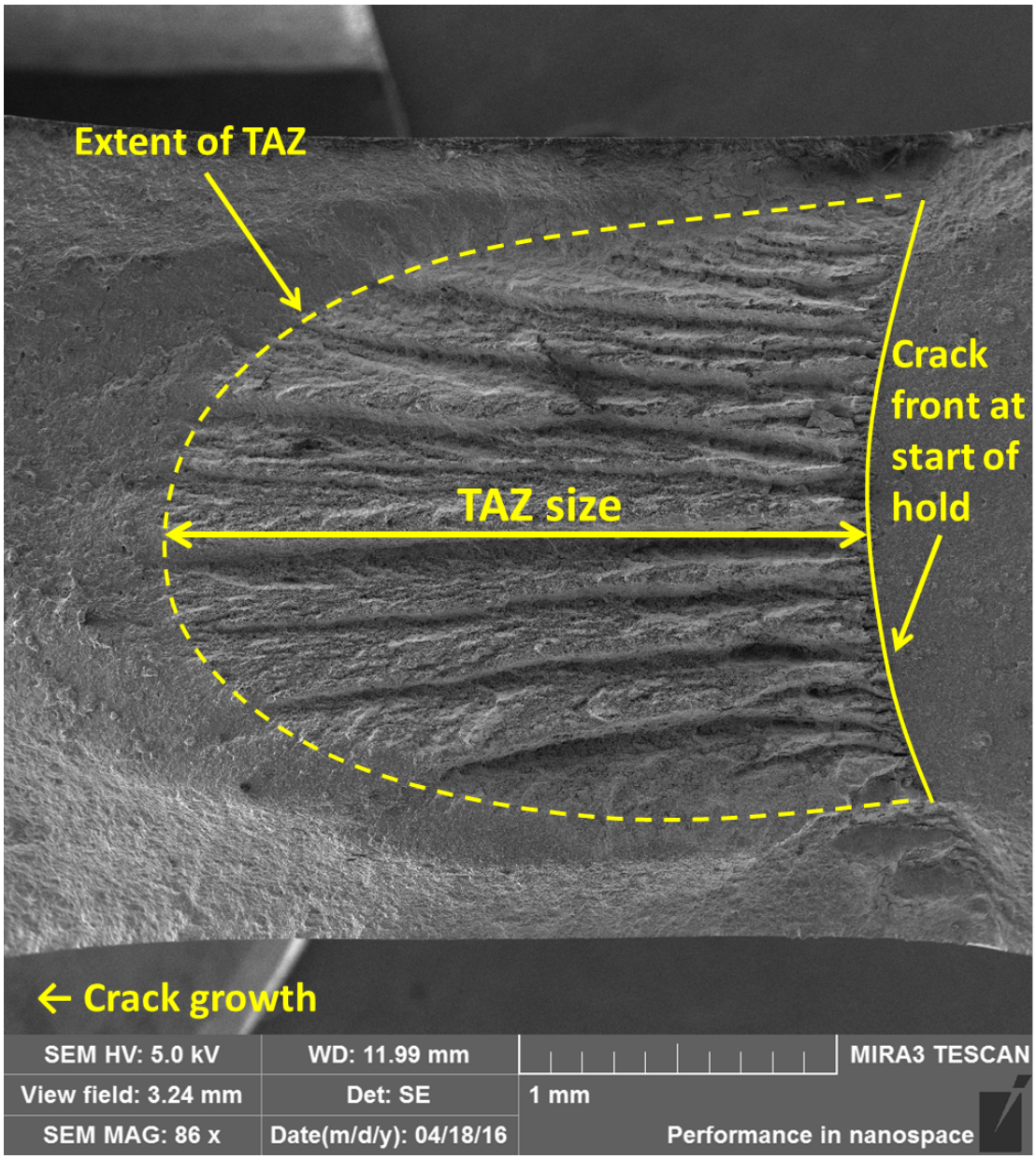

Figure 4.16: Temperature affected zone created by a K_{hold} of 45 MPa $\sqrt{m}$ for 3600 seconds at 650°C indicating where the TAZ size measurements were taken

Table 4.3: Temperature affected zone size created by a for various hold stress intensities, hold temperatures, and hold durations

K_{hold} (MPa $\sqrt{m}$)	Temperature (°C)	Hold Duration (sec)	TAZ size (μm)
25	550	90	26
		300	29
		3600	86
		18200	197
	600	30	40
		90	67
		300	126
		3600	336
	650	30	37
		90	53
		300	77
		3600	118
35	550	90	49
		300	67
		3600	83
		18200	298
	600	30	60
		90	81
		300	141
		3600	250
	650	30	100
		90	245
		300	378
		3600	861
45	550	3600	213
		15675	503
	600	30	133
		90	158
		300	207
		3600	827
	650	30	164
		90	148
		300	223
		3600	1985

4.3.1 Fractography

4.3.1.1 Specimen Geometry and Specimen History Driven Temperature Affected Zone Characteristics

There was an obvious difference in the size of a TAZ as one moved from the center of the specimen where plane strain dominated to the edges of the specimen where plane stress dominated as Figure 4.10 shows. This indicates that the plane strain dominated region where dilatational forces are greatest at the center of the specimen is more susceptible to the development of a TAZ.

Additionally, the crack length at which a hold was executed affected the TAZ size. Figure 4.17 shows how two test points executed at the same stress intensity, temperature, and duration of hold produced different TAZ sizes. Several factors may have contributed to this variation. First, the TAZ created at a shorter crack length resulted in a relatively constant TAZ size in the center of the specimen extending toward the free surface further than at longer crack lengths where the maximum TAZ size is only observed very near the center of the specimen. This is probably due to plane strain dominating more of the specimen width at shorter crack lengths allowing for a more consistent shape of the TAZ. Also, though care was taken to minimize the effects of previous test points executed on the same specimen, their effects (previous high temperature exposure, previous loading, etc.) may have also contributed to the difference in TAZ size as the crack length of the hold changes.

In addition to the factors mentioned above, the fact that the TAZ size varies with a constant stress intensity of hold suggests that the stress intensity factor in its current form may not be a complete characterizing parameter for TAZ size. The multiple physics occurring at the crack tip in thermomechanical loading makes identification of any characterizing parameter difficult. Even so, as will be discuss later, there were distinct trends observed with variation of the stress intensity of the hold and for lack of a better characterizing parameter, the stress intensity of the hold was used as a

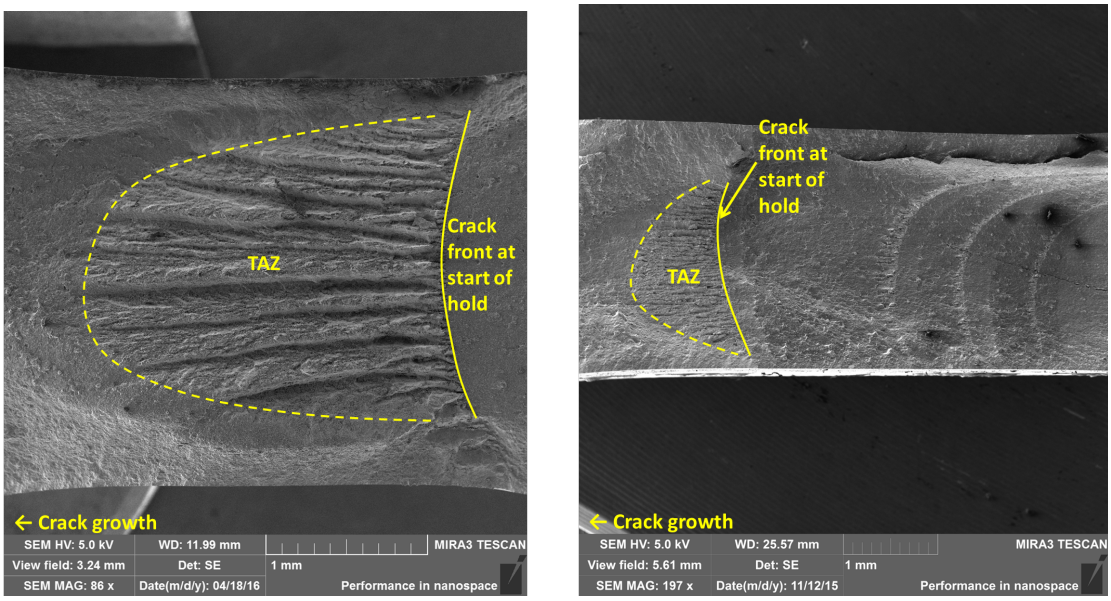

(a) TAZ at a crack length of 10.15 mm **(b)** TAZ at a crack length of 31.7 mm

Figure 4.17: Comparison of how TAZ size and shape vary early in the specimen compared to later in the specimen for a TAZ created by a K_{hold} of 45 MPa $\sqrt{m}$ for 3600 seconds at 650°C

characterizing parameter for TAZ size.

As there were not a sufficient number of test specimens to execute all test points at short crack lengths, a simple linear correction factor was applied to the measured TAZ size depending on the crack length the hold was executed at. This was done to correct the TAZ size to an equivalent size to had the hold been executed at a short crack length where plane strain would dominate and history effects would be minimized. Figure 4.18 shows the transition from plane strain dominated, to mixed plane stress and plane strain, to plane stress dominated crack growth for one of the TMF spectrum tests executed with this project and these transition points were used to correct the TAZ size measurements. A hold executed when the crack length was in the plane strain dominated area, corresponding to crack lengths less than 12 mm, was assumed worst case and was the basis for the TAZ size effect. Additionally, a hold executed when the crack length was in the plane stress dominated area, crack lengths greater than 18 mm, was multiplied by a factor of 2.0. The value of 2.0 was

chosen based on the relationship of the TAZ size for holds executed at crack lengths in the plane strain dominated area were about 2.0 times larger than holds executed in the plane stress dominated area. A linear interpolation for the correction factor was applied for TAZ measurements at crack lengths within the mixed region.

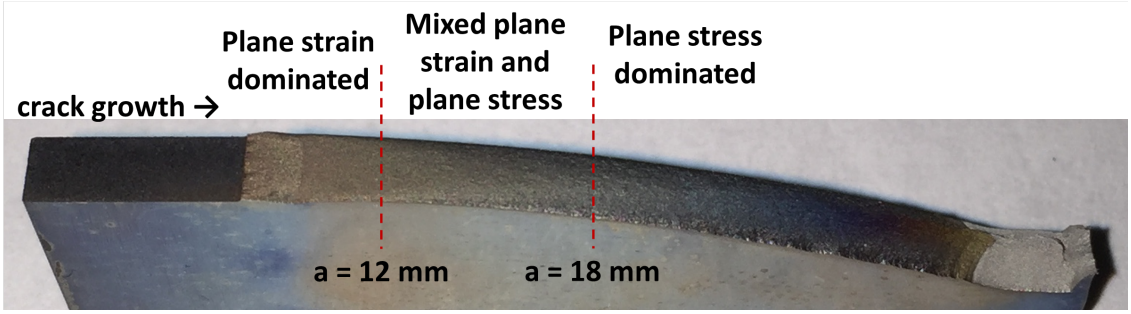

Figure 4.18: Top view of the failure surface of a TMF spectrum test with plane strain, mixed plane strain and plane stress, and plane stress regions identified

Based on these geometry driven TAZ characteristics, a different specimen geometry where there is not such a rapid transition from plane strain to plane stress as one moves from the center to the edge of the specimen would be better for single TAZ characterization.

4.3.1.2 Low Temperature Cycling Impact on Temperature Affected Zone

The TAZ for each hold left evidence on the failure surface, however, due to the torturous nature of the crack growth at lower temperatures as discussed in Section 4.1, there are inconsistencies in their overall shape. Figure 4.19 shows a segment of one specimen subjected to several constant stress intensity tensile holds. Some TAZs spanned most of the width of the specimen while others were fragmented across the width. Overall, holds executed at shorter crack lengths were less influenced by the torturous crack growth. However, due to the limited number of specimens, test points executed at longer crack lengths could not be avoided. In cases where it was felt that the specimen geometry effects had significantly impacted TAZ development,

the hold condition was repeated on another specimen. This was accomplished for about one third of the hold conditions. Additionally, as opposed to the cycling being accomplished at elevated temperature before and after holds discussed in Section 4.2, cycling after these holds were executed at low temperatures to better highlight the width of the TAZ on the fracture surface. The elevated temperature cycling utilized for the test points discussed in Section 4.2 allowed for hold conditions producing larger TAZs to be visible and prevented torturous crack growth, however the exact limits were hard to discern and hold conditions that produce smaller TAZs were very difficult to identify. For these reasons, quantitative results on the influence of the stress intensity, duration, and temperature of a hold require more data to produce conclusive results. However, qualitative results on the overall trends for the impact of these variables on TAZ size could be determined and are discussed below.

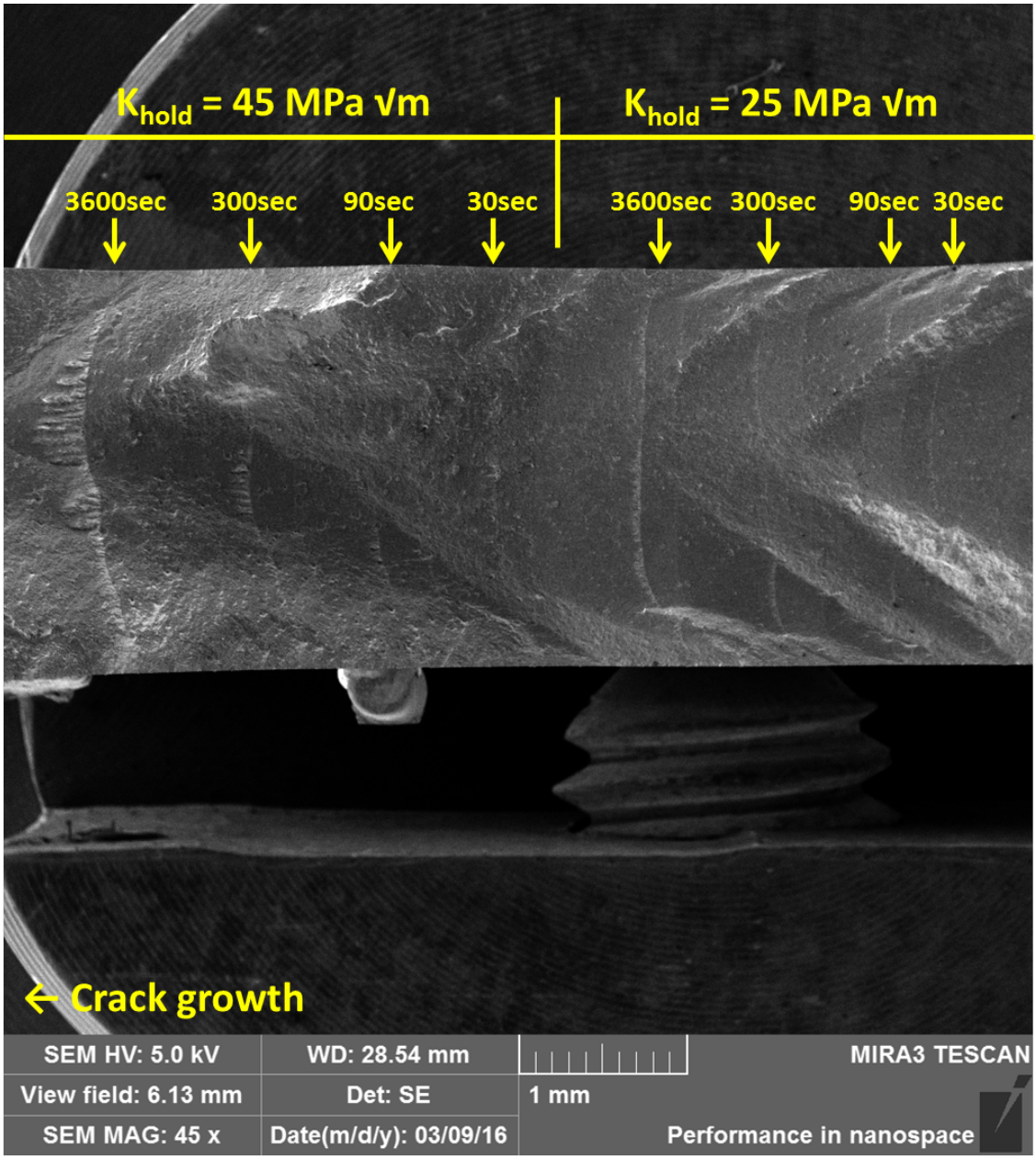

Figure 4.19: Top view of multiple TAZ hold conditions created at 650°C for various hold durations and K_{hold} levels highlighting the impact of the torturous nature of crack growth on the TAZ

4.3.1.3 Temperature Affected Zone Qualitative Characteristics

As Figure 4.10 shows, the level of damage to the failure surface varies depending on how severe the environment conditions are. In general, as the stress intensity of hold, hold duration, and/or hold temperature increased, the amount of oxidation and

secondary cracking assumed a larger proportion of the TAZ surface compared to the transgranular cyclic crack growth. Each TAZ created was qualitatively characterized based on how severe the oxidation and secondary cracking appeared. Figure 4.20 shows a representation of how the TAZ appearance changed with changing stress intensity, hold duration, and hold temperature. Figure 4.21 shows samples of each of the categories described in Figure 4.20.

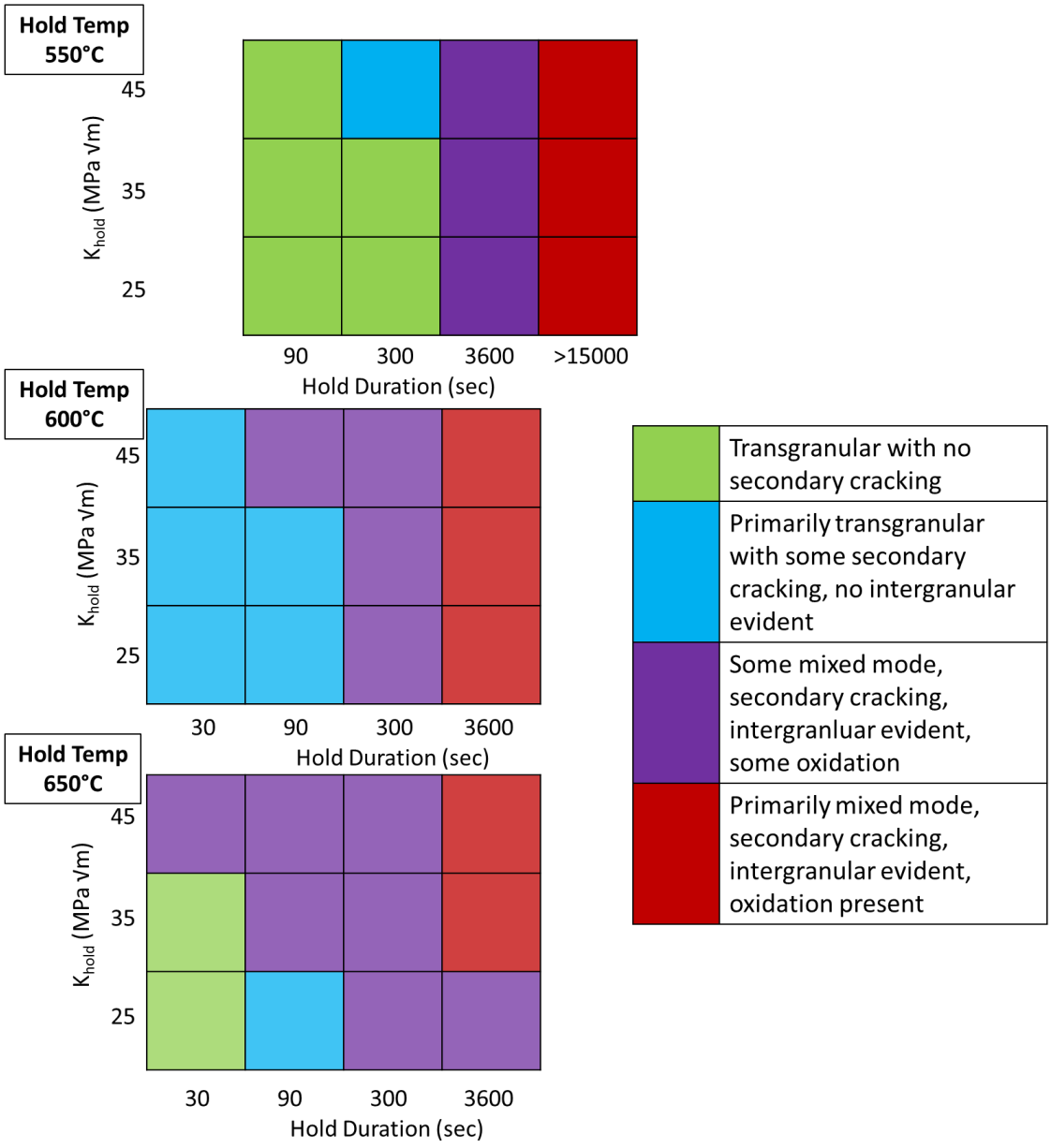

Figure 4.20: Qualitative characterization of the TAZ surface appearance for various hold stress intensities, hold durations, and hold temperatures

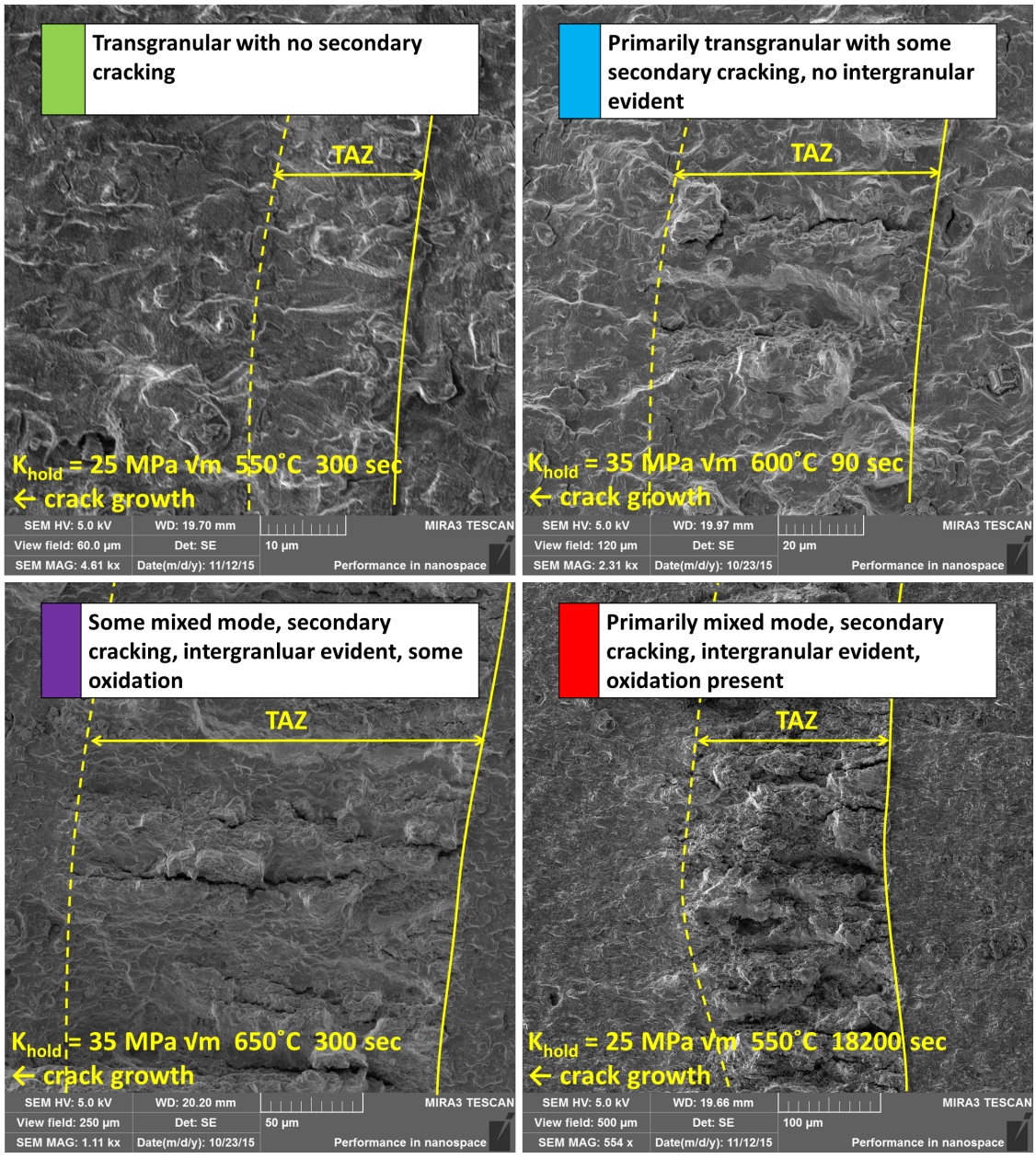

Figure 4.21: Sample images of the qualitative characterization categories of the TAZ surface appearance described in Figure 4.20

4.3.1.4 Temperature Affected Zone and Time-dependent Crack Growth

For all TAZ holds executed during this project, no time-dependent crack growth was observed with the optical method of crack length measurement. Additionally, due to the noise induced by the induction heater, the EPD system did not record any time-dependent crack growth as well. To confirm that the creation of a TAZ is not traditional time-dependent crack growth, a test point was executed where a TAZ was created and instead of cyclically loading the specimen after the tensile hold, it was pulled apart similar to a fracture toughness test. The failure surface is shown in Figure 4.22. It shows how the TAZ is clearly visible, but instead of striations in the sections of TAZ not weakened, as Figure 4.13 shows, dimples similar to ductile rupture are visible. This indicates that though the weakened areas of the TAZ may appear similar to time-dependent crack growth, the non-weakened areas of the TAZ do not and there is a complex interaction between the two that influences crack growth through that region.

Additionally, the TAZ sizes measured in this project, specifically for the longer duration holds, exceeded the depth of oxidation penetration of 150 μm reported by Miller et al. for time-dependent crack growth in IN 718 [47]. This indicated that though oxidation is an important factor for a TAZ, it is not the only mechanism.

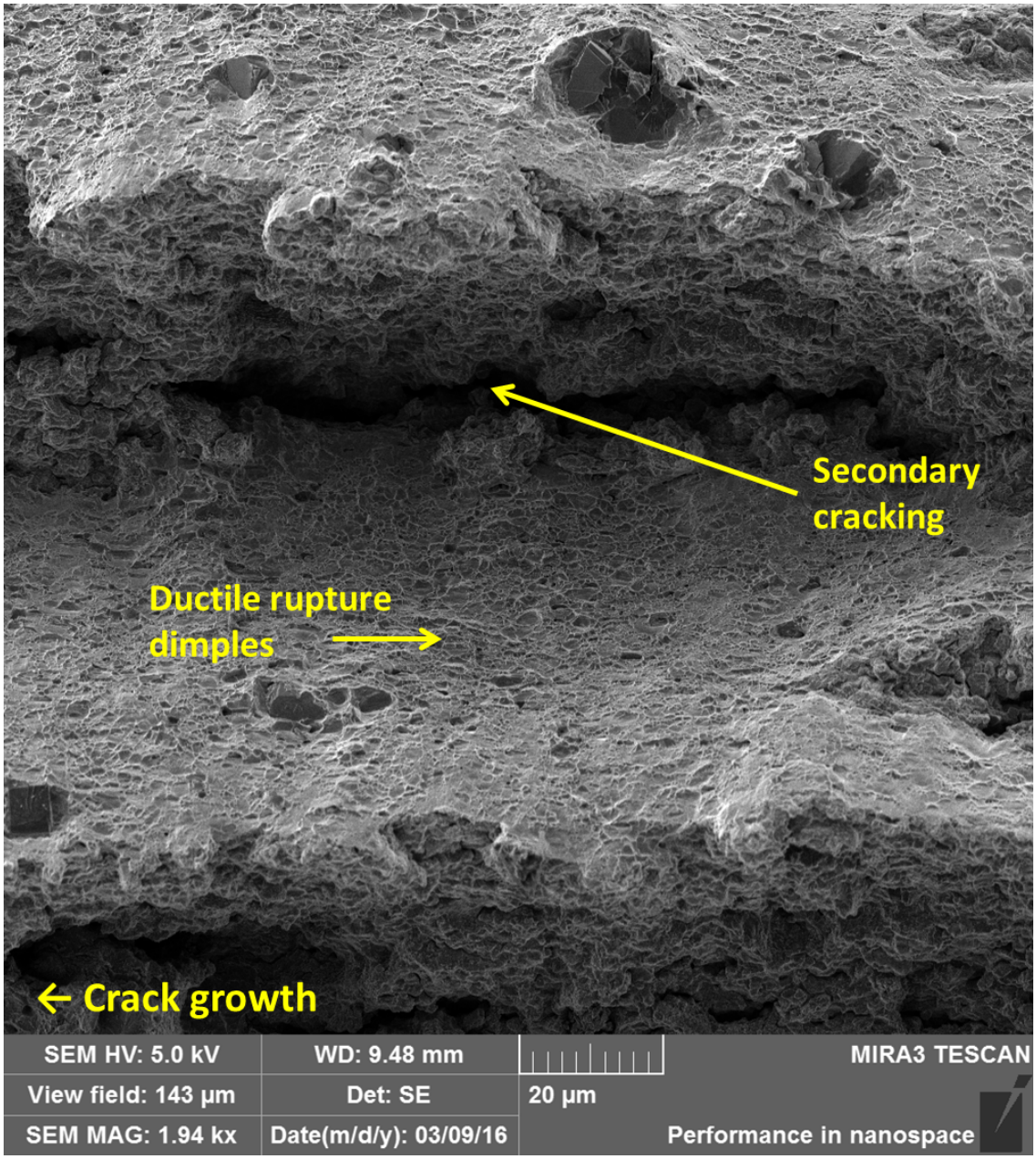

Figure 4.22: Dimples in non-weakened area of TAZ created by a tensile hold of K_{hold} of 45 MPa $\sqrt{m}$ for 3600 seconds at 650°C and subsequently pulled apart instead of cycled

4.3.1.5 Oxidation Penetration at the Crack Tip within a Temperature Affected Zone

As discussed in Section 2.6, oxidation is thought to be a significant contributer to the development of a TAZ. Figure 4.23 shows a view of the TAZ shown in Figure 4.16

zoomed in on the portion in the center of the specimen and showing the point at which the high temperature tensile hold was conducted. An area of predominately intergranular crack growth is evident immediately after the point at which the tensile hold was conducted. This intergranular crack propagation is indicative of oxidation weakening of the grain boundaries. Additionally, since no time-dependent crack growth was observed during any of the tensile holds conducted in this research, this intergranular crack growth was assumed to have occurred once the hold was completed and the cycling was resumed. Additionally, the test parameters used to create this TAZ were the worst case parameters used in this research at a $K_{hold} = 45$ MPa $\sqrt{m}$ at 650°C for 3600 seconds. The width of the intergranular region was approximately 55 μm. The work done by Miller et al. indicated that for time dependent crack growth at 700°C halted at a stress intensity of 60 MPa $\sqrt{m}$, a more worst case situation in terms of temperature and stress intensity than the current example, an oxidation affected region extended 150μm ahead of the crack tip into unbroken material [47]. On the failure surface they observed a transition from intergranular crack growth to transgranular crack growth within this region. The width of their measured oxidation affected region and the fractographic appearance shows good correlation to the experimental data shown here.

Once the crack propagates through the region of primarily intergranular crack growth, the secondary cracking extending perpendicular to the crack front in preferential channels show a similar intergranular appearance. These channels are evidence that the weakening nature of the oxidation was able to penetrate in channels ahead of the crack tip similar to what Viskari et al. reported [48]. This secondary cracking extends well beyond the 150 μm oxidation affected region described by Miller et al. The visible evidence of oxidation on the surface in the form of the grainy appearance shown in Figure 4.23 follows and remains close to these channels.

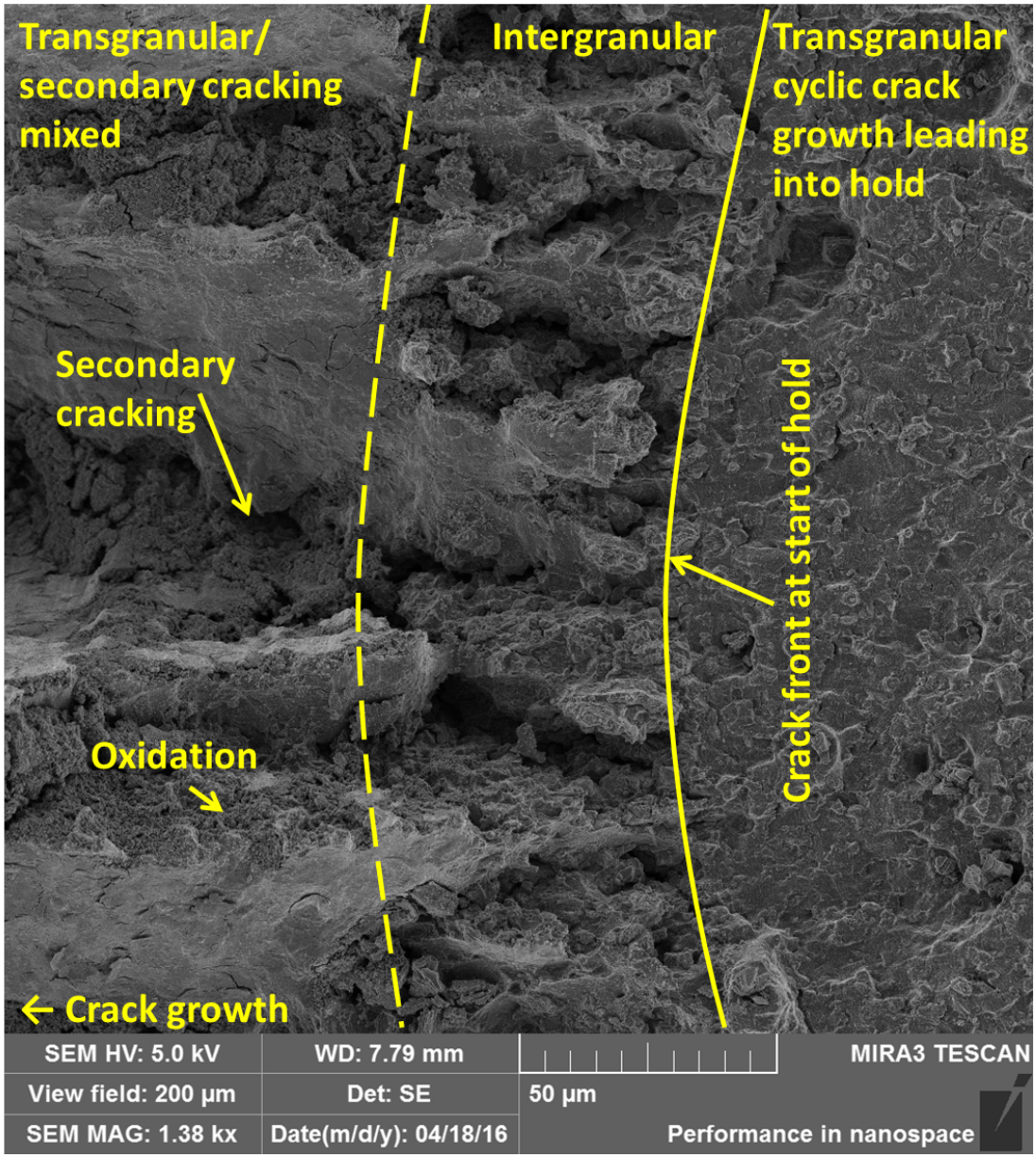

Figure 4.23: Failure surface of a TAZ created by a tensile hold of K_{hold} of 45 MPa $\sqrt{m}$ for 3600 seconds at 650°C highlighting the transition from cycling prior to the hold to the beginning of the TAZ

4.3.1.6 Sectioning of the Temperature Affected Zone

To further investigate the characteristics of the TAZ created by a high temperature tensile hold, a specimen was sectioned through the TAZ perpendicular to the crack growth direction as Figure 4.24 shows. It was subsequently hot mounted and polished with a 0.5μm diamond slurry.

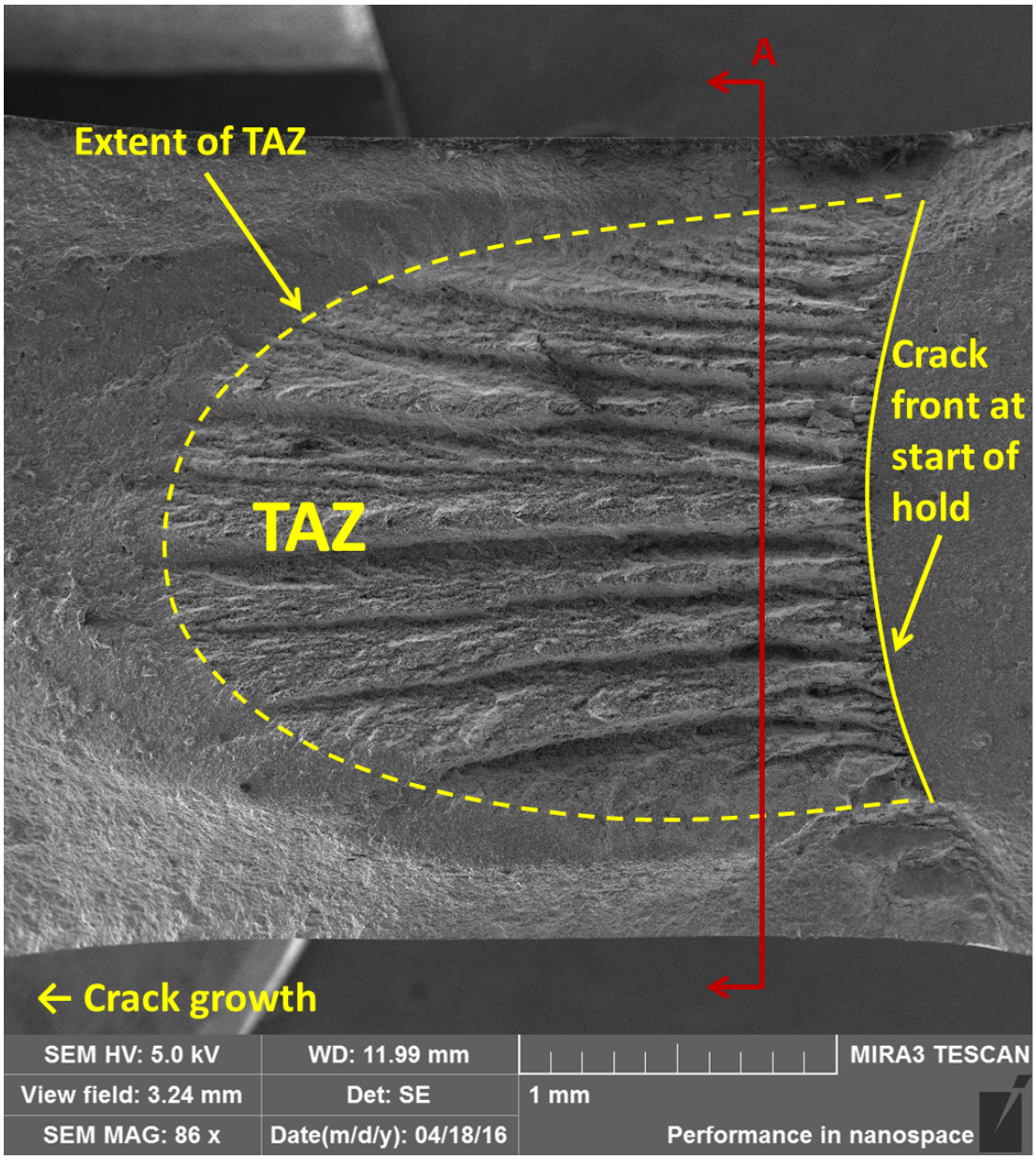

Figure 4.24: TAZ created by tensile hold at a K_{hold} of 45 MPa $\sqrt{m}$ for 3600 seconds at 650°C highlighting where section A was taken

Figure 4.25 shows the highly non-planar TAZ when compared to the portions near the free surface that exhibited no TAZ. A closer inspection of the TAZ in Figure 4.26 shows the secondary intergranular cracking observed at the bottom of the depressions in the TAZ.

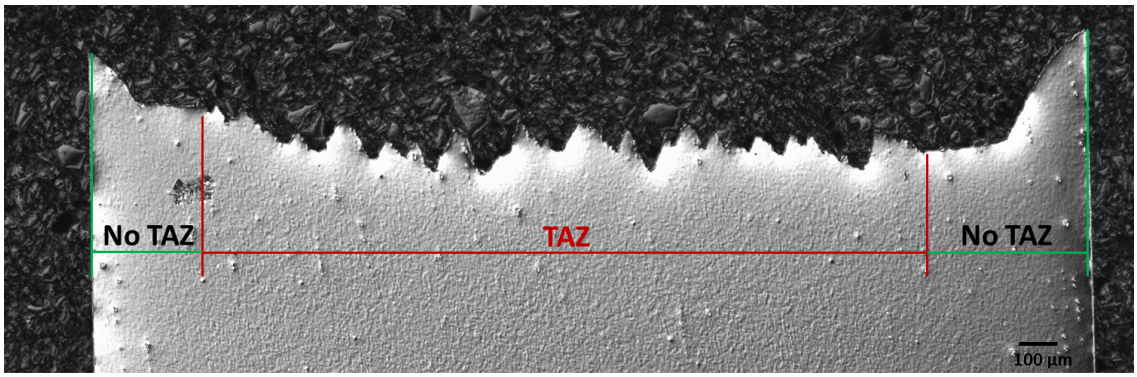

Figure 4.25: Optical image of section A view across the thickness of the specimen created by tensile hold at a K_{hold} of 45 MPa $\sqrt{m}$ for 3600 seconds at 650°C

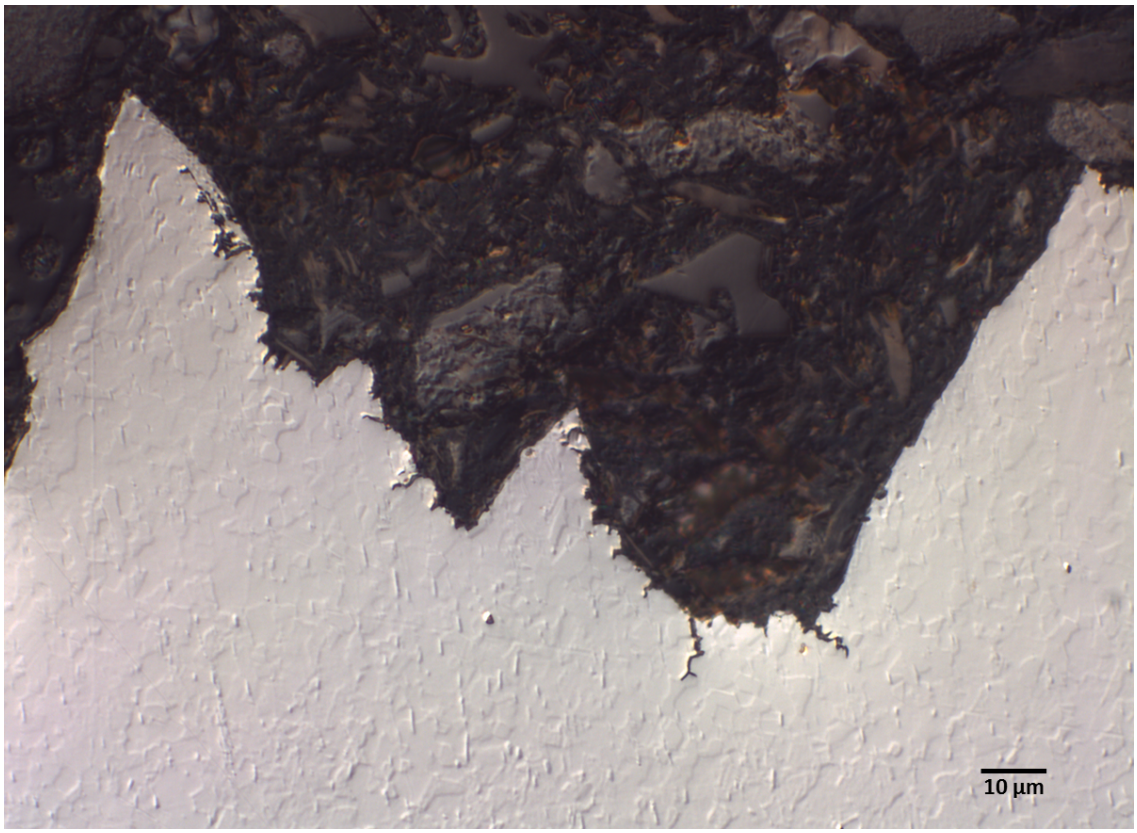

Figure 4.26: Higher magnification optical image of section A view in TAZ region created by tensile hold at a K_{hold} of 45 MPa $\sqrt{m}$ for 3600 seconds at 650°C

4.3.2 Effect of Tensile Hold Stress Intensity on Temperature Affected Zone Size

As the stress intensity of a tensile hold was increased, the size of the TAZ also increased as Figure 4.27 shows.

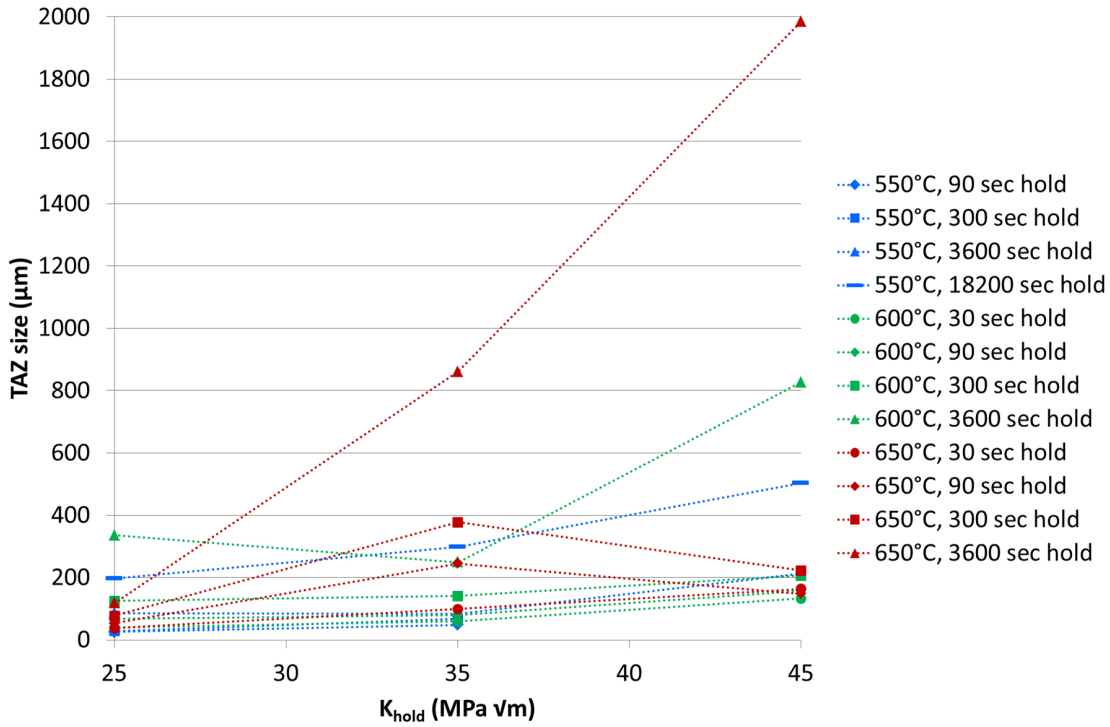

Figure 4.27: Effect of the stress intensity of a hold on the TAZ size for various temperature and hold durations

As the stress intensity increases, the amount of the tensile dilatational forces in the material ahead of the crack tip increases allowing for more and deeper penetration of oxygen at the crack tip to weaken the grain boundaries and hence create a larger TAZ.

4.3.3 Effect of Tensile Hold Duration on Temperature Affected Zone Size

As the duration of a tensile hold increased, the size of the TAZ also increased as Figure 4.28 shows.

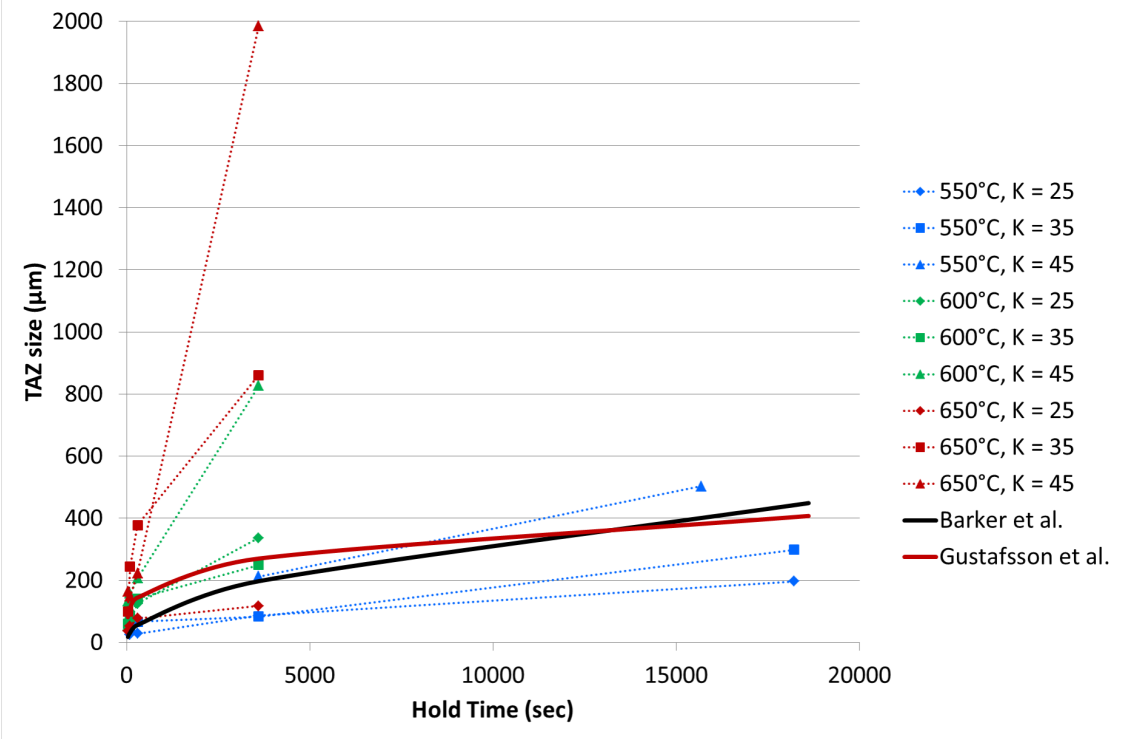

Figure 4.28: Effect of the duration of a hold on the TAZ size for various hold temperatures and hold stress intensities with comparison to published sources from Barker et al. [58] and Gustafsson et al. [57]

The diffusion of oxygen into and oxidation of Ni-base superalloys is time-dependent. As the hold time increases, more diffusion of oxygen and oxidation can occur to weaken grain boundaries. Favorable comparisons to TAZ size models from Barker et al., which was independent of the stress intensity of the hold and the hold temperature, and Gustafsson et al. which was for a TAZ created at 550°C and independent of the stress intensity of the hold are also shown in Figure 4.28 [57, 58].

4.3.4 Effect of Tensile Hold Temperature on Temperature Affected Zone Size

As the temperature at which a tensile hold was executed increased, the size of the TAZ also increased as Figure 4.28 shows. As energy is provide to the specimen in the form of heat, it is easier for the diffusion of oxygen to take place and for the potential effects of creep to occur. This increase in penetration ability of the oxygen can lead

to weakening of the grain boundaries and therefore create a larger TAZ.

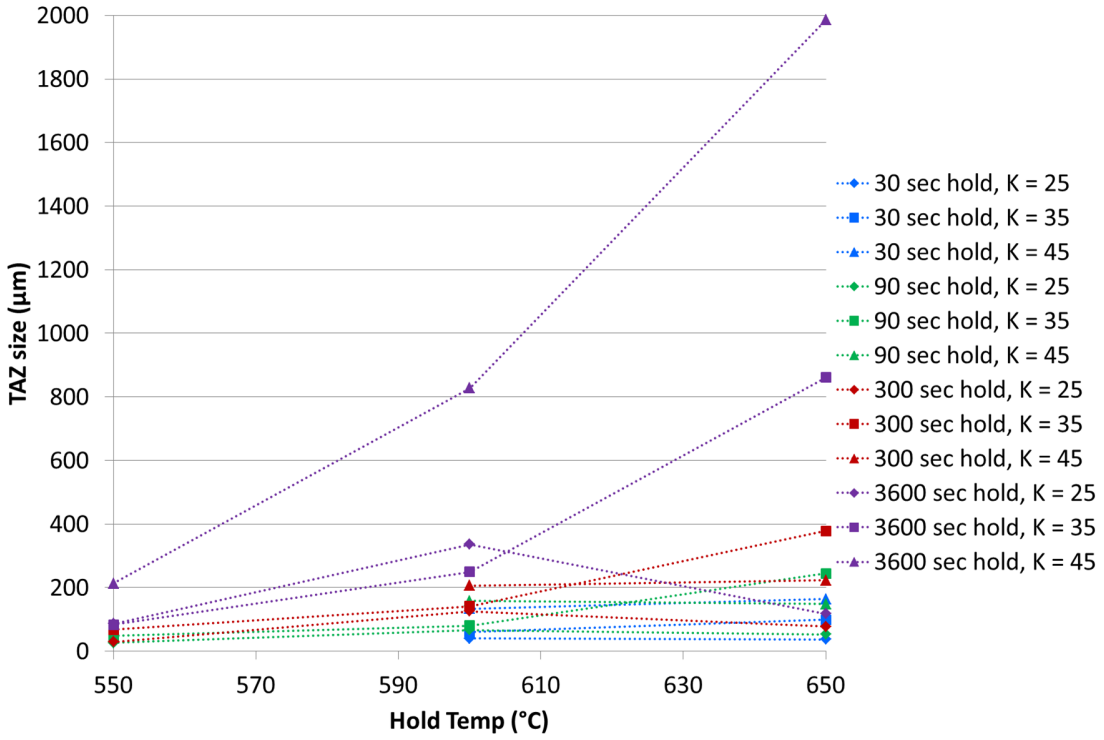

Figure 4.29: Effect of the temperature at which a tensile hold was executed on the TAZ size for various hold stress intensities and durations

4.3.5 Temperature Affected Zone Size Empirical Fit

Utilizing the trends observed in the TAZ size with variations of the hold stress intensity, hold duration, and hold temperature shown in Section 4.3, a simple empirical fit was created. The data in Figures 4.27, 4.28, and 4.29 indicate a power-law type relationship between the stress intensity of hold, the duration of hold, and the hold temperature with respect to TAZ size. A power-law type relationship between TAZ size and the stress intensity of hold and hold duration was implemented. Additionally, as a significant contributor to TAZ creation is the diffusion of oxygen at the crack tip, a temperature-dependent process, an Arrhenius type equation was utilized to fit temperature's contribution to TAZ since it is the form typically used to describe diffusion. The empirical fit is given by:

$$TAZsize = Ct^{n_1} {K_{hold}}^{n_2} e^{n_3 \frac{-Q}{RT}} \tag{4.1}$$

where TAZ size is in mm, t is the duration of the hold in seconds, K_{hold} is the stress intensity of the hold in MPa $\sqrt{m}$, T is the temperature of the hold in Kelvin, and R is the universal gas constant. The activation energy, Q, was taken from the activation energy for the high temperature oxidation of Ni-base superalloys as reported by Chang [76]. The parameters, C, n_1, n_2, and n_3 were obtained through regression analysis of the data reported in Figures 4.27 - 4.29. The values used for the parameters shown in Equation 4.1 are shown in Table 4.4. The parameters n_1, n_2, and n_3 effectively scale the contribution of the duration of the hold, stress intensity of the hold, and the temperature of the hold, respectively, to the development of a TAZ.

Table 4.4: TAZ size empirical fit parameters

C	0.291	$(\text{sec})^{-n_1}$ $(\text{MPa}\sqrt{m})^{-n_2}$
n_1	0.48	
n_2	2.6	
n_3	0.38	
Q	255000	J/mol
R	8.31446	J/mol*K

The parameters were selected and fit to match the overall trends observed. Figures 4.30 - 4.32 show a sampling of how well the fit matched the experimental data.

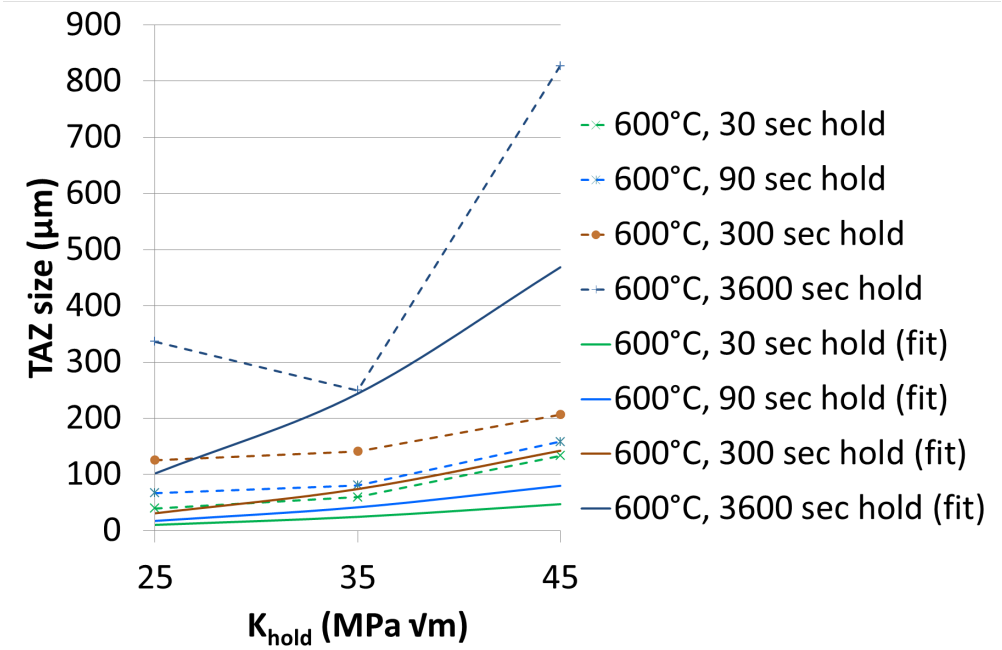

Figure 4.30: Empirical fit of the TAZ size based on the stress intensity of the hold

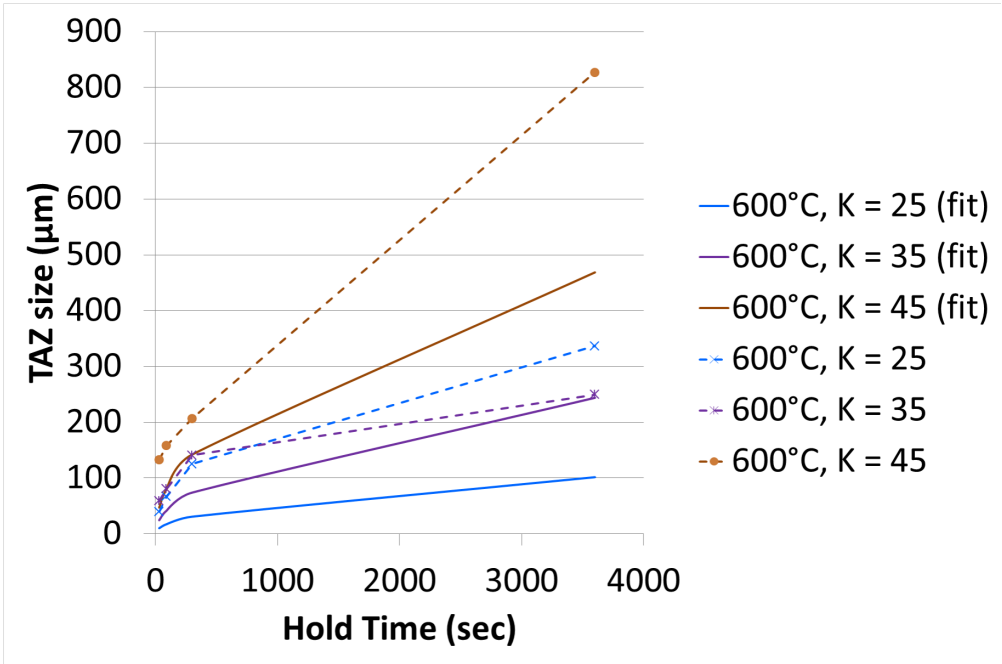

Figure 4.31: Empirical fit of the TAZ size based on the hold duration

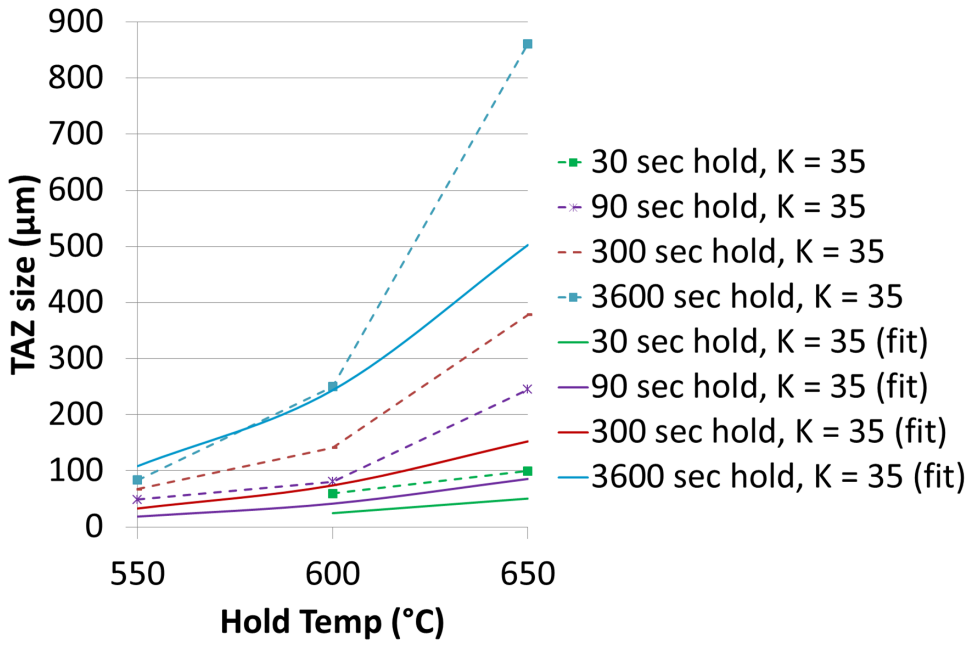

Figure 4.32: Empirical fit of the TAZ size based on the duration of the hold

4.3.6 Impact of Temperature Affected Zone on Fatigue Crack Growth Rate

Since the optical method of crack length measurement could not capture the affect of a TAZ on FCGR, three additional holds with subsequent cycling were executed using an EPD system with the cycling temperature reduced from 260°C to room temperature (about 26°C). These holds were executed at short crack lengths to limit any history effects of prior loading, ensure plane strain dominated crack growth, and to remain within the geometry bounds of Equation 3.10. Figure 4.33 shows a comparison of the crack length measurements for a TAZ created with a K_{hold} of 45 MPa $\sqrt{m}$, a hold duration of 3600 seconds, and a hold temperature of 650°C. It is clear that an initial portion of acceleration is observed immediately following the tensile hold using EPD for crack length measurement whereas the crack growth measured with the optical method shows no acceleration as observed with the other TAZ test points.

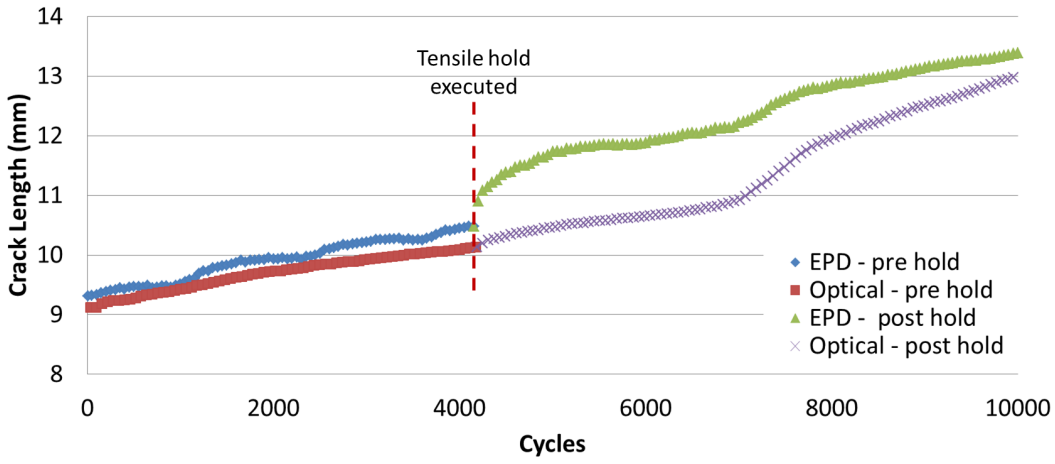

Figure 4.33: Crack growth before and after a TAZ created by a K_{hold} of 45 MPa $\sqrt{m}$, a hold duration of 3600 seconds, and a hold temperature of 650°C comparing the optical method of crack growth measurement and EPD

To capture the effect of the acceleration on FCGR and to limit the noise inherent in crack length measurements, a third order polynomial was fit to the crack length measurements immediately following resumption of cycling after the hold as Figure

4.34 shows. This smoothed curve was used to generate the crack growth increment plots to determine the impact of a TAZ on FCGR. Figure 4.35 shows the impact of a TAZ on FCGR at three different stress intensity levels. A maximum acceleration of 4.75 times the unaffected FCGR was observed. This was significantly less than the up to 300 times acceleration shown in Figure 2.11 where steady time-dependent crack growth was allowed to develop during the tensile hold before cycling was resumed. As stated earlier, in a realistic application, time-dependent crack growth under sustained loading is not a significant concern for IN 718 and as such, the measured impact of a TAZ on FCGR is realistic.

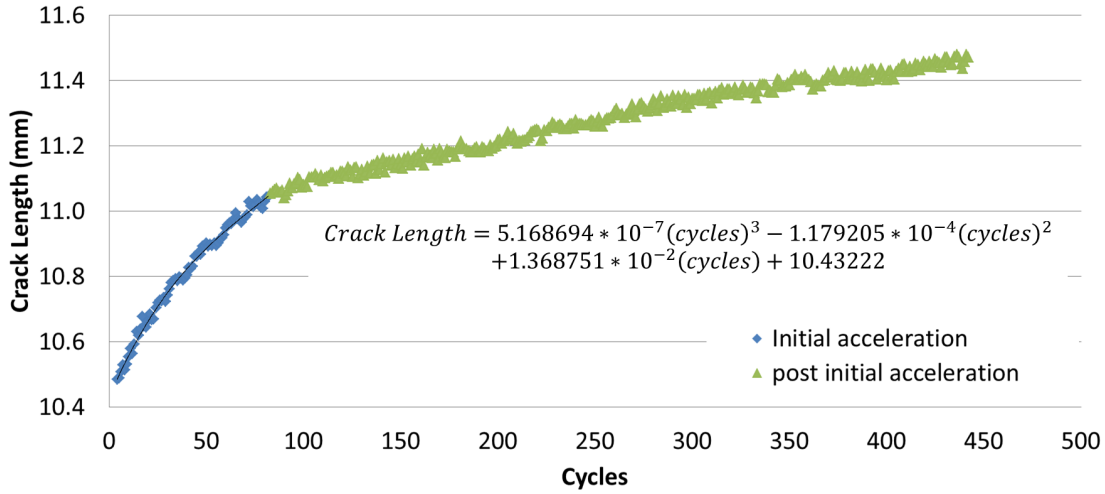

Figure 4.34: Crack growth immediately following resumption of cycling following a TAZ created by a K_{hold} of 45 MPa $\sqrt{m}$, a hold duration of 3600 seconds, and a hold temperature of 650°C with a polynomial fit to the significant initial acceleration

The slope of the data in Figure 4.35 is decreasing as the stress intensity level is increasing indicating the effects of TAZ on FCGR are more significant at lower stress intensity levels. At lower stress intensity levels, the plastic zone size is smaller and hence there is a larger proportion of plain strain dominating the specimen. As was mentioned earlier, the higher proportion of plain strain in the specimen will increase the tensile dilatation of the material at the crack tip and lead to an increased risk of

developing and subsequently being impacted by a TAZ.

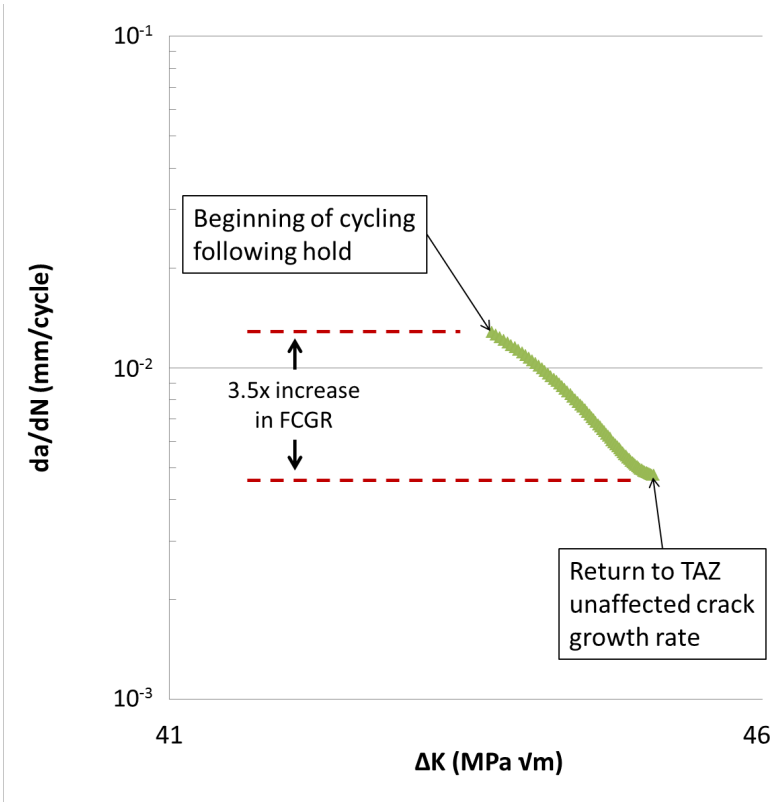

(a) TAZ created by K_{hold} of 45 MPa $\sqrt{m}$ for 3600 seconds at 650°C

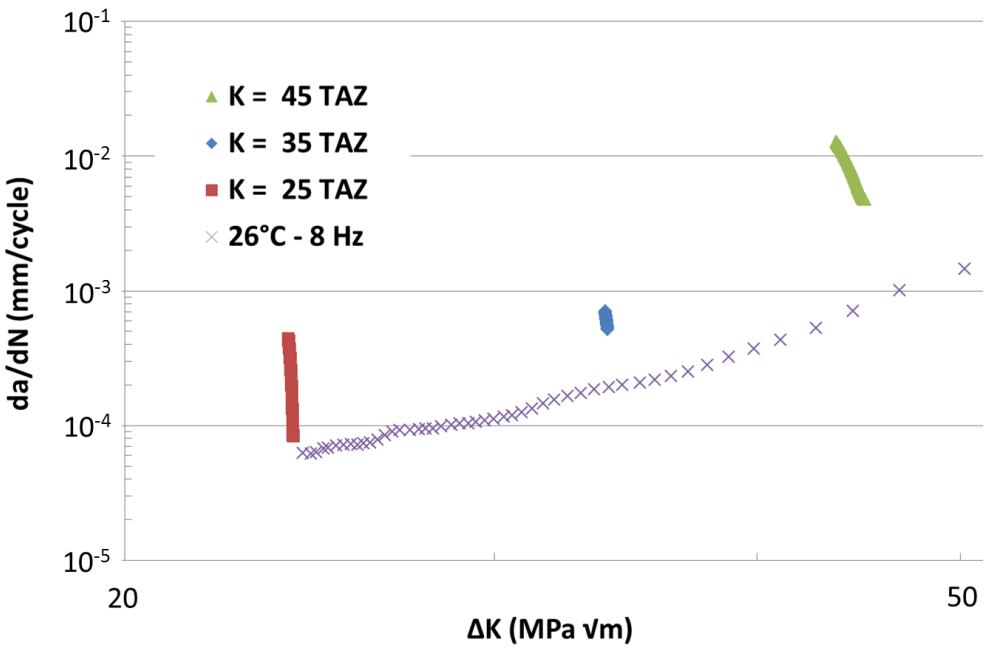

(b) FCGR following a 3600 second hold at 650°C (K = 45 TAZ and K = 25 TAZ) or 600°C (K = 35 TAZ) for different K_{hold} compared to isothermal FCG at room temperature at 8 Hz

Figure 4.35: Impact of TAZ on FCGR

4.3.7 Impact of Temperature Affected Zone on Fatigue Crack Growth Rate Empirical Fit

As was clearly shown in Section 4.3.6, the presence of a TAZ at the crack tip leads to an accelerated crack growth rate. An empirical fit was develop to account for the accelerating effect of a TAZ on crack growth rate. The equation developed utilizes the current TAZ size and the plastic zone size to calculate a multiplication factor (TAZ acceleration factor (TAF)) indicating how much faster the crack is propagating:

$$TAF = 1 + D\left(\frac{TAZsize_{current}}{r_p}\right)^p \tag{4.2}$$

where TAZ size$_{current}$ is the current TAZ size in mm, r$_p$ is the plastic zone size in mm, and D and p are fitting parameters. As the TAZ is consumed by crack growth, the TAF will also decrease until no TAZ remains and the TAF value becomes unity.

Utilizing fitting parameters of D = 6.0 and p = 0.5, Figure 4.36 shows a good correlation of the TAF to experimental data.

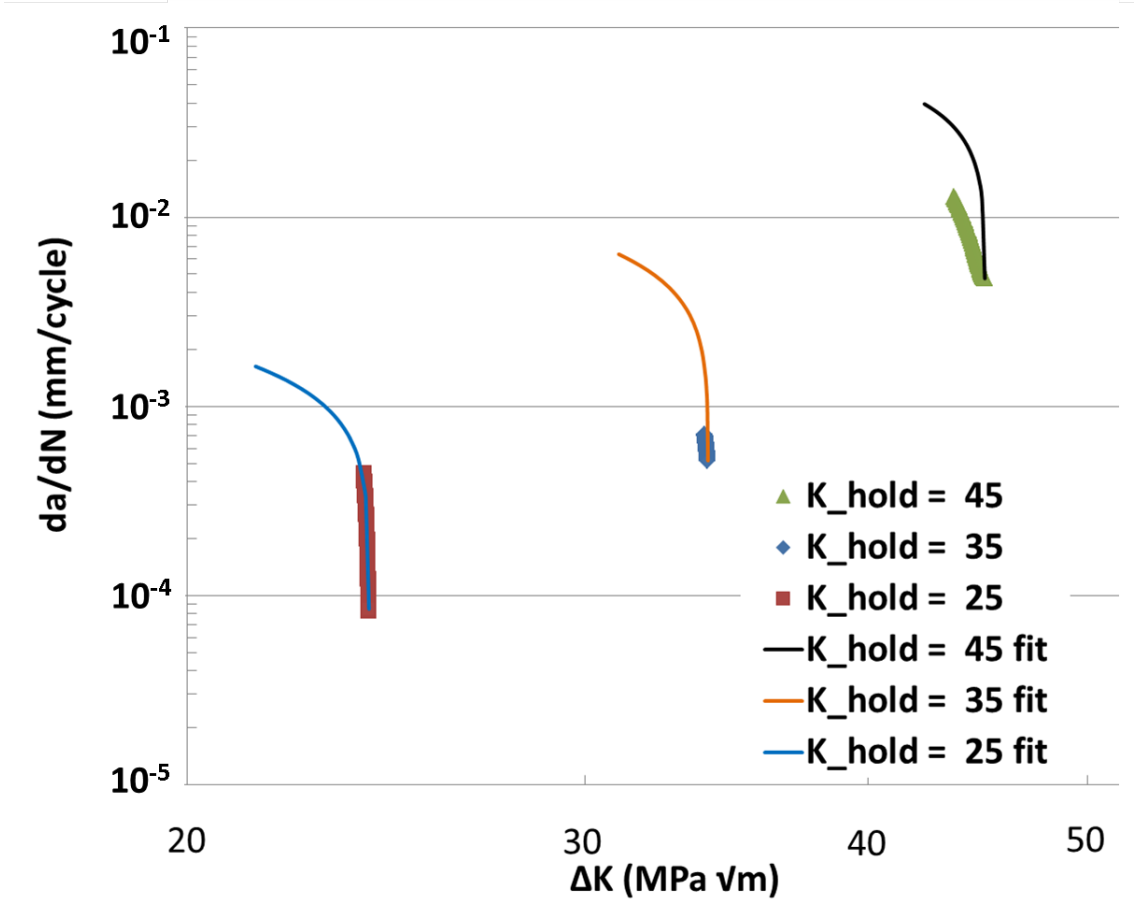

Figure 4.36: Fit of TAZ impact on FCGR following a hold using Equation 4.2

The form of Equation 4.2 allows for the effect of TAZ to be reduced as the state of stress transitions from plane strain dominated to plane stress dominated. The TAZ failure surfaces indicate that as the state of stress varied from plane strain dominated at the center of the specimen to plane stress dominated at the free surface, the amount of embrittled material in the form of TAZ reduced. Additionally, the experimental observations in Figure 4.36 show how as the stress intensity increases, and similarly the plastic zone size increases, the slope of the crack growth data becomes less negative (i.e. less significant). Equation 4.2 effectively captures this effect.

4.3.8 Significant Findings

Definite trends were observed in TAZ size with changes in the stress intensity of a hold, the duration of a hold, and the temperature of a hold. Holds at the highest stress intensities for the longest durations at the highest temperatures resulted in the most severe impact on the failure surface in the form of secondary cracking and oxidation. The impact of a TAZ on FCGR was captured for several holds using the EPD crack length measurement technique and showed initial acceleration upon resumption of cycling following a hold. Utilizing a power-law relationship to account for the effect of the stress intensity of a hold and the duration of a hold and an Arrhenius type equation to account for the temperature of a hold provided for accurate modeling of the TAZ size for a hold with specific stress intensity, duration, and temperature. Additionally, the empirical fit of the impact of a TAZ on FCG shown in Equation 4.2 provides an accurate fit of the impact of a TAZ on FCGR as shown in the experimental data.

4.4 Effect of Compressive Hold on Thermomechanical Fatigue Crack Growth

In addition to evaluating the effect of a tensile hold on FCGR, tests were conducted to characterize the effect of a high temperature compressive hold in a TMF spectra.

4.4.1 Crack Growth Rate

The fatigue crack growth rate for the consortium developed aircraft spectrum (Figure 3.12) and triangular OP TMF waveform (Figure 3.13) are shown in Figures 4.37 and 4.38, respectively. When a compressive hold at the maximum temperature was imposed, minimal impact on FCGR was observed compared to the spectra without a compressive hold. This was observed for both the consortium developed spectrum as well as the triangular waveform.

Additionally, compressive hold comparisons were done at temperatures above the

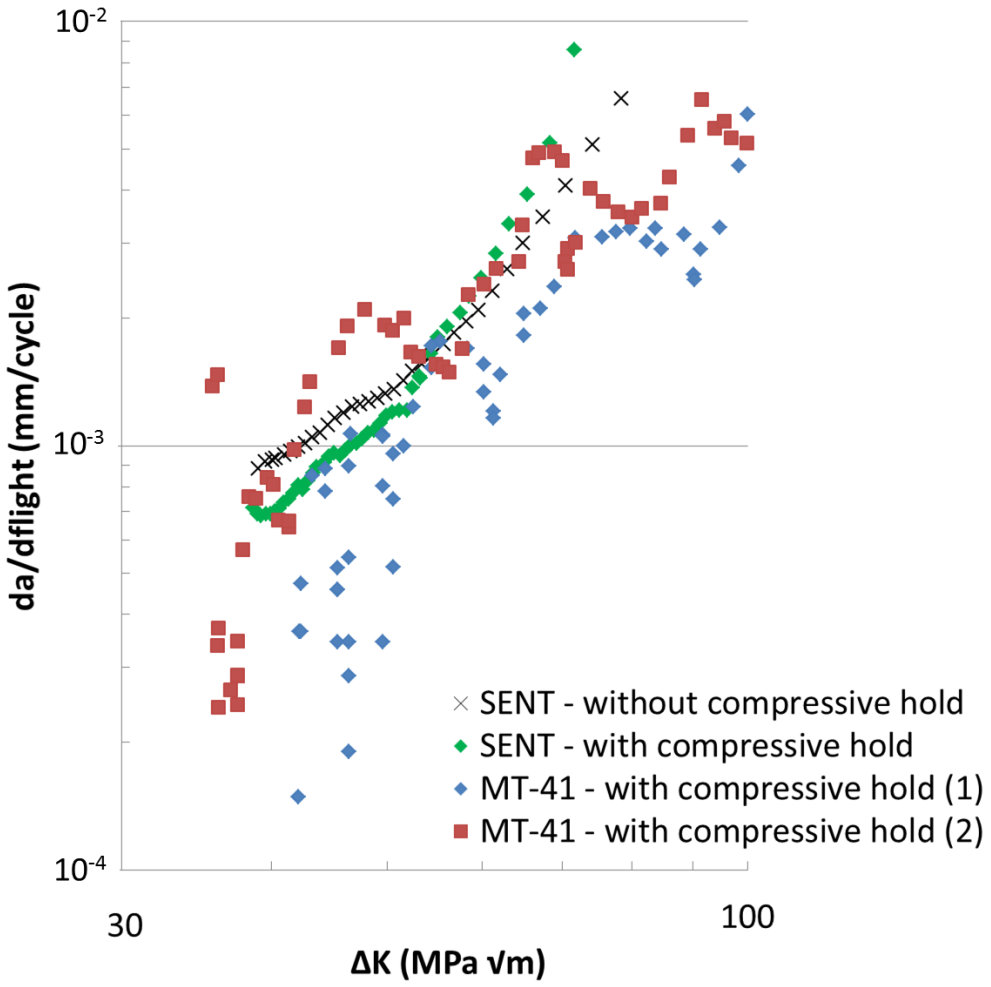

Figure 4.37: Impact of compressive hold on OP TMF for the consortium developed aircraft spectrum for both the SENT and MT-41 specimen geometries T_{max} = 600°C, T_{min} = 260°C, overall R = -0.2

typical maximum usage temperature of 650°C to determine if the oxidation mechanism would appear and increase crack growth rate. Again, imposing a 30 second compressive hold at temperatures up to 725°C showed minimal indication of increased crack growth rate after the hold as Figure 4.39 shows. This minimal indication of increased crack growth rate does not necessarily suggest that the oxidation mechanism begins to play a larger role. At these higher temperatures, the effects of creep and stress relaxation begin to play a larger role. Utilizing a plastic yield zone approach, the time spent at high temperature under global compressive loading will have the

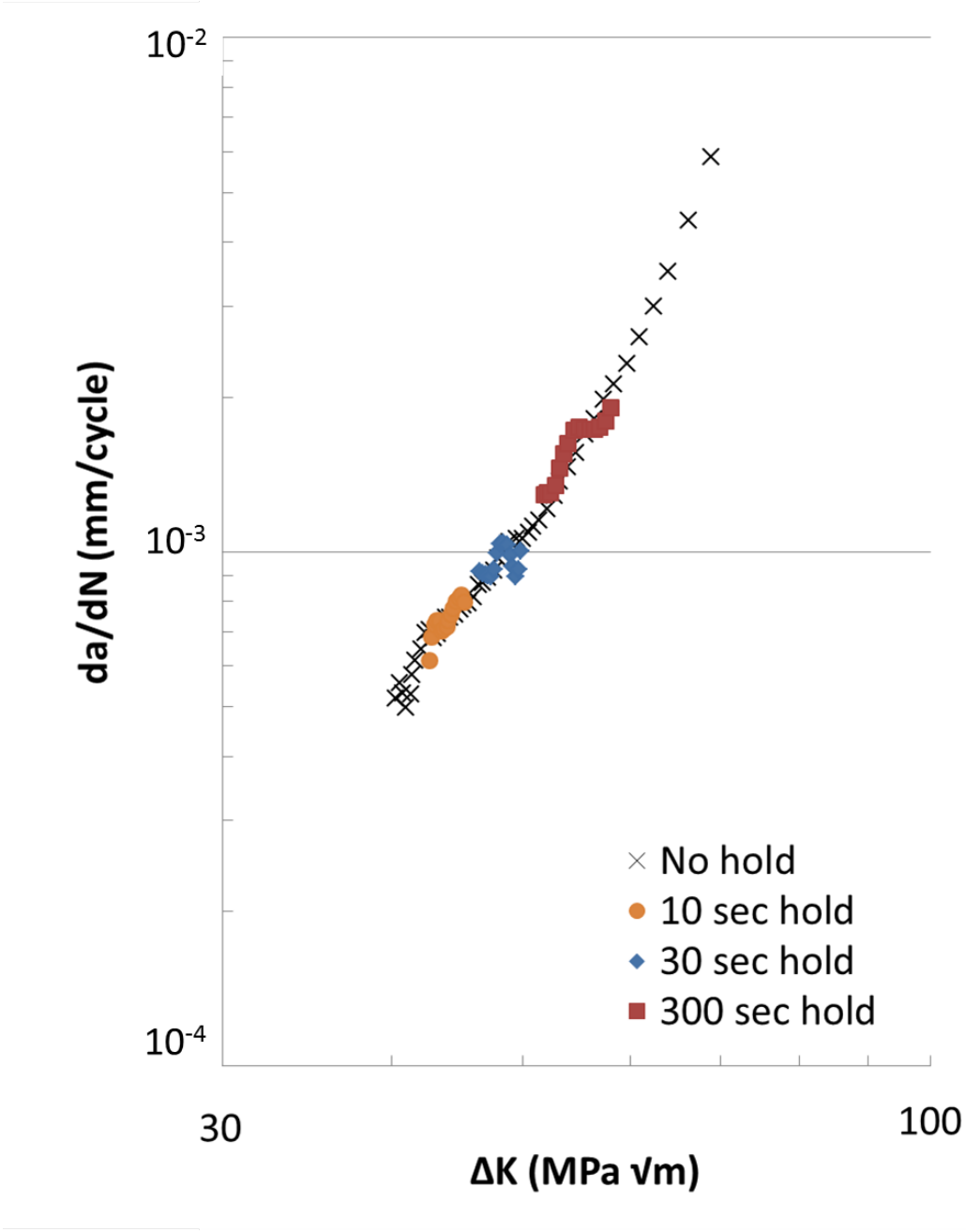

Figure 4.38: Impact of compressive holds of various durations on FCGR for an OP TMF triangular waveform T_{max} = 650°C, T_{min} = 315°C, overall R = -0.2

effect of relaxing the compressive residual stresses in the plastic zone ahead of the crack tip. As long as the hold is not approaching negative yield strength, any hold at these high temperatures will relax the stress even further. The stress relaxation

will effectively increase the loading ratio, R, for the subsequent tensile cycle. The spectrum with the hold will experience an increase in the loading ratio more than the spectrum without the hold, leading to faster crack growth with the hold than without. As can be seen in Figure 4.39, this effect is minimal even after the hold temperature is 75°C above the typical maximum usage temperature for IN 718.

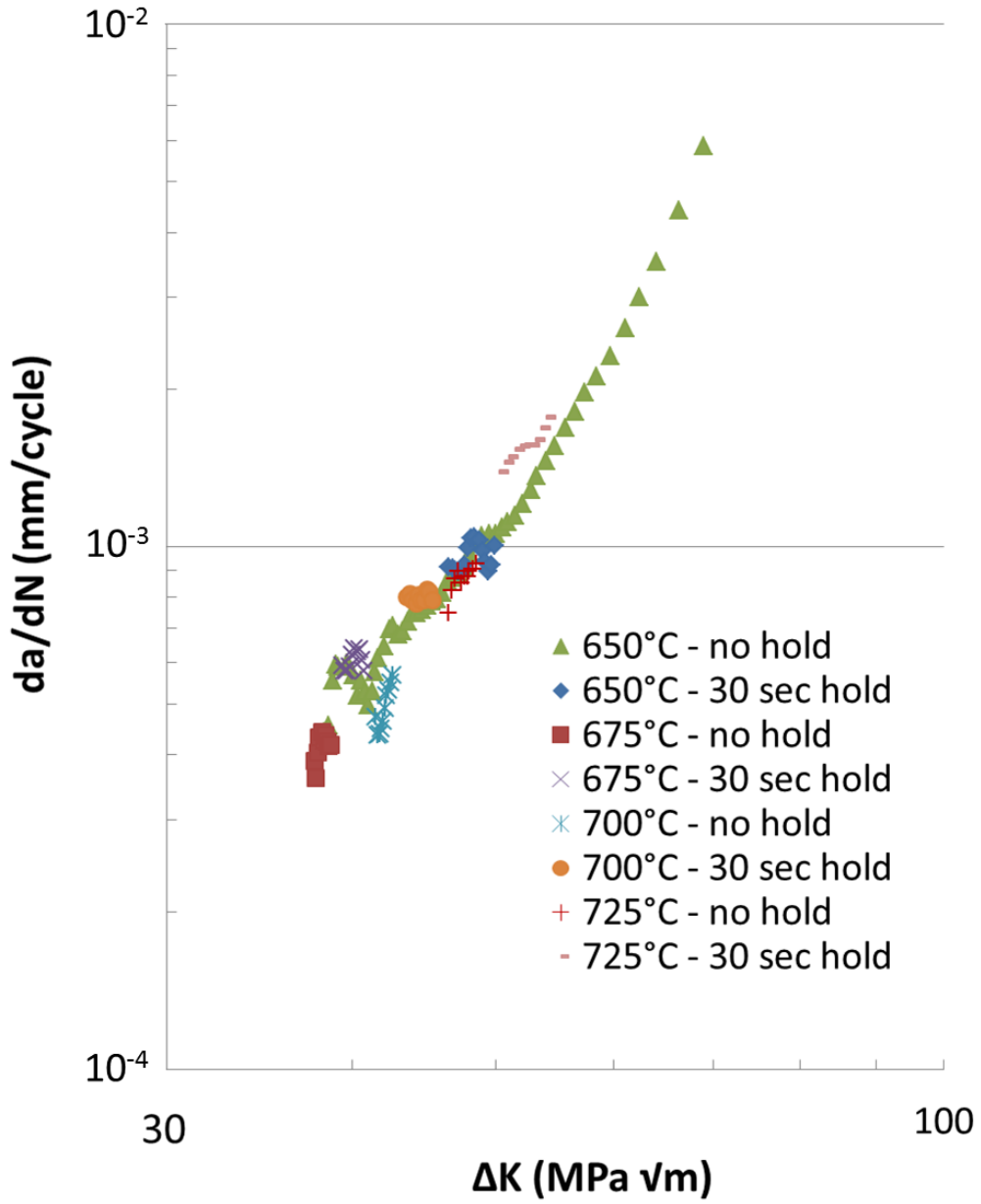

Figure 4.39: Impact of 30 second compressive holds on FCGR for an OP TMF triangular waveform of various maximum temperatures T_{min} = 315°C, overall R = -0.2

4.4.2 Fractography

Consistent characteristics of the failure surfaces for the OP TMF test points with and without a compressive hold were also observed. Figure 4.40 shows a relatively

flat failure surface indicative of all of the OP TMF test spectra executed to evaluate the effect of compressive hold. Clearly evident is the lack of any of the chevron characteristics observed in the lower temperature isothermal failure surfaces shown in Figure 4.3. For an OP TMF cycle, the maximum load occurs at a low temperature. It can be reasoned that since the maximum tensile load drives crack growth, the temperature at maximum load (low for an OP TMF cycle) should be representative of the crack growth response. However, even though the minimum temperature for the OP TMF cycles executed here were well below 427°C where the chevron shapes were observed for the isothermal tests, the OP TMF crack growth response is not represented by the temperature at maximum load but could be represented by the crack growth expected at some intermediate temperature between the maximum and minimum temperatures of the cycle. This coincides with the discussion of Section 2.5.

Figure 4.40: Failure surface for the consortium developed OP TMF spectrum with compressive hold

A SEM view of the failure surfaces for the OP TMF with compressive hold crack growth tests are shown in Figure 4.41. They exhibited a primarily transgranular failure surface with striations present and some secondary cracking. For an isothermal test at 650°C and this low loading frequency, one would expect an intergranular failure surface had the elevated temperatures occurred during the tensile portion of the cycle as is shown in Figure 2.5 [25]. All failure surfaces observed, regardless of whether a compressive hold occurred, or its duration, showed a similar transgranular failure surface with striations present. Occasional grain boundary tearing was also

observed but not a significant proportion of the failure surface. These failure surface characteristics were also observed for the specimens subjected to temperatures up to 725°C.

As there was limited secondary cracking observed on the failure surface for the OP TMF specimens, any impact on fatigue crack growth rate observed in the specimens subjected to temperatures over 650°C can most likely be attributed to creep and stress relaxation effects as mentioned above.

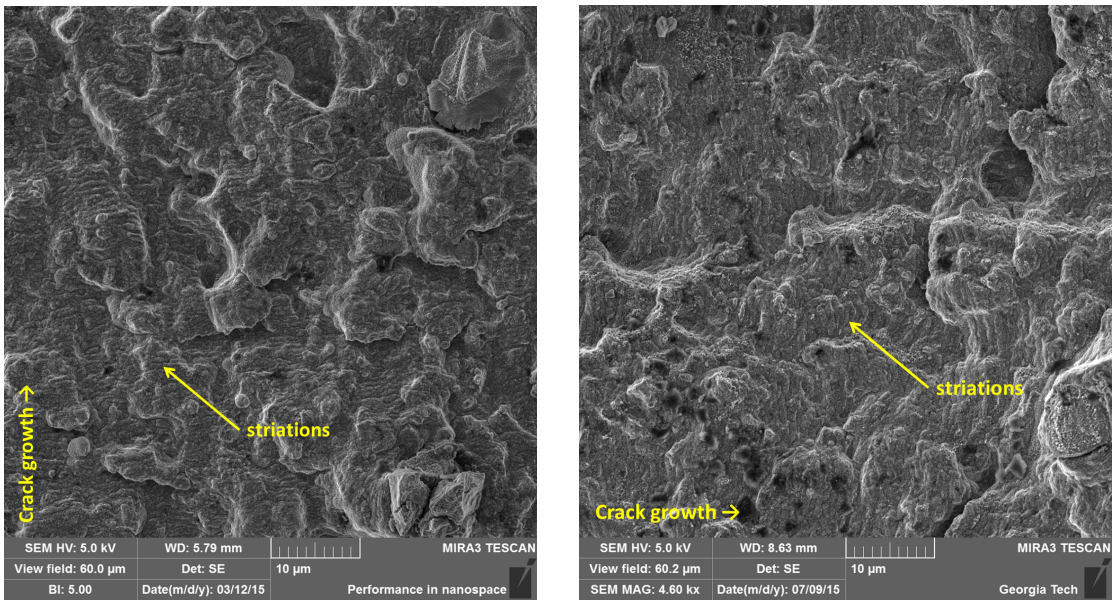

(a) Observed transgranular failure surface with striations present $T_{max} = 650°C$

(b) Observed transgranular failure surface with striations present $T_{max} = 725°C$

Figure 4.41: Observed transgranular failure surface for OP TMF with compressive hold FCG tests

The transgranular failure surface is more indicative of a faster loading frequency where there is no time for oxidation penetration, as Figure 4.5 shows, or a vacuum environment where there isn't any oxygen present. The appearance of a transgranular fracture surface suggests that although the specimens were subjected to temperatures up to and above the typical maximum operating temperature at a frequency slow enough to cause weakening of the grain boundaries to occur, the fact that most of the high temperature time was spent in compression limited how far the oxidation

could penetrate at the crack tip. Without oxygen penetration, the material's plastic response will drive the crack growth rate, and a hold time will have minimal effect. Both the FCGR data and the failure surfaces agree with this conclusion.

The penetration of the oxidation is dependent on the stress and strain state of the affected grain boundaries [77–79]. With global compressive loading, the grain boundaries in close proximity to the crack tip are compressed together, limiting the opportunity for oxygen to penetrate, as opposed to a tensile situation where the grain boundaries are strained apart allowing oxygen to more easily penetrate. It is possible for tensile residual stresses to develop at the crack tip when subjected to compression-compression loading in the presence of a notch due to reversed yielding which could provide the tensile strains to the grain boundaries needed for oxygen penetration. However, for the OP TMF conditions evaluated in this project, tensile residual stresses do not develop as the global compressive stress completely closes the crack and the material ahead of the crack tip does not yield in compression due to a stress concentration as it does with a notch present. Therefore the oxygen does not encounter tensile strains at the grain boundaries that would offer an easy path to penetrate the material at the crack tip during the hold and subsequently affect crack growth rate.

Additionally, good correlation was made between the striation spacing and the crack growth rate measured with the optical method of crack length measurement. Figure 4.42 shows the transgranular failure surface with striations of an OP TMF with compressive hold test specimen. Taking the average of striation spacing from several points in the SEM image, a crack growth rate of 6.51 x 10^{-4} mm/cycle was measured while the measured crack growth rate at this point in the specimen was measured as 8.38 x 10^{-4} mm/cycle using the optical method of crack length measurement.

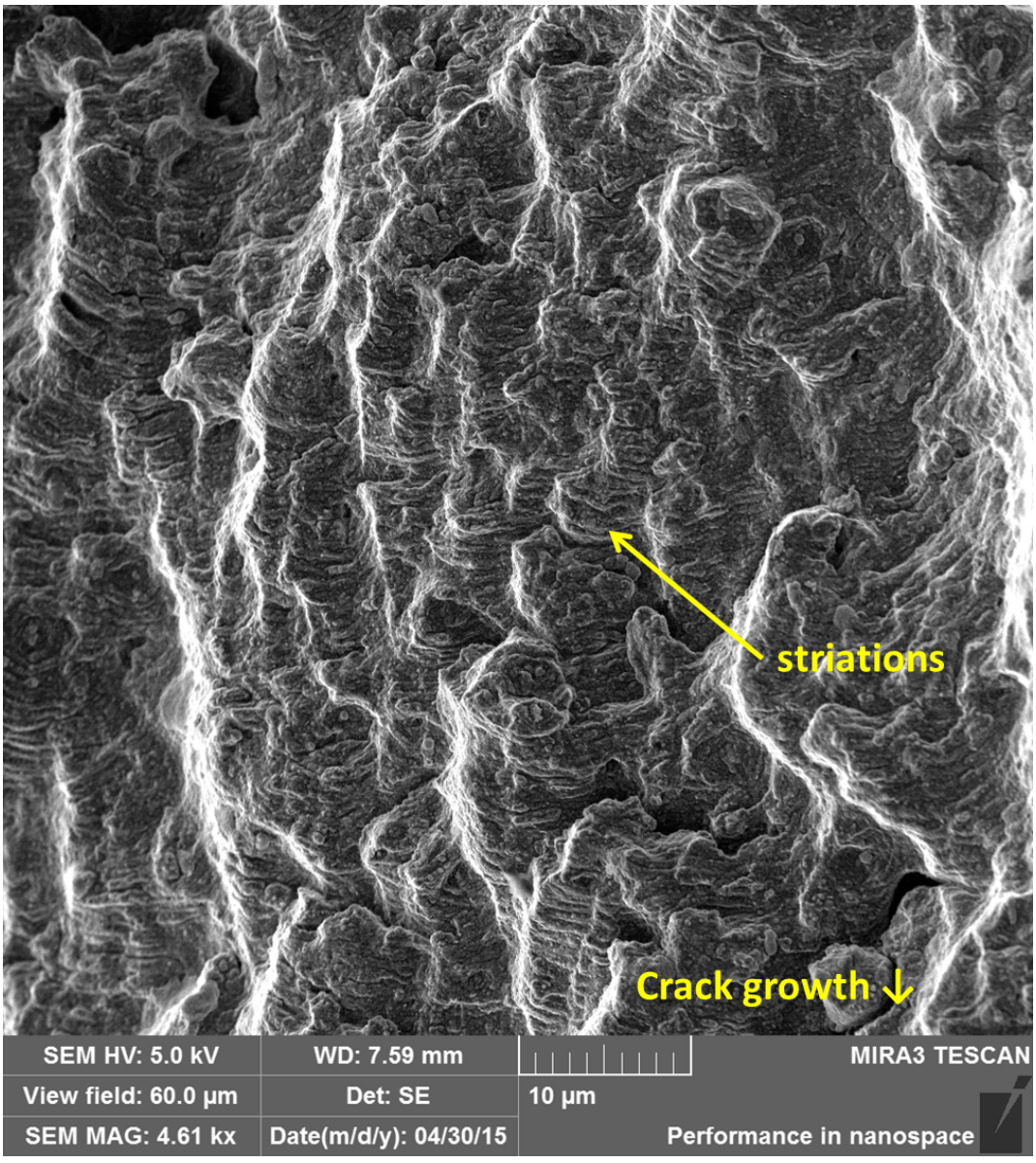

Figure 4.42: Observed transgranular failure surface with striations for the OP TMF with compressive hold FCG tests highlighting striation spacing

4.4.3 Significant Findings

There is no significant impact of a compressive hold at high temperature on FCGR. This includes compressive holds up to 75°C hotter than the typical maximum usage temperature.

4.5 Tensile Hold Sequence Effects on Out-of-Phase Thermomechanical Fatigue Crack Growth

To best simulate realistic applications, the test spectra shown in Figure 3.14 were executed to evaluate the impact of loading or unloading immediately prior to a tensile hold.

4.5.1 Crack Growth Rate

Figure 4.43 show how an increasing load immediately prior to tensile hold (forward) allowed a crack to propagate more quickly than a tensile hold coming off of an unload (backward). The overall impact was about a 30% increase in FCGR for the forward spectrum. If one were to approach these two spectra from a load interaction perspective, the underload immediately prior to the tensile hold for the forward spectrum has the effect of reducing the crack growth retardation effects of the prior maximum load, effectively reducing the beneficial residual stresses at the crack tip induced by the overload. Similarly, from a temperature interaction perspective, the underload immediately prior to the tensile hold (forward spectrum) allows for higher tensile dilatational forces at the crack tip. This will allow more oxygen penetration at the crack tip which will more significantly weakening the material and lead to a faster crack growth rate. These results agrees with the isothermal work of Ponnelle et al. [36] and the isothermal results of Section 4.2.

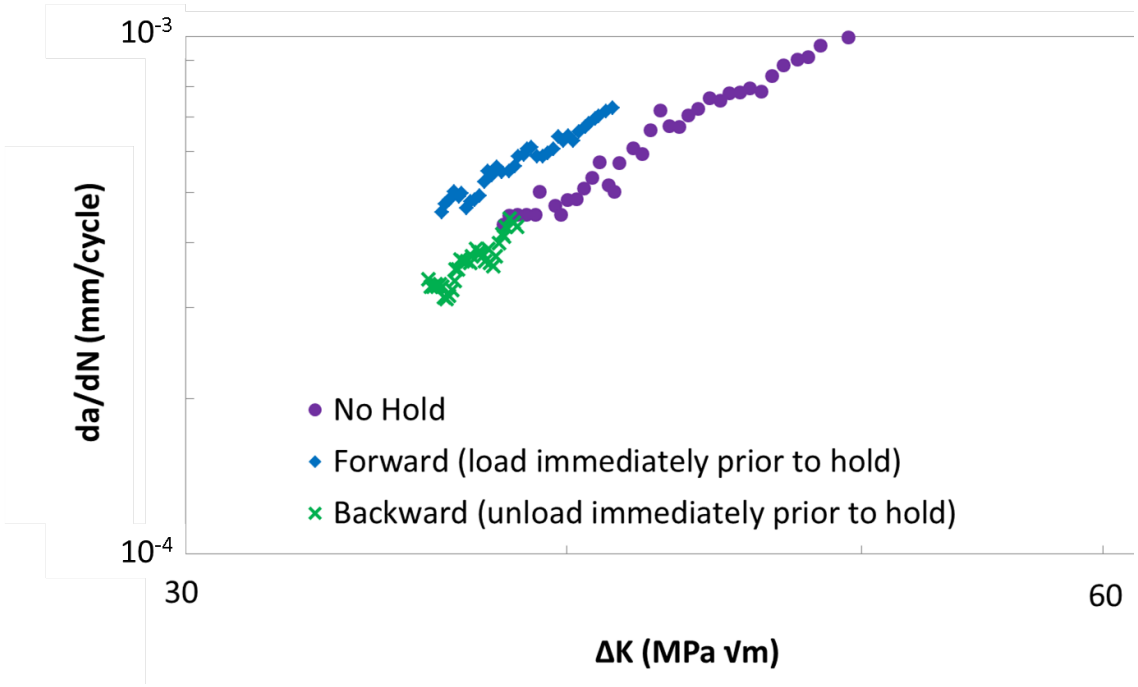

Figure 4.43: Impact of loading (forward) or unloading (backward) immediately prior to a tensile hold at high temperature on FCGR compared to the same OP TMF spectra without a subsegment

4.5.2 Fractography

Figure 4.44 shows the failure surfaces for the tensile hold sequence effects tests. Although both appear to be primarily transgranular, there are significantly more striations visible for the backward test point. Additionally, though there was no observed secondary cracking for the forward spectrum, the surface itself has a rougher appearance indicating that the crack was not allowed to propagate as smoothly as the backward spectrum allowed. These factors indicate that prior weakening of the material ahead of the crack tip leading to more torturous crack propagation was present for the forward spectrum and would therefore contribute to a faster FCGR. This agrees with the crack growth data collected.

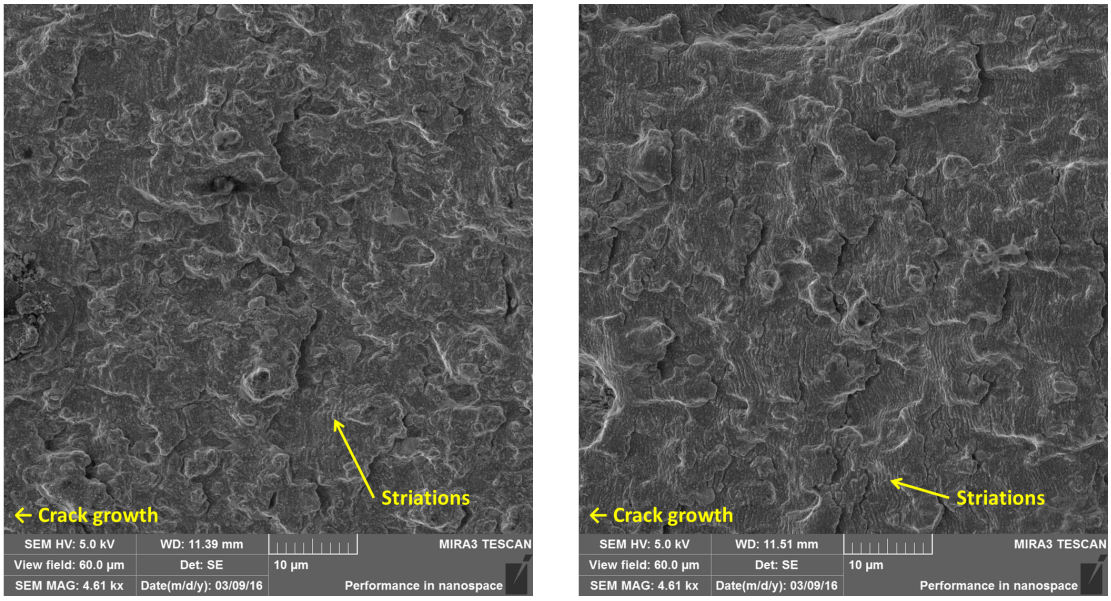

(a) Forward spectrum (loading immediately prior to hold) at $\Delta K = 39$ MPa $\sqrt{m}$ showing transgranular crack growth with some striations

(b) Backward spectrum (unloading immediately prior to hold) at $\Delta K = 38$ MPa $\sqrt{m}$ showing transgranular crack growth with numerous striations

Figure 4.44: Failure surfaces of tensile hold sequence effects specimens

4.5.3 Finite Element Analysis

To confirm that the forward spectrum leads to higher tensile dilatational forces at the crack tip, a FEA simulation was executed using the same model as discussed in Section 4.2.3. Figure 4.45 shows how for the forward TMF spectrum, the von Mises stresses immediately ahead of the crack tip are tensile and higher than for the backward TMF spectrum. These higher tensile von Mises stresses will allow more oxidation to penetrate and lead to faster crack propagation for the forward TMF spectrum.

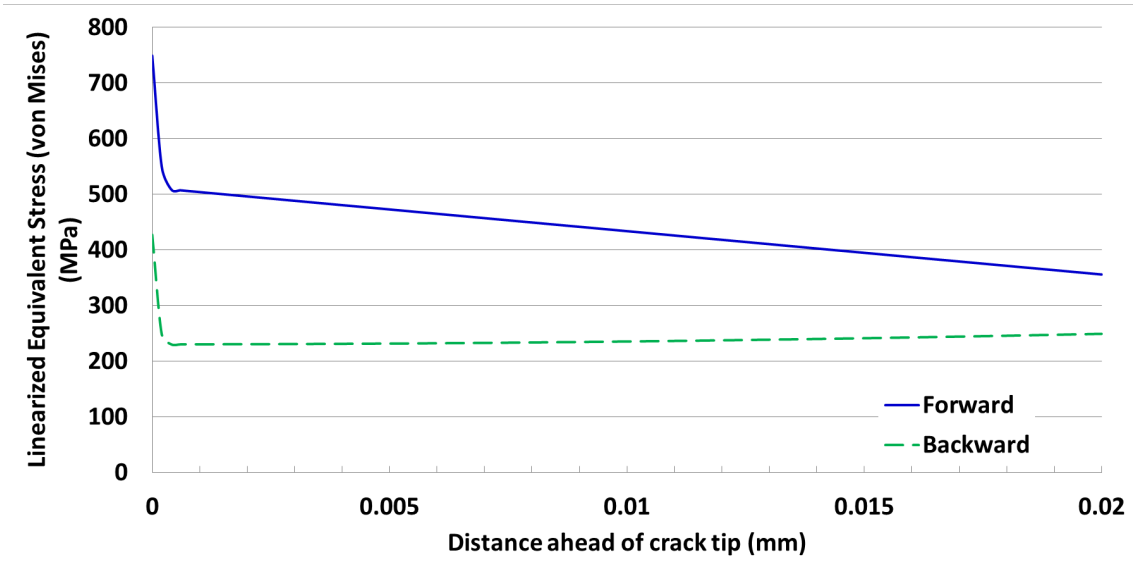

Figure 4.45: Finite element analysis prediction of the von Mises stress ahead of the crack tip at the beginning of the tensile hold for the forward and backward TMF spectra

4.5.4 Significant Findings

For a TMF spectrum, tensile holds at high temperature immediately following an unload showed no increase in FCGR whereas tensile holds at high temperature immediately following an increase in load showed an increased FCGR. Fractographic evidence indicated slight weakening of the failure surface for the tensile hold following an increase in load. Finite element analysis indicates that increased tensile stresses at the crack tip may be responsible for the increased FCGR of the forward TMF spectrum.

4.6 Representative Thermomechanical Fatigue Spectra

In addition to the OP TMF tests conducted to evaluate the impact of a compressive hold on FCGR and the sequence effects of a tensile hold, two tests were conducted to simulate realistic application spectra. These spectra were designed to be representative of fighter aircraft and transport aircraft applications.

4.6.1 Crack Growth Rate

The effect of the tensile subcycles imposed during a tensile hold to simulate a fighter aircraft spectra (see Figure 3.15) was shown by noticeably faster crack growth when compared to the spectra with tensile hold run without the subcycles to simulate a transport aircraft spectra (see Figure 3.16) as Figure 4.46 shows.

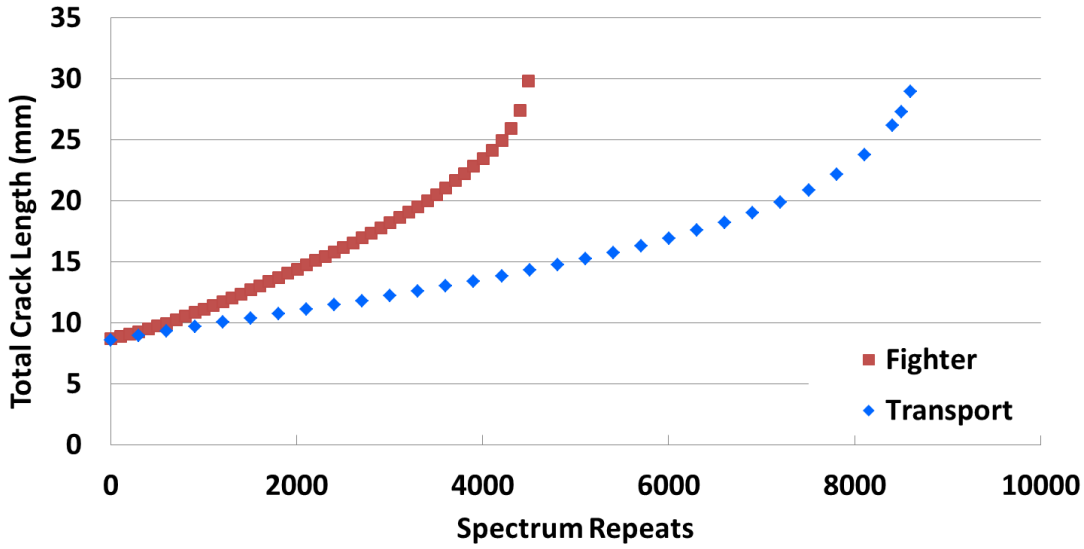

Figure 4.46: Crack growth comparison of representative fighter and transport aircraft TMF spectra

Both the representative fighter and transport aircraft spectra are expected to develop a TAZ, especially during the tensile hold. As mentioned in Section 4.5, the unloading effect just prior to the second and third tensile holds in the fighter spectrum should lead to those hold segments being subject to limited weakening at the crack tip due to oxygen penetration. Since the overall life for the fighter spectrum is shorter, it would indicate that the weakening of the material developed in the first 30 seconds of tensile hold plays a much more significant role when combined with the subcycles than the weakening developed during the longer duration transport aircraft spectrum's tensile hold.

Additionally, for subcycles of the form found in the representative fighter aircraft

spectrum (subcycle mean load is the same as the tensile hold load), the second and third hold segments have a limited contribution to weakening of the material at the crack tip, however, if the subcycles were executed backward (load-unload-load instead of unload-load-unload) the second and third tensile holds would more significantly contribute to the weakening of the material at the crack tip and hence, faster crack growth would be expected.

4.6.2 Fractography

The failure surfaces shown in Figure 4.47 indicate that the representative fighter aircraft spectra was subject to a similar amount of embrittlement as the representative transport aircraft spectrum. The overall transgranular nature of the spectrum with some secondary cracking was in approximately the same proportion on both failure surfaces. This indicates that the TAZ developed for both spectra were similar in magnitude and that the subcycles themselves are what drove faster crack growth for the representative fighter aircraft spectrum.

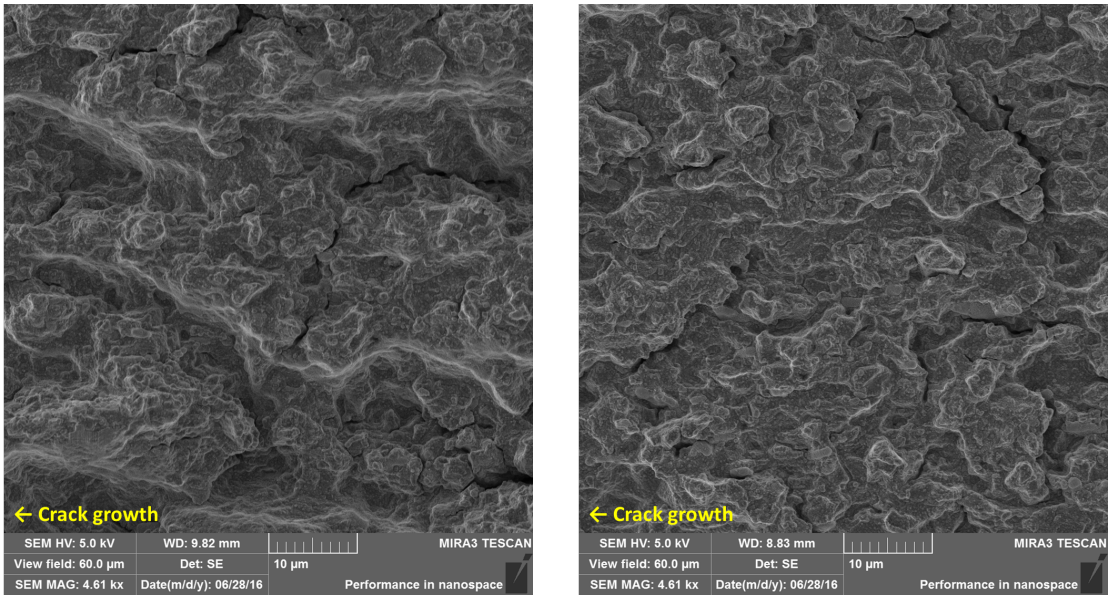

(a) Representative fighter spectrum at $\Delta K = 40$ MPa $\sqrt{m}$ showing transgranular crack growth with secondary cracking

(b) Representative transport spectrum at $\Delta K = 40$ MPa $\sqrt{m}$ showing transgranular crack growth with secondary cracking

Figure 4.47: Failure surfaces for FCG of representative aircraft spectra

4.6.3 Significant Findings

The representative fighter TMF spectrum showed significantly faster crack growth than the transport aircraft spectrum. Though reduced oxygen penetration is expected with the fighter aircraft spectrum compared to the transport spectrum, the subcycles of the fighter spectrum are large enough to provide crack growth increments that have a net result of shortening the overall life.

CHAPTER V

FATIGUE CRACK GROWTH MODELING

Accurate modeling of the propagation of cracks is critical to ensure safe operation of components. The thermomechanical environment of a turbine engine provides a particularly harsh environment that must be accurately accounted for. The focus of this project is on polycrystalline Ni-base superalloys that typically make up turbine engine disks and as such, a model was developed to better account for this harsh environment on these materials. The yield zone based fatigue crack growth model, MPYZ-TMF, discussed in Section 2.7.2.1 was utilized as a foundation due to its ability to account for load interaction effects (previous overloads and underloads and their effects on subsequent crack growth) with varying temperature. There are several limitations with the original model, namely an inability to evaluate representative spectra without simplification and a basic implementation of the effect of time at temperature on FCGR.

5.1 Model Overview

The overall modeling algorithm from the original MPYZ-TMF model, shown in Figure 5.1 was maintained for the updated version of the model. Specific modules highlighted were modified in the current project. These modifications include: adjusting how spectra are read into the program, the incorporation of additional specimen geometries, adjusting how the model handles temperature variations within the spectra for crack growth calculations, and calculation of how a TAZ accelerates crack growth. More specific discussion of the parts of the algorithm and code not addressed in this project can be found in the work of Barker [67].

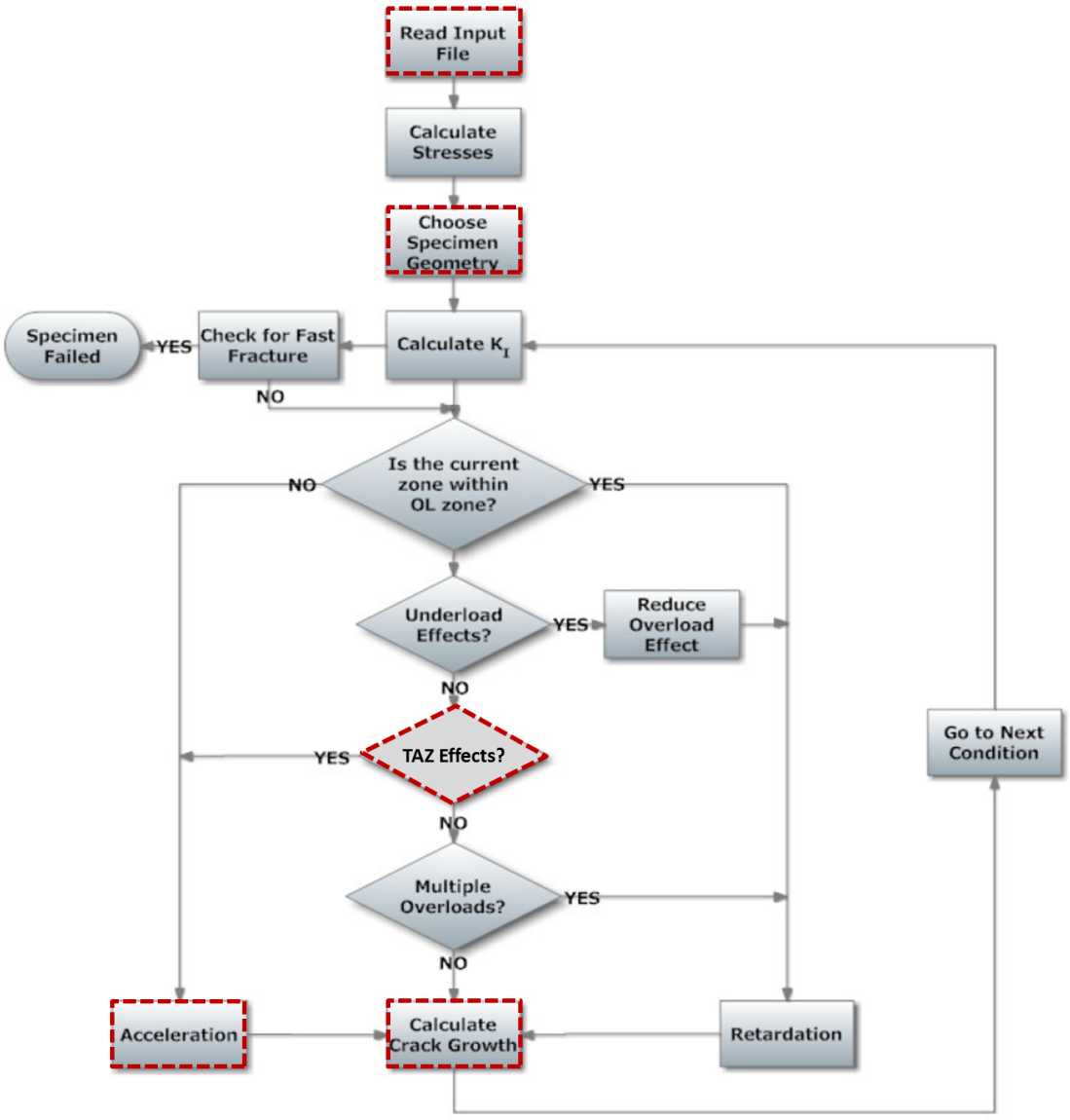

Figure 5.1: Overall modeling algorithm highlighting areas from the original model that were improved [67]

5.2 Model Inputs

Inputs to the model are provided by the user in two text files. The first describes the specimen geometry and experimentally determined material parameters. The other file contains the specific thermomechanical loading spectrum to be evaluated.

5.2.1 Specimen Geometry

The model developed in this project utilized the stress intensity of a crack to calculate the crack growth increment with either a Paris or Foreman-type crack growth law. As the stress intensity varies with loading and specimen geometry, to accurately predict a test specimen's crack growth during a loading spectra, the specimen specific stress intensity solution must be utilized. The original MPYZ-TMF model included calculations for five common geometries. The stress intensity solution for the MT-41 specimen was added during the current project. Its stress intensity solution is discussed in Section 3.2.2. The specimen geometries currently implemented in the model include:

1. Single Edge Notched Tension (SENT)
2. Single Edge Notched Bending
3. Center Cracked Tension
4. Double Edge Notched Tension
5. Compact Tension
6. MT-41 Cylindrical Specimen with Single Starter Hole

Any specimen dimensions needed for the stress intensity solution must be provided by the user in the input file. Additional specimen geometries and their corresponding stress intensity solution can be implemented at a later date as needed.

5.2.2 Temperature-dependent Material Data

In addition to specimen specific geometry, temperature-dependent material properties must be provided by the user. Except where specified later, material properties are linearly interpolated between the data at the three different temperatures provided by the user.

5.2.2.1 Yield Strength

The coefficients for a 2^{nd} order polynomial fit for how the yield strength, in MPa, varies with temperature, in degrees Celsius, are provided by the user. The equation takes the form:

$$\sigma_y = aT^2 + bT + c \tag{5.1}$$

In addition to the temperature-dependent yield strength, the ultimate strength and Poisson's ratio are also provided by the user at a single temperature. For the purposes of this project, the values utilized were taken at 26°C. The coefficients for yield strength, ultimate strength, and Poisson's ratio used for this project were obtained from the MMPDS [15].

5.2.2.2 Crack Growth Rate Parameters

The temperature dependent crack growth rate of the material must also be provided by the user. As discussed in Chapter 2, since the fatigue crack growth rate at elevated temperature is dependent on loading frequency, care must be taken to utilize FCG data where the embrittling effects of time at temperature can be minimized (i.e. at fast frequency, in an inert environment, or in a vacuum). Paris and Forman parameters fit to the experimental data collected in this project were used for the model. The parameters are shown in Table 5.1. Parameters for the fit to crack growth data must be derived from data in units of MPa $\sqrt{m}$ for ΔK and mm/cycle for the crack growth increment per cycle, da/dN.

Table 5.1: Fatigue crack growth rate parameters, ΔK in units of MPa $\sqrt{m}$ and da/dN in units of mm/cycle

Temperature	Paris Equation		Forman Equation		
°C	C_p	n_p	C_f	n_f	K_C' MPa $\sqrt{m}$
26	1.85 x 10^{-9}	3.26	2.40 x 10^{-7}	3.1	116
427	7.10 x 10^{-9}	2.95	1.31 x 10^{-6}	2.7	119
650	5.32 x 10^{-7}	1.93	3.93 x 10^{-4}	1.2	95

5.2.2.3 Fracture Toughness

Values for the temperature dependent fracture toughness of IN 718 at room temperature and 427°C were utilized from the work of Mills et al. [80]. The fracture toughness at 650°C was determined by extrapolating Mills et al. data using a second order polynomial. The fracture toughness values utilized are shown in Table 5.2.

Table 5.2: Fracture toughness values [80]

Temp °C	Fracture Toughness MPa $\sqrt{m}$
26	131
427	126
650	75

5.2.3 Threshold Stress Intensity Range

Since spectrum segments of small stress intensity range are not expected to be able to extend a crack, a threshold stress intensity range is employed. A threshold stress intensity range of 8 MPa $\sqrt{m}$ was utilized for the model based on the work of Clavel and Pineau with IN 718 at 550°C [81].

5.2.4 Load Interaction Parameters

Load interaction parameters to fit Equations 2.10, 2.11, and 2.13 were not specifically determined for IN 718 during this project. Parameters were utilized from the work of Barker et al. on a similar Ni-base superalloy, Inconel 100 [67]. Inconel 100 is

also an equiaxed fine grained Ni-base superalloy with similar strength to IN 718 so use of its parameters for load interaction effects should sufficiently coincide with the performance of IN 718 . The load interaction parameters are shown in Table 5.3.

Table 5.3: Load interaction parameters used for modeling [67]

Load Interaction Parameters	
A	1.0
B_a	3.85 x 10^{-5}
B_b	1.99
Y	0.0
Z	0.5

5.2.5 Temperature Affected Zone Size Fitting Parameters

Parameters to describe the growth of the TAZ must also be provided by the user to account for the weakening effects of time spent at elevated temperature on FCGR. The TAZ size parameters determined in Chapter 4 and utilized in Equation 4.1 were utilized for the model and are shown in Table 5.4.

Table 5.4: TAZ size parameters

C	0.291	$(\text{sec})^{-n_1}$ $(\text{MPa}\sqrt{m})^{-n_2}$
n_1	0.48	
n_2	2.6	
n_3	0.38	

5.2.6 Temperature Affected Zone Acceleration Parameters

The user must also provide a parameter to describe the impact of a TAZ on FCGR. The TAZ acceleration exponent determined in Chapter 4 and utilized in Equation 4.2 of D = 6.0 and p = 0.5 were utilized for the model.

5.2.7 Specimen Geometry and Material Parameter Input File

The input file specifying the specimen geometry and experimentally determined material parameters is provided by the user as a text file and a sample is shown in Figure

5.2 with the corresponding values used in this project.

```
Specimen Geometry (mm)
width = 38.1
thickness = 2.54
initial crack length = 8.62
radius = 0
cross sectional area = 96.77

Temperature Values
Temp1 = 27
Temp2 = 427
Temp3 = 649

Material Strength vs Temperature Coefficients (2nd Order Poly)
YSvTa = -2.000e-4
YSvTb = -1.076e-1
YSvTc = 1.016e3
Ultimate Strength = 1280
Poissons ratio = 0.3333333

Paris Parameters
CP1 = 1.82e-9
CP2 = 7.10e-9
CP3 = 5.32e-7
nP1 = 3.26
nP2 = 2.948
nP3 = 1.9305

Foreman Parameters
CF1 = 2.40e-7
CF2 = 1.31e-6
CF3 = 3.93e-4
nF1 = 3.1
nF2 = 2.7
nF3 = 1.2
Kcp1 = 116
Kcp2 = 119
Kcp3 = 95

Fracture Toughness
Kc1 = 131
Kc2 = 126
Kc3 = 75

Threshold DK = 8

Load Interaction Parameters
A = 1.0
B_a = 3.85e-5
B_b = 1.99
Y = 0.0
Z = 0.5

Temperature Affected Zone Parameters
C = 0.291
n1 = 0.48
n2 = 2.6
n3 = 0.38

Temperature Affected Zone impact on FCGR
D = 6.0
p = 0.5
```

Figure 5.2: Input file specifying specimen geometry and material parameters

5.2.8 Thermomechanical Spectra

The second text file provided by the user describes the spectrum to be evaluated. As Figure 2.13 shows, a representative TMF spectrum for a turbine engine is not a simple constant amplitude loading cycle executed isothermally. There are ever changing relationships between load and temperature. The original MPYZ-TMF model lacked the ability to evaluate a representative TMF spectrum without first converting it into complete cycles (a load and unload) executed isothermally. When this is done, loading sequence effects are lost. Additionally, the question of what temperature to assign to each complete cycle remains since the loads for the cycles could have been originally executed at different temperatures.

The model developed in this project has the ability to allow the user to enter a TMF spectrum on a point-to-point basis. The user provides each point based on the time it occurs (in seconds), the load at that time (in newtons), and the temperature at that time (in degrees Celsius) in a text file for each specific time point in the TMF spectra to be evaluated as Figure 5.3 shows.

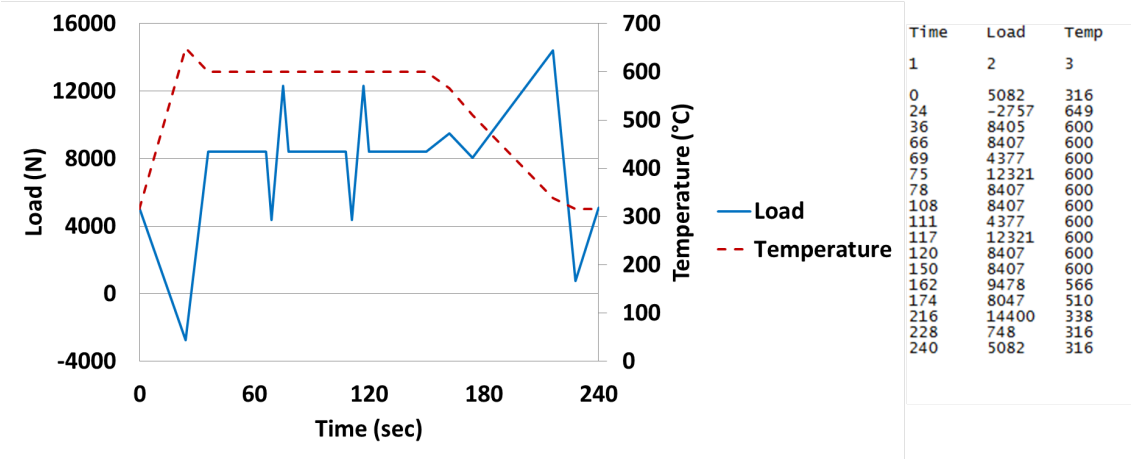

Figure 5.3: Sample TMF spectra and corresponding model input

5.3 Model Algorithm

5.3.1 Spectrum Input Impact on Crack Growth Increment and Load Interaction Effects

Care must be taken to ensure crack growth calculations are accurately executed when using the point-to-point spectrum method discussed above. As the model traverses from point-to-point in the TMF spectrum, it assigns a maximum stress intensity and minimum stress intensity for that segment. It then makes adjustments for load interaction effects in the same way as the original model does (i.e. retarding crack growth if there were previous overloads, or reducing retardation effects if there was a previous underload) and calculates a crack growth increment for that segment using the user selected Paris or Foreman crack growth model. However, the calculated crack growth increment is only allowed to contribute to the crack growth prediction if the load is increasing in the current segment of the spectrum. If the load is decreasing or constant, the crack growth increment is set equal to zero for that segment.

The model uses the average temperature of the segment for calculation of the crack growth increment. This was based on the discussion of Section 4.4.2 which stated that for an OP TMF cycle, the temperature at maximum load is not representative of the crack growth response. Additionally, for a given stress intensity range, as the temperature increases, the crack growth rate also increases. Utilizing the maximum temperature of the segment would be too conservative. Therefore, an intermediate temperature between the segment maximum and minimum would represent the crack growth response best. Lacking the resources to specifically explore an effective temperature for a TMF cycle, the average temperature of the segment was utilized.

Since the previous version of the MPYZ-TMF model required the user to enter a full cycle (minimum-to-maximum-to-minimum load) at a isothermal temperature and a frequency and the model developed during this project uses a point-to-point

methodology, a sample isothermal spectrum with an overload was run using both methods to ensure that the point-to-point methodology still accurately accounted for the load interaction effects. Figure 5.4 shows a good correlation between the full cycle and point-to-point spectrum input methods. Therefore, the methodology used to account for load interaction effects was left unmodified for the model developed in this project.

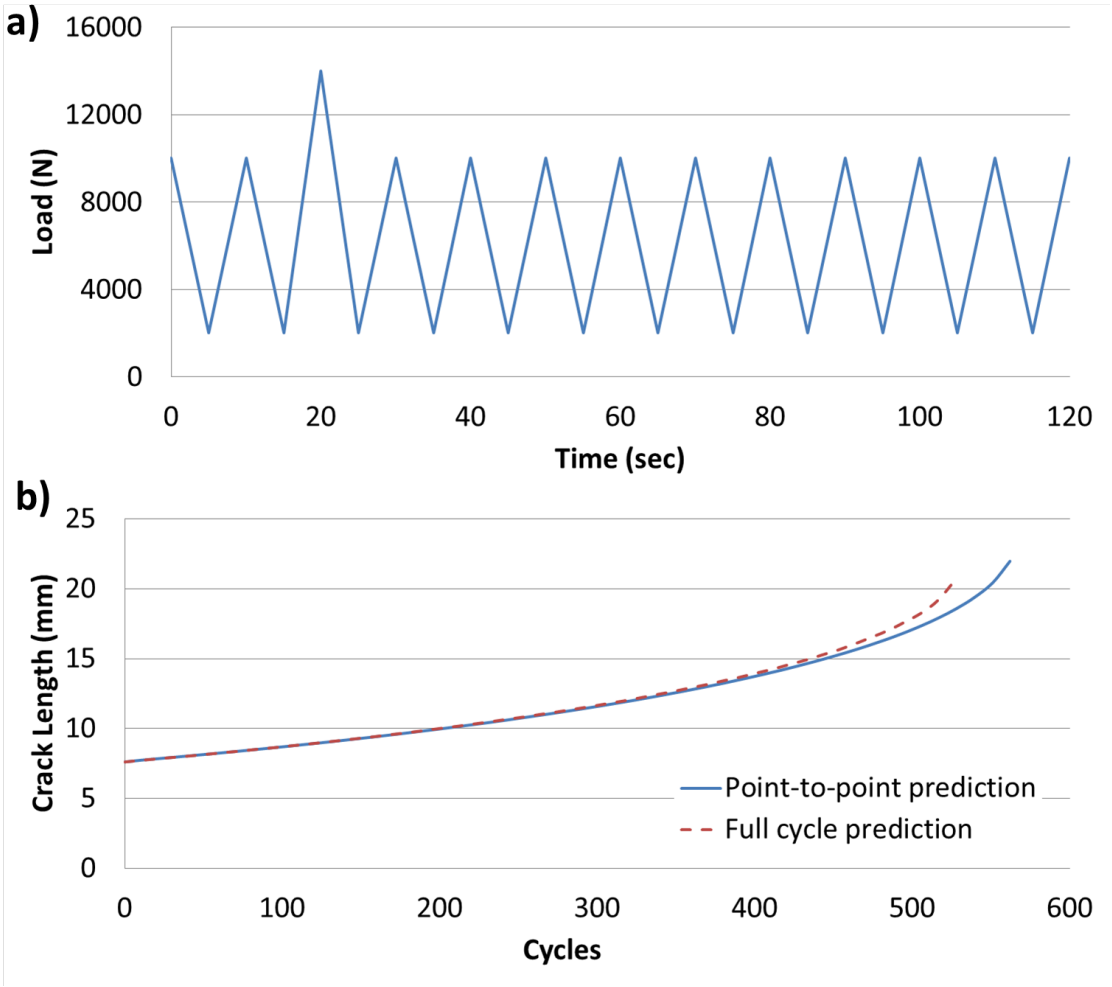

Figure 5.4: Comparison of a point-to-point and full cycle modeling methodology: a) sample isothermal spectra at 650°C repeated until predicted failure, b) crack growth prediction of the original MPYZ model (full cycle) and the model developed with this project (point-to-point)

5.3.2 Limits of Temperature Affected Zone Development

Based on the experimental observations discussed in Chapters 2 and 4, a TAZ is expected to occur only under certain conditions and therefore, several limits were imposed. Specifically, it is assumed that TAZ does not develop when:

1. The temperature is below 500°C.
2. The stress intensity is less than or equal to zero.
3. The stress intensity is less than or equal to 75% of any of the previous three spectrum points.

These limits are justified from the experimental observations and the discussion below. Experiments shown in Section 4.4.1 indicated that when a crack is held in compression at elevated temperature, no impact on FCGR will result. This result drove the selection of lower limit of TAZ development at a stress intensity of zero. Since oxidation penetration is allowed to more easily occur under tensile strains, a more accurate lower limit would specify the point at which the crack tip starts to open. This could be accounted for by a method such as Newman's crack tip opening displacement [63], however, since the foundation of the MPYZ-TMF is a yield zone approach, a limit of only positive stress intensities was utilized.

Additionally, the model looks back several segments within the spectrum to ensure any unloading effects are accounted for in mitigating TAZ development. The model looks back at the stress intensities of the three previous segments of the spectrum to account for any portions of the loading spectrum that may have a general downward trend over several points. For the spectra utilized in this project, looking back three points satisfied the ability to accurately account for the unloading effect on TAZ development. Looking back three segments is not a user option, but can be changed with future iterations of the model.

5.3.3 Spectrum Partitioning for Temperature Affected Zone Calculation

Due to the complex nature of TMF spectra, it is probable that segments of the spectra will traverse the limits of when TAZ is expected to develop discussed above. To ensure that the model accounts for the parts of the segments of the spectrum expected to develop a TAZ, the segments were partitioned in to five equal parts, or subsegments. The number of subsegments is not user selectable but can be changed with future iterations of the model. The selection of five is arbitrary but was selected for a number of reasons. First, it allowed for a segment that traverses the limits discussed above to still develop TAZ during the portions of the segment before those limits are reached. Second, the empirical fit for TAZ size was fit to experimental data collected from hold durations from 30 to 18200 seconds. For the realistic spectra tested in this project, having too many partitions would shorten the partitions to durations not as well fit by the TAZ empirical fit. Lastly, increasing the number of partitions is less computationally efficient. Figure 5.5 shows the TMF spectra from Figure 3.14 highlighting the portions of the spectra the model predicts will develop TAZ based on the limits discussed in the previous section.

Once the segments are partitioned, an expected TAZ for each partition in mm is calculated:

$$TAZsize_{partition} = C\Delta t^{n_1} {K_{partition}}^{n_2} e^{n_3 \frac{-Q}{RT_{partition}}} \tag{5.2}$$

where Δt is the partition's duration in seconds, $K_{partition}$ is the stress intensity at the end of the partition in MPa $\sqrt{m}$, and $T_{partition}$ is the temperature at the end of the partition in Kelvin. The fitting parameters C, n_1, n_2, n_3 are provided in Table 4.4. The activation energy, Q, utilized is discussed in Section 4.3.5, and R is the universal gas constant.

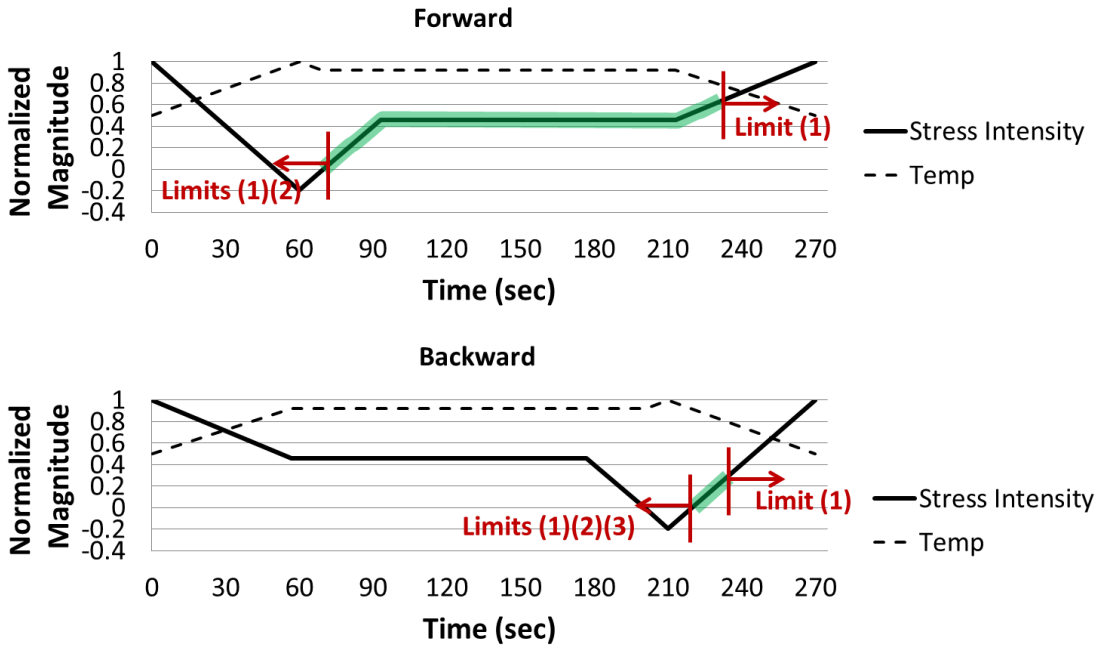

Figure 5.5: Sample TMF spectra highlighting where the model predicts TAZ will develop base on the limits discussed in Section 5.3.2

5.3.4 Temperature Affected Zone Accumulation

As a specimen spends time in tension at elevated temperature, a TAZ will develop. The empirical model, Equation 4.1, was established from observations after holds of a crack tip without an existing TAZ. However, a TMF spectrum may subject the crack to cases where a TAZ is expected to be developed while an existing TAZ is present ahead of the crack. Understanding how the TAZ will continue to develop in these situations is critical. One approach is to design a discriminating experiment to understand this influence. One possibility is an approach similar to that discussed in Section 3.4.3.2 except the specimen would be subject to a second tensile hold of differing parameters (hold stress intensity, duration, and temperature) immediately after the first hold and prior to any cycling to see if a trend could be observed in TAZ accumulation. A schematic of this approach is shown in Figure 5.6.

Since oxidation is a primary contributor to the development of a TAZ, a form for the addition of portions of TAZ was approached similar to the parabolic oxygen

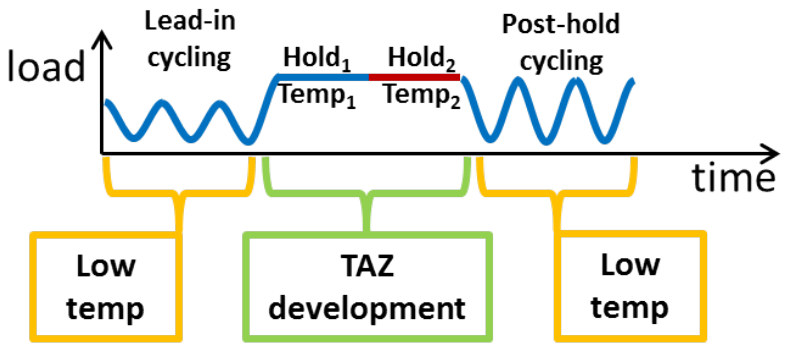

Figure 5.6: Suggested spectrum to identify the characteristics of TAZ accumulation

diffusion law used by Ghonem et al. as shown in Equation 2.2 [25]. In effect, the degrading species needs to diffuse through existing TAZ to further develop the TAZ and each new portion of TAZ can only contribute a part of the TAZ estimated from single hold tests. The summation of TAZ portions is described by:

$$TAZsize_{newtotal} = TAZsize_{existing} + \frac{TAZsize_{newsegment}}{(TAZsize_{existing} + 1)^{TAC}} \tag{5.3}$$

where TAZ size is in mm and TAC is the TAZ accumulation coefficient. The TAC was chosen as 2.0 for this project. Figure 5.7 shows how the percentage of contribution to an existing TAZ of the predicted TAZ for a new portion diminishes as the existing TAZ gets larger. When the existing TAZ is small, a larger percentage of new TAZ portion will contribute to extending the existing TAZ, whereas, when the existing TAZ is larger, a smaller percentage of the new TAZ portion will contribute to extending the TAZ.

It is important to point out that using this method to account for TAZ accumulation is sensitive to the number of partitions used for each segment. For example, when increasing from the five partitions used for this project to a higher number, there is a higher number of TAZ segments to account for and as such the overall TAZ ends up larger resulting in faster crack growth and a more conservative prediction. This dependence on number of partitions is not ideal, but is sufficient when the calibrating

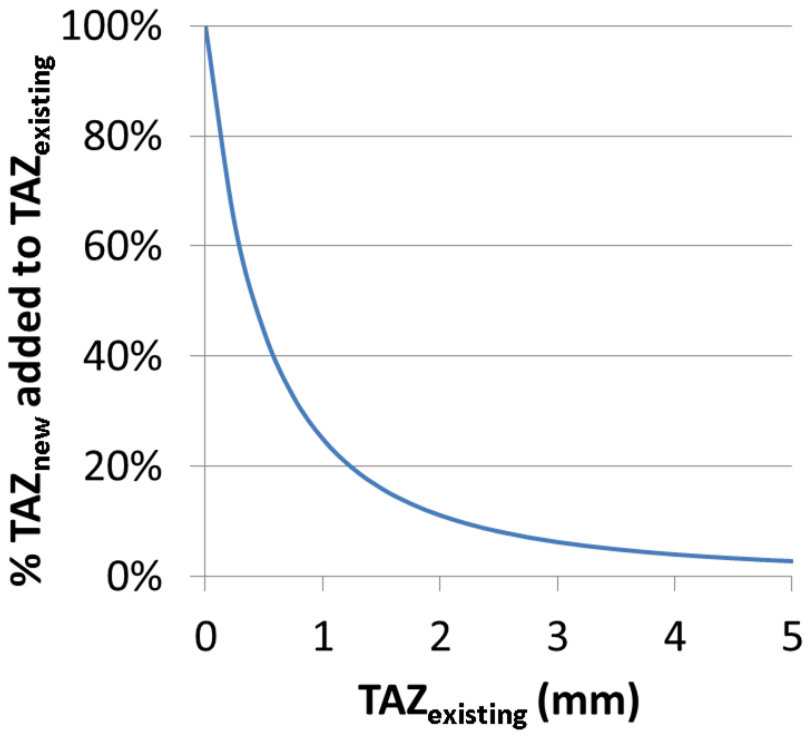

Figure 5.7: Percentage of a new TAZ portion that will contribute to the existing TAZ

spectrum is similar to the spectrum trying to be predicted. Additionally, it had the advantage of being easily applied to any spectrum the user inputs.

Other methods of partitioning to account for TAZ development are possible, but have their own limitations. For example, setting each partition to a fixed duration could require smoothing of the spectra so that the input spectrum points coincide with the fixed spacing of the partitions. Another possible TAZ accumulation methodology would be to base it on the rate of TAZ development. The rate of TAZ development was used by Lundstrom et al. but failed to account for existing TAZ [59]. As stated previously, the existing TAZ will impact any future TAZ accumulation and must be accounted for.

5.3.5 Impact of Temperature Affected Zone on Crack Growth Increment

Any new TAZ developed during the current segment is accounted for before the TAF calculation for that segment. The crack growth increment predicted by the Paris or Forman equations, and adjusted for any load interaction effects, is multiplied by the TAF. This new value is the final crack growth increment for the segment and is added to the existing crack length for a new total crack length.

An important feature of the equation used to calculate the TAF, Equation 4.2, is its ability to account for the transition from a state of plane strain to a state of plane stress as the crack grows. The model adjusts the plastic zone size calculation, shown in Equation 2.8, based on this transition.

5.3.6 Temperature Affected Zone Consumption by Crack Growth Increment

As the crack grows an increment forward, it consumes a commensurate amount of the existing TAZ, reducing its value. The new crack length and existing TAZ are used for the next segment of the spectrum. The crack propagates in the model until the fracture toughness of the specimen is reached.

5.4 Model Output

When the model predicts failure, it notifies the user of the number of segments, number of spectrum repeats, and the final crack length at failure. Predictions from the model are output as a text file. The user can specify the number of data points to output and the model evenly samples the predicted crack growth and outputs the requested number of data points. The primary parameters the model outputs include the spectrum repeats count and the crack length. The secondary parameters output include, the maximum, minimum, and range of stress intensity, the crack growth increment, the TAF and the TAZ. It is important to note that all output points are specific to the number of data points the user requests to be output, meaning that

the values are tied to only one specific segment within the spectrum, not the entire spectrum. This sampling technique is sufficient for tracking the crack length as the cycle count increases and allows for the user to check to ensure the other parameters are being calculated as expected. If the user wants a full picture of every segment, they need only request the number of output points equal to the number of segments at failure.

5.5 Model Predictions

Fatigue crack growth predictions, in the form of crack growth curves, for the isothermal and TMF spectra were conducted to exercise the model.

5.5.1 Fundamental Fatigue Crack Growth

As shown in Figure 2.4, the frequency of loading plays a significant role in the FCGR of IN 718. Though the primary utilization of a TAZ is to account for temperature interaction effects (i.e. where temperature history affects crack growth at different temperatures), the model was exercised to evaluate how well it could also account for frequency effects for isothermal loading. As discussed in Section 3.4.2, isothermal FCG tests were conducted at fast frequency to attempt to avoid any influence of the weakening effect ahead of the crack tip of elevated temperature exposure. As discussed in Section 4.1, these effects could not be completely eliminated for the test at 650°C. Since the Paris and Forman fits to this data were used as input into the model, this data, which inherently has some elevated temperature exposure weakening effect already present will compound with the effect of any TAZ developed leading to a faster than expected FCGR. Figure 5.8 shows how if the TAZ effects are not utilized, the prediction fits the experimental data well as expected. If the TAZ effects are utilized, even with the fast cycling, some TAZ can develop leading to faster crack growth.

Figure 5.9 shows the impact of frequency effects from a different perspective. A

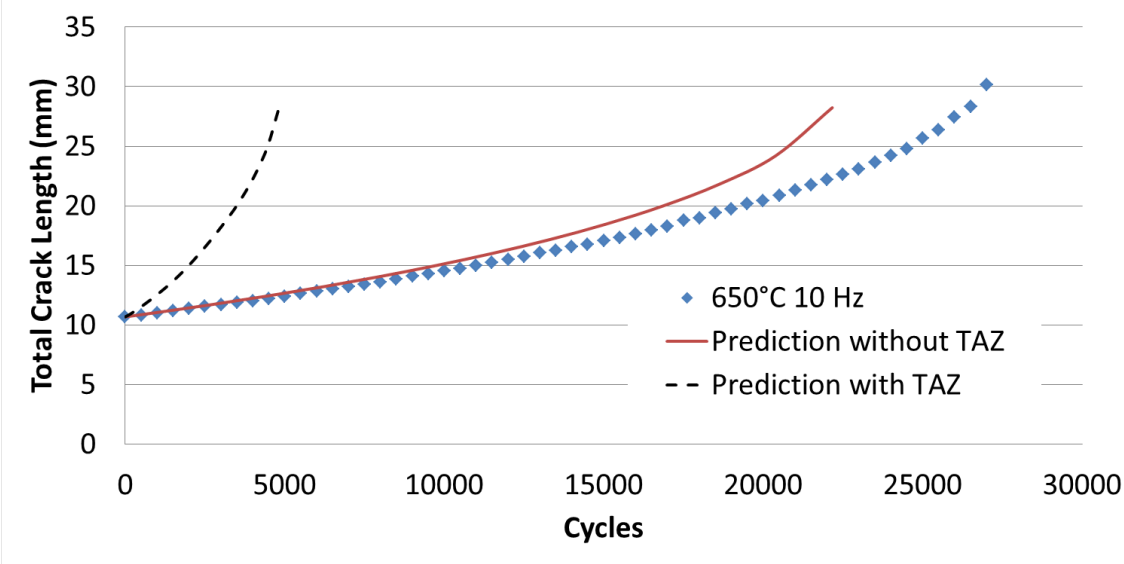

Figure 5.8: Model predictions of crack growth for isothermal FCG at 10 Hz at 650°C comparing the predictions with and without TAZ effects

comparison of the FCGR curve for the prediction is made to the experimental data at 10 Hz along with the Forman crack growth equation fit and shows that the crack growth prediction without TAZ effects matches exactly the Forman equation fit as expected. The prediction with TAZ effects shifts the curve up indicating faster crack growth. A small segment of slow frequency (0.1 Hz) isothermal cycling at 650°C at a high stress intensity range with the same loading ratio as the fast frequency loading (R = 0.05) (data extrapolated back to lower stress intensity ranges as indicated by the dashed red line) was accomplished and the experimental data is also presented in Figure 5.9 along with the model's prediction. For the slower frequency loading, the model does a better job of accounting for the frequency effects though the prediction is still conservative.

As discussed in Section 5.2.2.2, ideally, crack growth data that has not been influenced by the weakening effect of exposure to time at temperature should be used to ensure the TAZ calculated in this model is not compounding with the TAZ inherent in the fundamental crack growth data entered by the user.

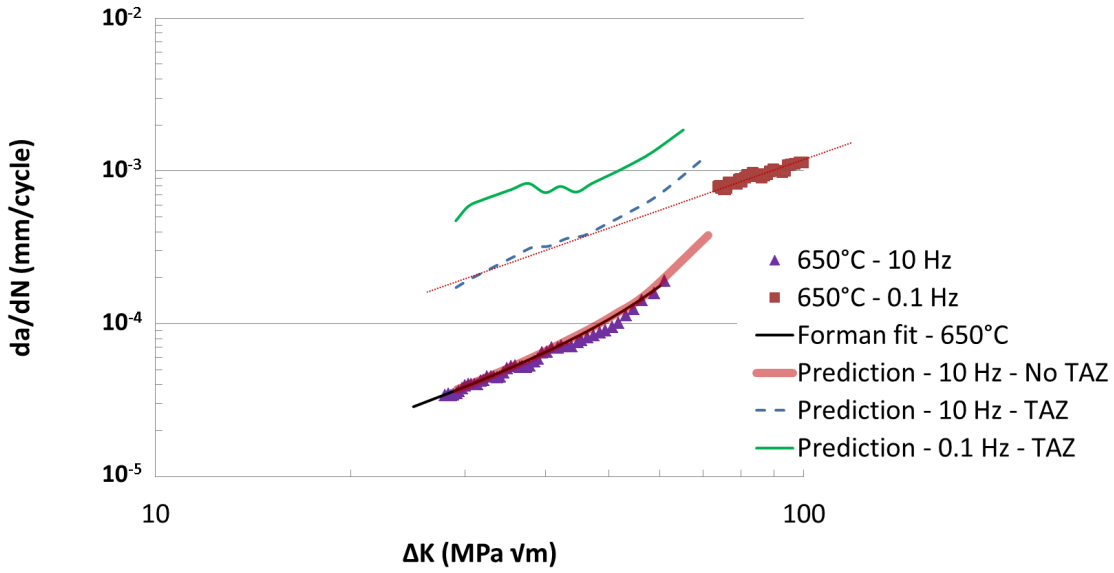

Figure 5.9: Model predictions of FCGR for isothermal cycling at 10 Hz at 650°C comparing the predictions with and without TAZ effects to experimental data and the Forman crack growth equation fit

5.5.2 Tensile Hold Sequence Effects on Triangular Waveform Out-of-Phase Thermomechanical Fatigue Crack Growth

5.5.2.1 Prediction without Tensile Hold

The prediction of life for a triangular waveform OP TMF spectrum without hold as shown in Figure 3.13 is shown in Figure 5.10. The prediction is non-conservative in this case. Similar to the Backward OP TMF spectrum shown in Figure 5.5, only a limited portion of the spectrum is expected to produce a TAZ and the model predicts that the TAZ is completely consumed every cycle by the crack growth increment. Without any overloads or underloads, this leaves the fundamental crack growth prediction as the driving force for the overall crack growth prediction. Since Paris or Forman equations are implemented using the average temperature of the segment for model calculations and the FCGR is slower at lower temperatures, this indicates that selection of a temperature value higher than the average would be necessary to produce a better prediction. However, even when the model was run utilizing the maximum

temperature of the segment, essentially predicting isothermal crack growth at 650°C, the prediction was still non-conservative as Figure 5.10 shows. This indicates that the slow cycling, TMF nature of this spectrum has not been fully captured by this model. More significant TAZ accumulation, or a larger TAF for the TAZ produced each cycle would be required to predict faster crack growth. Despite the limitations just discussed, the average temperature for a segment for the Paris or Forman crack growth calculations was utilized for model calculations since the predictions better fit the more representative TMF spectra expected to produced significant amounts of TAZ in this project.

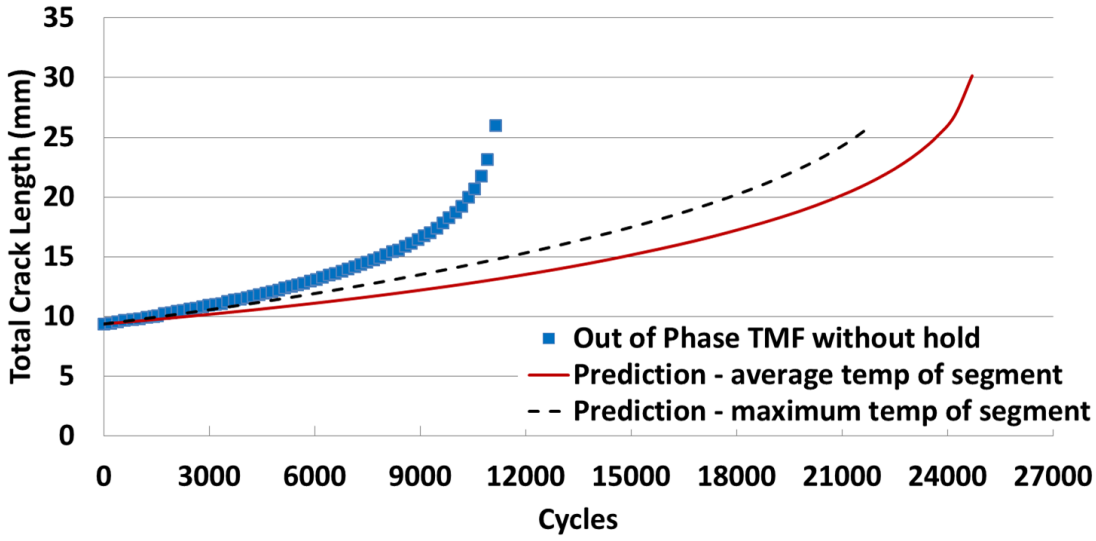

Figure 5.10: Model predictions for the crack growth of the triangular OP TMF spectrum utilizing both the average temperature of each segment and the maximum temperature for each segment compared to experimental data

5.5.2.2 Prediction with Tensile Hold

Figure 5.11 shows predictions for the crack growth of the triangular OP TMF spectra, as shown in Figure 3.14. The forward triangular spectra is expected to allow for more TAZ to be produced and as such has a higher TAF. The model provides a good fit to the experimental data. On the other hand, the backward spectrum, similar to the triangular OP TMF spectrum of Section 5.5.2.1, predicts limited TAZ development

and a correspondingly non-conservative life indicating an under-prediction of the slow cycling at elevated temperature effects on FCGR.

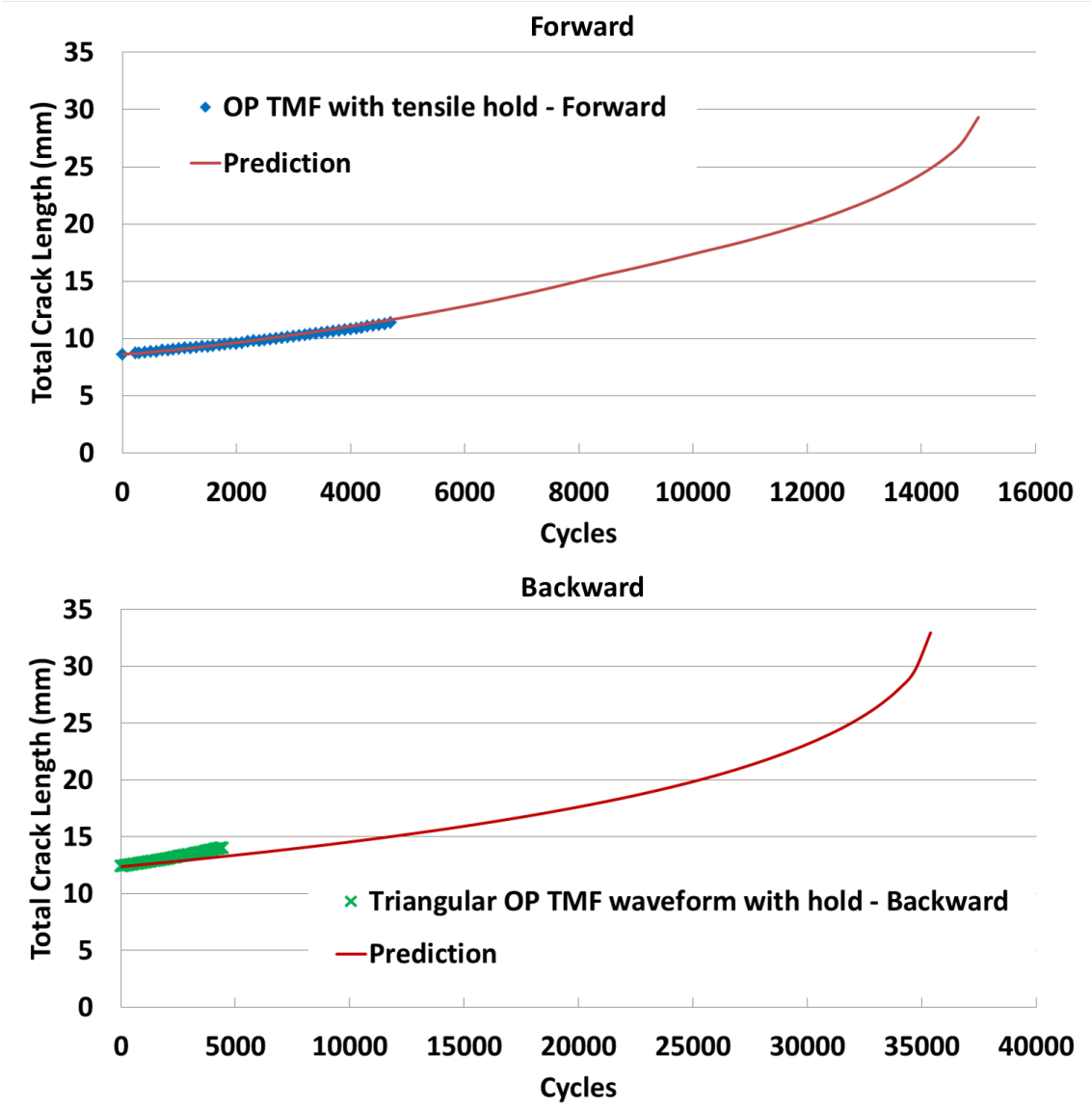

Figure 5.11: Model predictions for the crack growth of the forward and backward triangular OP TMF spectrum with tensile hold compared to experimental data

Since the experimental tests for the forward and backward spectra were executed in succession on the same specimen, direct comparison of their crack growth predictions are not available. However, a prediction of the crack growth of the backward

spectra, executed as if it started at the same initial crack length as the forward spectra is shown in Figure 5.12. It shows that the model correctly accounts for the effects of tensile hold sequence within a spectra.

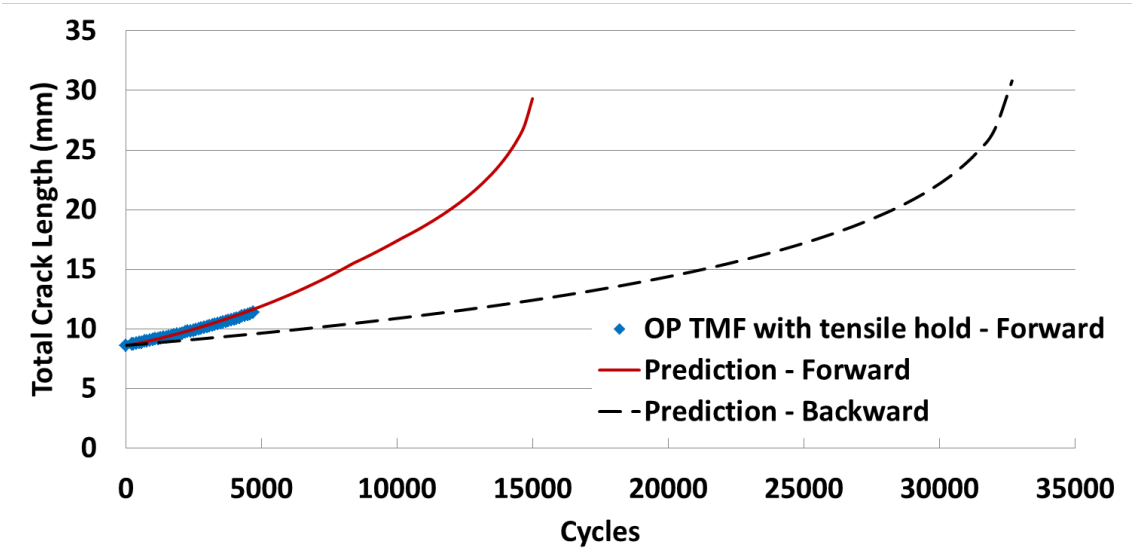

Figure 5.12: Model predictions for the crack growth of the forward and backward triangular OP TMF spectrum with tensile hold beginning with the same initial crack length compared to experimental data for the forward spectrum

5.5.3 Consortium Developed Thermomechanical Fatigue Spectra With and Without Compressive Hold

The model prediction for which portions of the engine consortium developed representative spectrum are expected to produce TAZ is shown in Figure 5.13. Additionally, the prediction for the crack growth of the spectrum with and without compressive hold is shown in Figure 5.14. A conservative life is predicted compared to the experimental data for the SENT specimen execute in load-control. The model shows the two consortium developed spectra, with and without compressive hold, as essentially the same spectra since the compressive hold does not contribute to TAZ development.

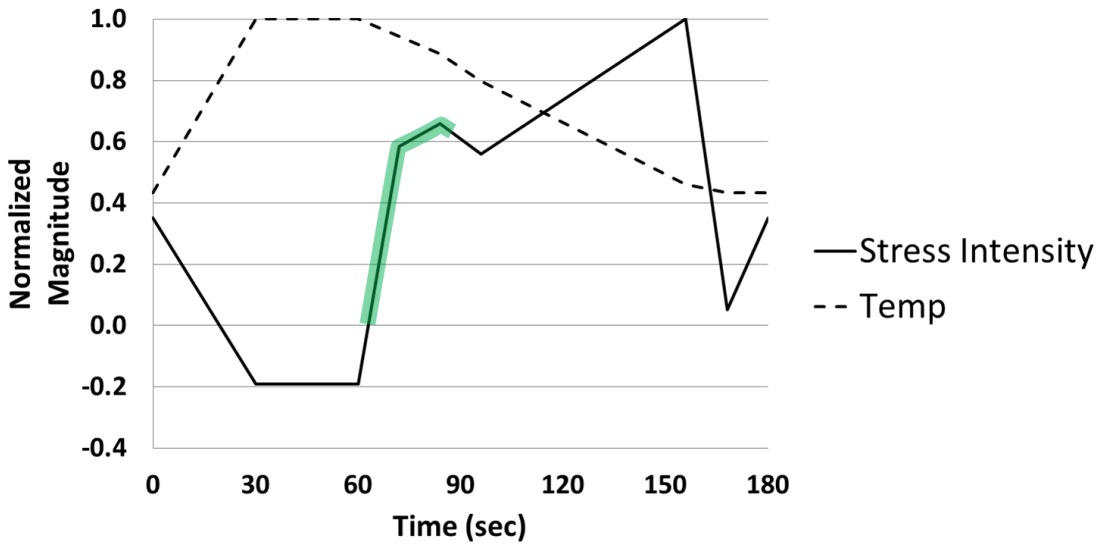

Figure 5.13: Consortium developed representative spectrum highlighting where the model predicts TAZ will develop

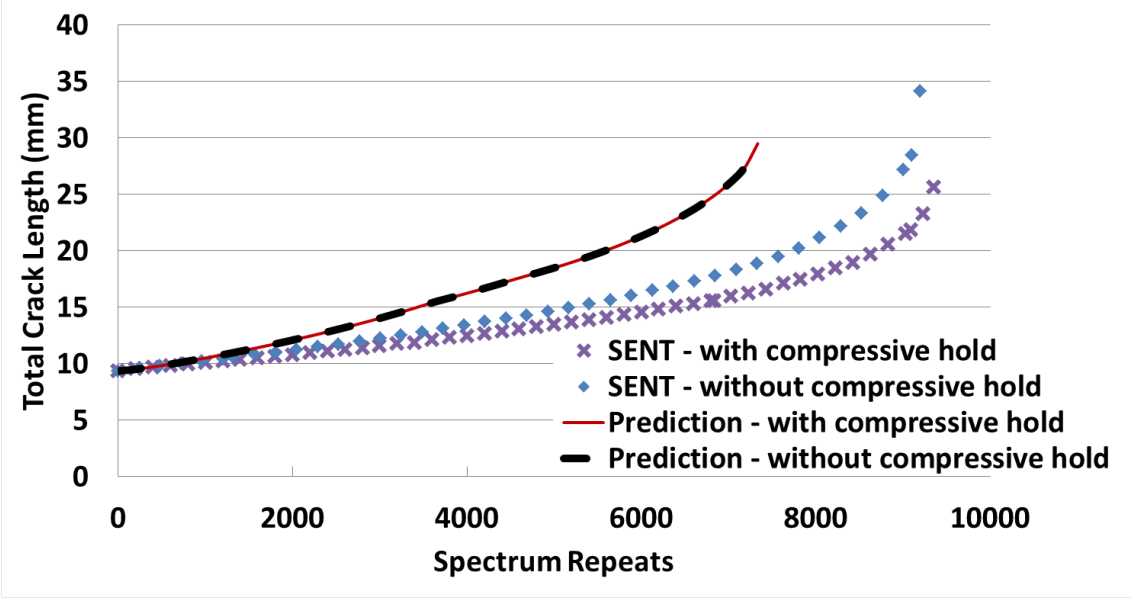

Figure 5.14: Model predictions for the crack growth of the engine consortium developed representative spectrum with and without compressive hold compared to SENT specimen experimental data

A prediction of the same consortium developed OP TMF spectrum with compressive hold run in displacement-control with the MT-41 specimen also results in a good prediction as Figure 5.15 shows. The prediction falls well within any scatter that may be expected from a typical FCG test. This prediction shows how the modeling

methodology employed for TAZ development and its impact on FCGR can effectively transition to other specimen geometries or test control methodologies.

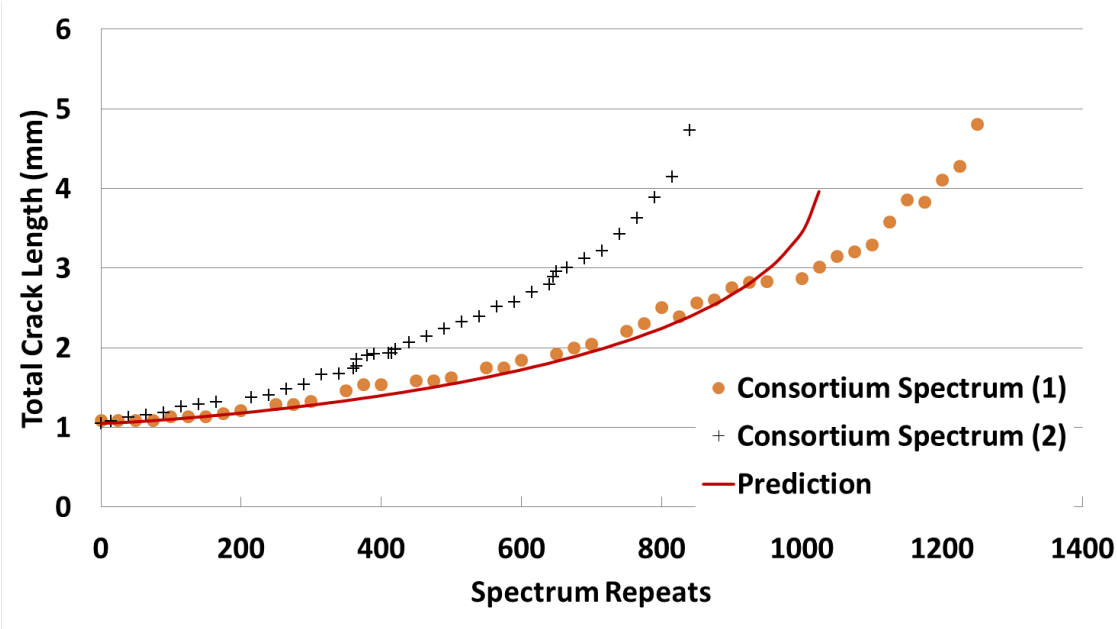

Figure 5.15: Model prediction for the crack growth of the OP TMF spectra with compressive hold compared to MT-41 experimental data

5.5.4 Representative Fighter and Transport Aircraft Turbine Engine Spectra

Predictions for the representative fighter and transport aircraft spectra were also executed. Figure 5.16 shows how the model accurately captures the portions of the representative fighter and transport spectra expected to produce a TAZ based on the discussion in Section 5.3.2. Additionally, Figure 5.17 shows how the model produces a good prediction for the fighter spectrum that is shorter than the conservative prediction for the transport spectrum coinciding with the experimental results. The model accurately predicts a larger TAZ accumulation for the transport spectrum, but the lack of significant subcycles during the hold leads to a longer life when compared to the fighter spectrum.

To highlight the significance of time spent at temperature on FCGR, a prediction of the representative fighter aircraft spectrum without TAZ effects was executed, as

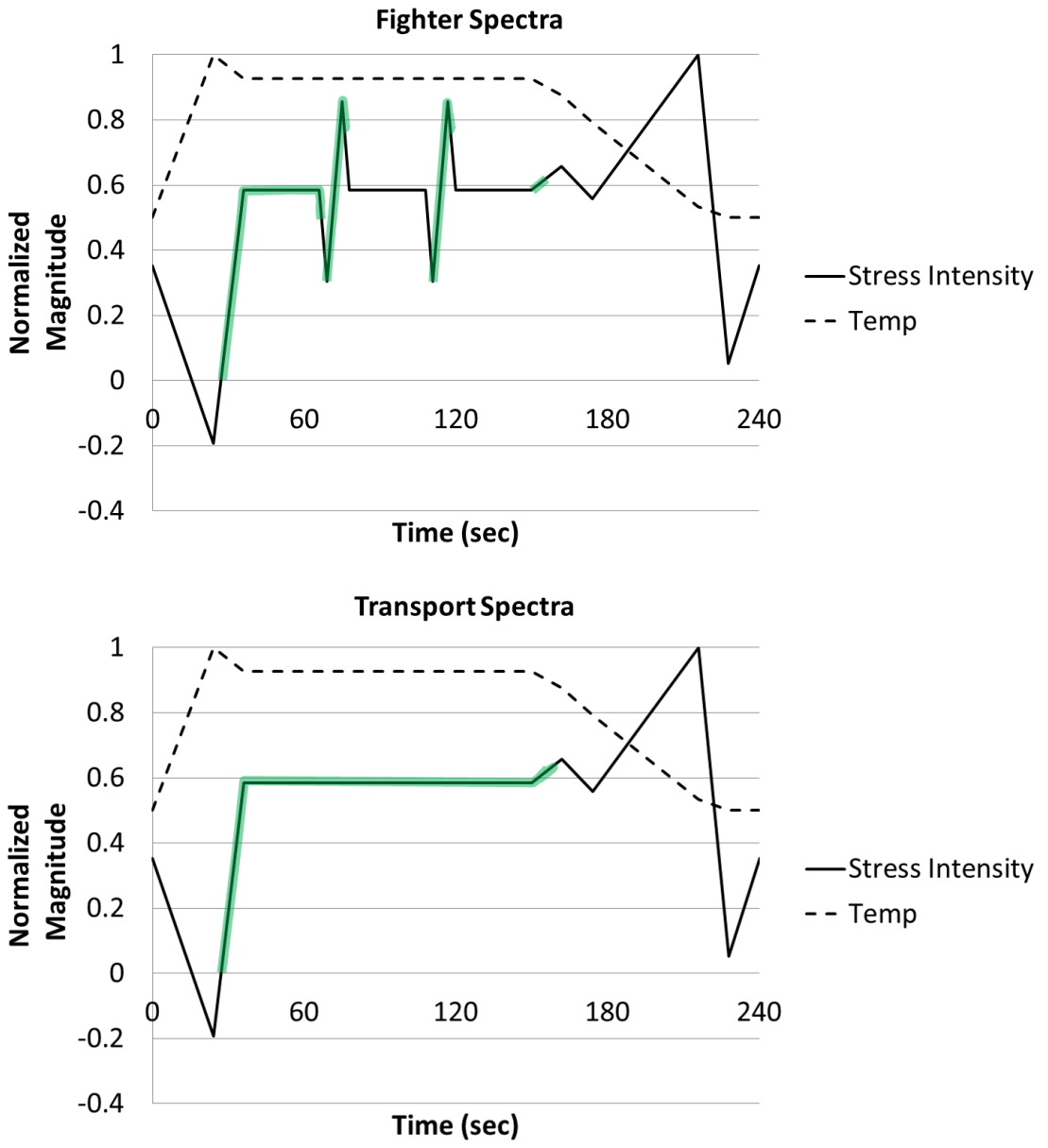

Figure 5.16: Representative fighter and transport aircraft spectra highlighting where the model predicts TAZ will develop

shown in Figure 5.18. Even with accounting for load interaction effects, the prediction is extreemly non-conservative. This highlights the significance of being able to accurately account for the temperature interaction effects on FCGR.

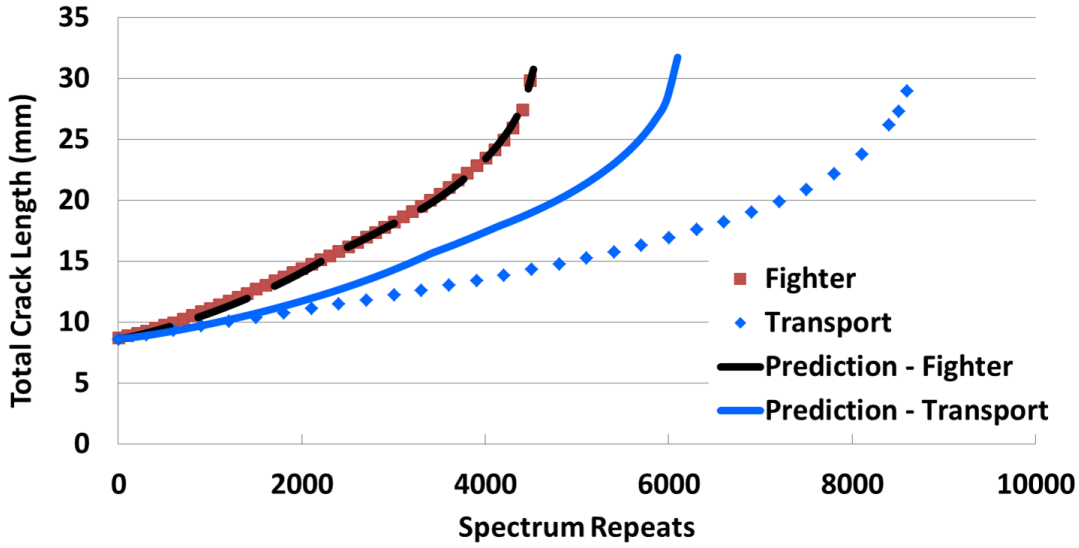

Figure 5.17: Model prediction for the crack growth of the representative fighter and transport aircraft turbine engine disk spectrum compared to experimental data

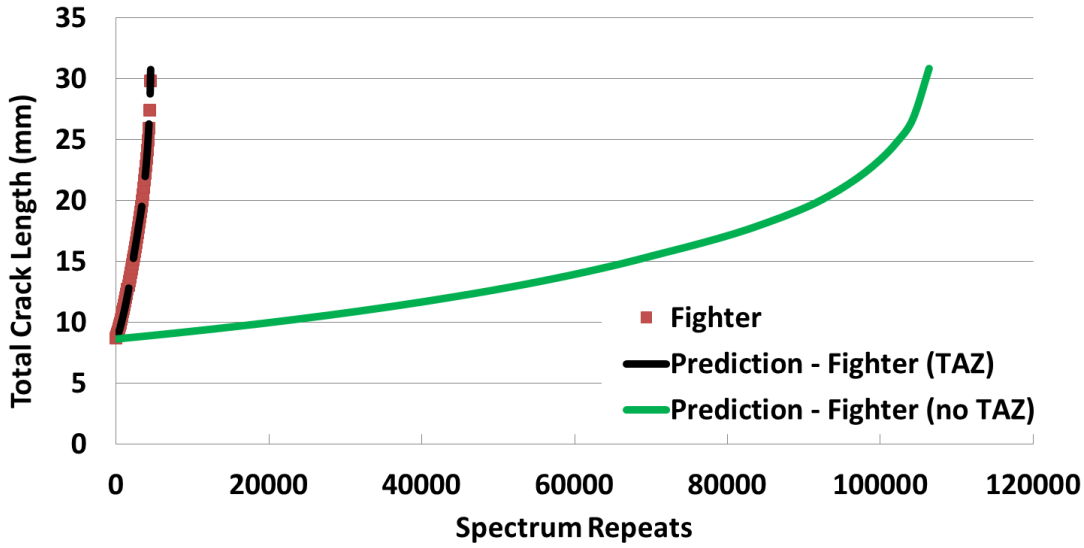

Figure 5.18: Model prediction for the crack growth of the representative fighter aircraft turbine engine disk spectrum with and without TAZ effects compared to experimental data

5.5.5 Evolution of the Temperature Affected Zone and the Temperature Acceleration Factor

A significant portion of the modeling effort was dedicated to capturing the development of the TAZ. Figure 5.19 shows the evolution of TAZ for the spectra predicted

to develop increasing TAZ (i.e. the TAZ developed within one spectrum repeat is not consumed by the crack growth for that spectrum repeat). Figure 5.20 shows the corresponding TAF for the same spectra.

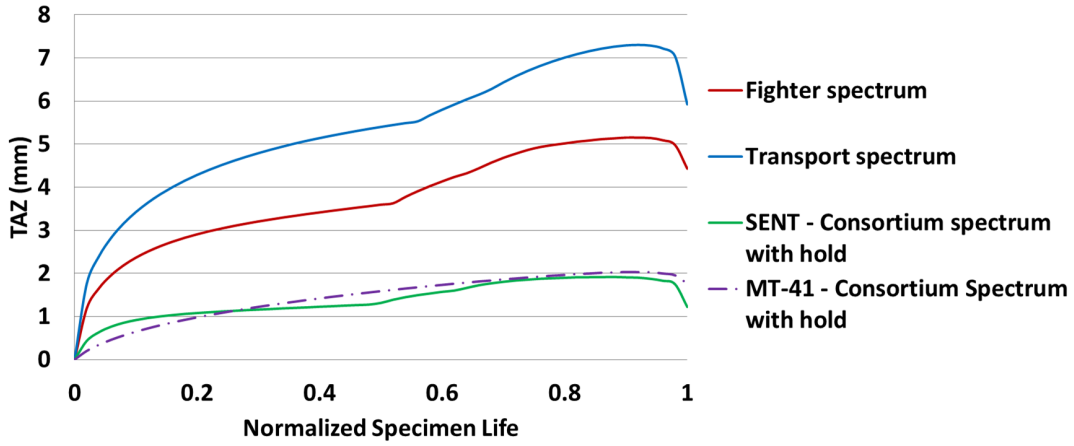

Figure 5.19: Evolution of the TAZ for all experiment spectra predicted to develop TAZ

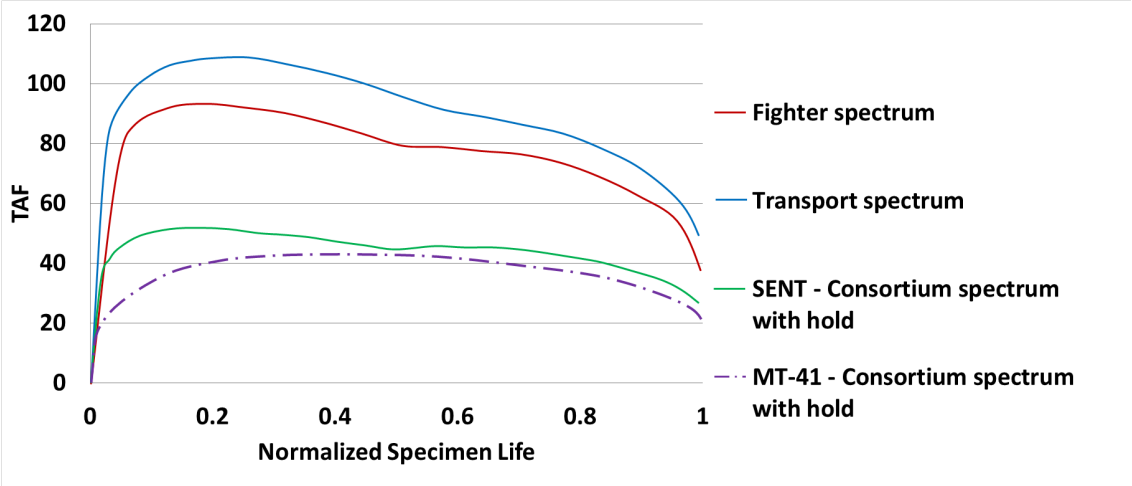

Figure 5.20: Evolution of the TAF for all experiment spectra predicted to develop TAZ

Several useful pieces of information can be gleaned from these two figures. First, a crack tip without TAZ will initially develop TAZ quickly, but eventually, as the TAZ gets larger and the contribution of new TAZ is reduced (as described in Section 5.3.4) a steady balance between the growth of the TAZ and the TAZ consumed by crack

growth is established. This trend in TAZ, when combined with the equation for the TAF, Equation 4.2, results in an initially high TAF that reduces as the crack length increases. This higher acceleration due to TAZ at shorter crack lengths coincides with where plane strain effects would be more prevalent. The TAF decreases as the crack length increases and plane stress effects begin to dominate. Second, the amount of TAZ and corresponding TAF for the consortium spectrum shows similar values between the SENT and MT-41 specimens indicating that the methodology to model temperature interaction effects is effective across multiple specimen geometries. Lastly, as discussed in Section 5.5.4, the model accurately predicts the TAZ, and correspondingly, the TAF for the transport spectrum to be larger than for the fighter spectrum.

5.5.6 Parametric Study

A parametric study was conducted to highlight the significance of temperature in a TMF cycle expected to be subject to temperature interaction effects and develop a TAZ. Predictions of the forward triangular OP TMF waveform with tensile hold (see Figure: 3.14) were conducted with the same temperature waveform scaled to different maximum temperatures of 550°C, 600°C, and 650°C. Figure 5.21 shows how the model correctly accounts for the higher temperature exposure with increased TAZ accumulation and an increased acceleration factor compared to a lower temperature cycle. This leads to the shorter life for the higher temperature spectra.

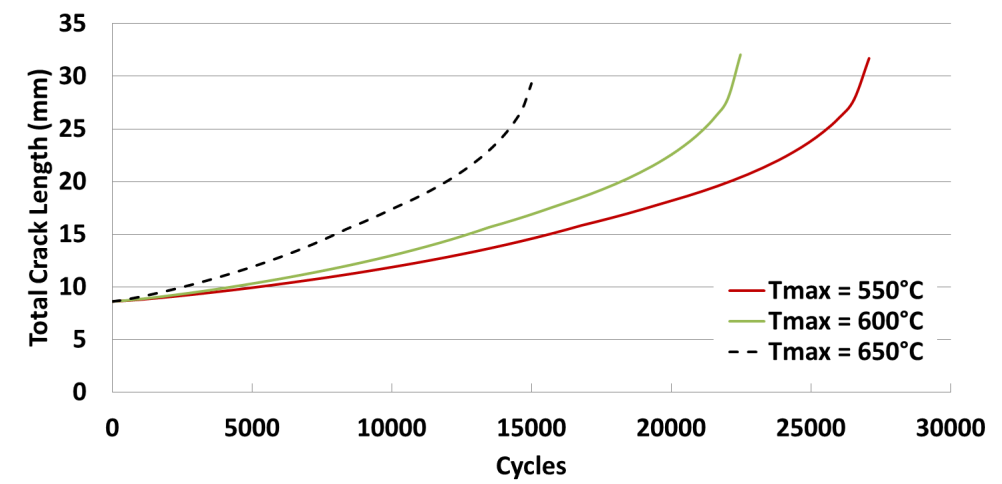

(a) Crack growth prediction

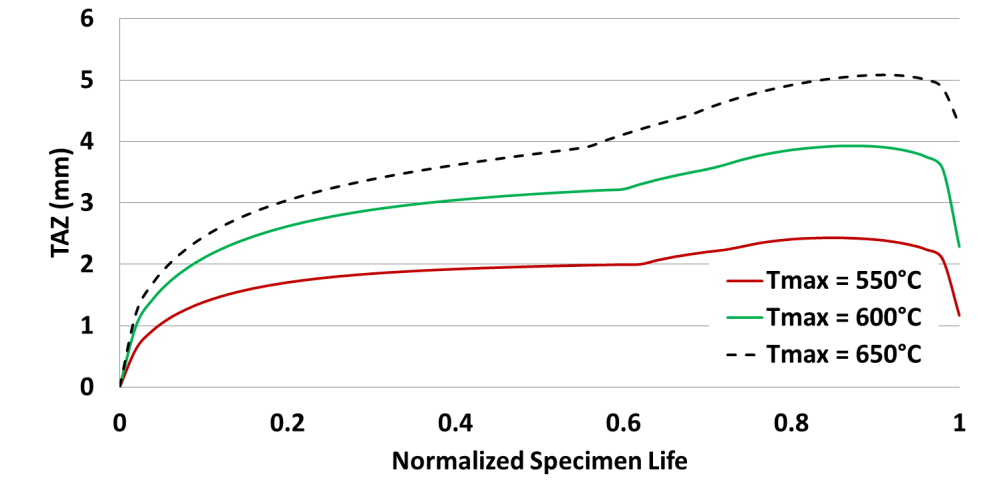

(b) TAZ evolution prediction

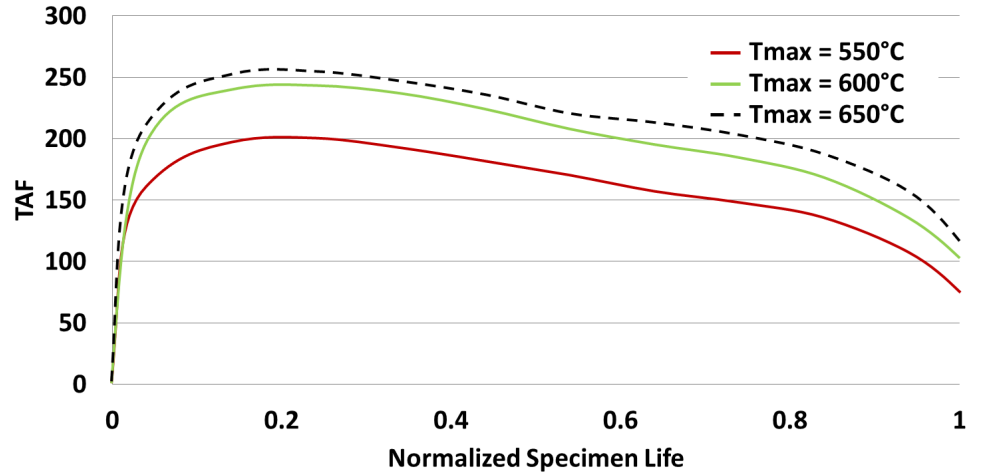

(c) TAF evolution prediction

Figure 5.21: Parametric prediction of the effect of varying the maximum temperature of the forward triangular OP TMF spectrum with hold

5.6 Significant Findings

Using a TAZ to account for the temperature interaction effects on FCGR for complex TMF spectra was shown to be a valid approach. Additionally, trends observed in experimental tests on the impact of tensile holds and their sequence effects were accurately captured by the model. The model predicts conservative life estimates for representative TMF spectra expected to be impacted by time at temperature effects.

CHAPTER VI

CONCLUSIONS, SIGNIFICANCE OF RESEARCH, AND RECOMMENDATIONS FOR FUTURE WORK

6.1 Conclusions

The primary purpose of this project was to characterize and model the fatigue crack growth performance of a polycrystalline Ni-base superalloy that is particularly sensitive to environmental effects when subject to a representative TMF spectrum. Unique experimental spectra were designed and executed to highlight the mechanisms observed during a TMF spectrum that were due to time spent at elevated temperature and to highlight specific characteristics of representative TMF spectra that influence the crack growth response. A FCG model was developed capable of accounting for representative TMF spectra without spectra simplification. The temperature interaction effects experienced due to previous time spent at elevated temperature were characterized using a temperature affected zone to describe a distance ahead of the crack tip weakened due to that previous exposure to time at high temperature. The IN 718 utilized in this project was from a forged disk and was a good analog for the material used in operational disks.

6.1.1 Characterization of Thermomechanical Fatigue Crack Growth in IN 718

The complicated interaction between applied loading, temperature, time, and the material's response, specifically at the crack tip was approached in a methodical way to best isolate specific response characteristics of the material. Additionally, unique spectra were specifically designed to best emulate characteristics of realistic applications. Conclusions were drawn from experimental crack growth data, fractographic

investigation, and finite element analysis simulation and include the following:

6.1.1.1 Isothermal Fatigue Crack Growth

- Isothermal fast frequency loading (10 Hz) at 650°C reduced the weakening effects of time spent at elevated temperature but did not completely eliminate them.

- For isothermal cycling below 427°C, shear dominated crack propagation occurs. Additionally, for cycling at these lower temperatures, the weakening effect of time spent at temperature in the form of secondary cracking or oxidation on the failure surface do not occur.

6.1.1.2 Effect of Tensile Hold at High Temperature: Hold Load Relation to Cyclic Loading

- Tensile holds conducted at high temperatures only create a TAZ when the tensile hold stress intensity is greater than 75% of the cyclic maximum stress intensity.

6.1.1.3 Effect of Tensile Hold at High Temperature: Constant Stress Intensity Factor

- An obvious TAZ ahead of the crack tip is observed when subject to a tensile hold at elevated temperature, both on the failure surface and in acceleration of the FCGR. This occurs for tensile holds at temperatures greater than or equal to 550°C.

- The TAZ is more pronounced in the center of the specimen where the tensile dilatational forces are greatest and plane strain effects dominate. As the state of stress changes from plane strain to plane stress and tensile dilatational forces decrease, the TAZ reduces.

- The TAZ extends in preferential channels ahead of the crack tip and is shown in the form of secondary cracking with oxidation on the failure surface. The

remaining material within a TAZ not weakened remains intact and fails in a ductile manner with visible striations when cycling resumes following a high temperature tensile hold. The reduced amount of material not weakened by the high temperature tensile hold ahead of the crack tip leads to a faster than expected FCGR.

- As the stress intensity of a tensile hold, the duration of a hold, or the temperature of a hold increase, the TAZ also increases.

- The larger the relative size of the TAZ, the higher the acceleration on FCGR.

6.1.1.4 Effect of Compressive Hold on Thermomechanical Fatigue Crack Growth

- Based on the results of conducting triangular waveform and representative OP TMF spectra, a compressive hold imposed at temperatures where one would typically expect material weakening and FCGR acceleration does not significantly impact fatigue crack growth rate. There is no significant influence of a compressive hold up to at least 725°C.

6.1.1.5 Tensile Hold Sequence Effects on Out-of-Phase Thermomechanical Fatigue Crack Growth

- For overall OP TMF loading, a high temperature tensile hold at 50% of the cyclic maximum load will increase the FCGR when the load is increasing as it approaches the tensile hold.

- When the cycle is run backward and the load is decreasing as it approaches the tensile hold, the tensile hold has no significant effect on FCGR.

6.1.1.6 Representative Fighter and Transport Aircraft Thermomechanical Fatigue Spectra

- Subcycles executed during a tensile hold during a representative fighter aircraft turbine engine spectra significantly increase the FCGR compared to the same

cycle executed with only a tensile hold and no subcycles.

- The weakening effects of time spent at elevated temperature are reduced by the introduction of subcycles, though the overall FCGR is increased due to the crack growth of the subcycles themselves. This highlights the significant differences between land based power generation turbines, where the engines are run for long durations (days or weeks) at constant load and temperature, transport aircraft where the holds aren't as long as land based turbines and there are more cycles, and fighter aircraft were the holds are shorter still and there are more intermediate cycles.

6.1.1.7 Experimental Methods

- Though an obviously weakened area is observed ahead of the crack tip due to a tensile hold at elevated temperature, the optical method for crack length measurement cannot capture the immediate impacts of the weakened area on FCGR. Stress redistribution in plane stress near the free surface reduces the tensile dilatational forces at the crack tip which in turn reduce the weakening effects of time spent at elevated temperature for the material near the free surface. The EPD method of crack length measurement is able to capture the accelerating effect of a single TAZ.

6.1.2 Temperature Affected Zone Modeling

The complex temperature and loading environment of realistic TMF spectra can weaken the material and lead to faster than expected FCG propagation. The modeling of the TAZ size, characterized with respect to the stress intensity of a hold, the duration of a hold, and the temperature of a hold, presents a unique capability to predict the amount of TAZ utilizing tensile hold parameters from across the full range of realistic TMF spectra. The unique model of the TAZ size due to a high temperature tensile hold was validated by a robust experimental matrix data.

Additionally, the impact of a TAZ on FCGR lessens as the state of stress transitions from plane strain to plane stress. The model developed accurately accounts for this transition by relating the TAZ size to the current plastic zone size.

6.1.3 Fatigue Crack Growth Modeling

A model was developed to capture the important features observed and their impact on the FCGR for realistic TMF spectra. Predictions for TMF spectra expected to be subject to the effects of time spent at elevated temperature accurately capture experimentally observed trends of those effects. The conclusions drawn from the modeling effort include:

- The unique implementation of TMF spectra segmentation within the model allowed for the effects of time spent at elevated temperature to be accurately captured and matched well to experimentally observed trends.
- The model provides the capability to account for the effects of loading history, both in terms of previous overload and underloads and in terms of the sequence effects of loading and holds, and weakening effect of time spent at elevated temperature on subsequent crack growth for complex TMF spectra in a robust manner without simplification of the spectra. The effects of features of realistic TMF spectra previously unaccounted for can now be captured.

6.2 Significance of Research

Designers and operators of jet turbine engines are dependent upon life predictions to effectively and efficiently ensure safe use of the components that make up the complex systems they are responsible for. The FCG performance is one measure that is critical to ensure a component's safe use, in setting efficient and effective inspection intervals, and in identifying manufacturing flaw tolerances. The harsh environment of turbine engines subjects components to a complicated loading, thermal, and environmental

situation. The ever changing nature of these factors makes prediction of the FCG performance of the material very difficult. The robust test matrix developed and executed with this project provides unique insight into the effect of different characteristics of realistic TMF spectra not previously available. The thorough evaluation of the development of a TAZ and its characteristics, both in terms of its appearance on the failure surface and its impact on FCGR provide insights not previously available. The data collected and characterizations made, particularly with regard to the weakening effect of time spent in tension at elevated temperature, will aid in identifying trends and modeling material response. Additionally, the observations made highlight the significance of understanding the difference between the response to TMF spectra of land-based energy generation turbines, transport aircraft turbine engines, and fighter aircraft turbine engines.

There are numerous isothermal FCG models available for predicting the FCG performance at elevated temperature. However, there are far fewer models able to account for a spectra with changing loads and temperatures, and still fewer able to also account for the effects of specific characteristics of the loading and temperature history. The complex characteristics of representative TMF spectra (variable temperature, stress, time, cyclic frequency, and sequence effects) necessitate the use of a model able to take the loading and temperature history into account to accurately predict crack growth. Load interaction effects due to previous overloads and underloads and temperature interaction effects due to the development of a TAZ are uniquely combined leveraging experimental data in a robust model capable of handling the complex TMF spectrum a component might see in service. This model will allow designers and operators the ability to evaluate more aspects of realistic TMF spectra in a robust manner not previously available to them. This will lead to safer and more cost effective operation of systems utilizing these materials.

6.3 Recommendations for Future Work

Though the findings of this project provide a good characterization of the effects of time spent at elevated temperature on FCG, the very complicated nature of TMF loading and the corresponding material response still requires further exploration. The recommendations for future work are:

- There are obvious differences in the TAZ between a plane strain dominated and a plane stress dominated situation. A more thorough characterization of the differences with regard to the weakening effects of a TAZ would provide designers the insights they need to make more informed decisions on the performance of the parts they are responsible for.

- Explore a more robust implementation of the TAZ accelerating effect on FCGR. Additional experimental data would elucidate the best methodology to characterize this effect.

- Though several representative TMF spectra were executed to capture the effects of the sequence of loading, unloading, and holds, due to resources limitations, more could not be accomplished. Additional tests to capture the effects of the complex loading, unloading, and tensile hold characteristics of realistic TMF spectra should be undertaken to better inform any models to their effects. Several characteristics were identified in this project but more remain to be determined such as how the loading sequence of intermediate load subcycles impact the effect of time spent at elevated temperature, the effect of non-synchronized application of load and temperature, the use of an effective temperature to represent FCG in a TMF spectrum, and the use of spectrum simplification techniques, such as rainflow counting, to accurately predict crack growth.

- Identification of the specific mechanisms active in the TAZ (oxidation, materials evolution, etc.) and their specific contribution to TAZ development and their impact on FCGR. For example, though creep effects are minimal at the maximum usage temperature of IN 718, the high strains present at a crack tip at a high temperature may allow for creep effects to become more significant than currently thought. Creep tests loaded near the yield strength of the material, to best simulate the high stresses at a crack tip, could provide further insight into the overall response of the material at the crack tip.

APPENDIX A

FINITE ELEMENT ANALYSIS MATERIAL MODEL INPUTS

Material models already incorporated in the finite element analysis software ANSYS were utilized for simulations. Published IN 718 material properties from the MMPDS-08 were utilized for all curve fits [15].

A 3-term Chaboche non-linear kinematic hardening model was selected due to its ability to handle cyclic softening. The coefficients used in ANSYS are shown in Table A.1. Figure A.1 shows how the Chaboche model compares to the published data [15].

Table A.1: ANSYS 3 term Chaboche non-linear kinematic hardening material model coefficients

Temp (°C)	Yield Stress (MPa)	C1 (MPa)	$\gamma 1$	C2 (MPa)	$\gamma 2$	C3 (MPa)	$\gamma 3$
21	1184.449	7589.426	136.2379	7562.012	144.7744	4996.795	10.79349
649	848.3492	11818.63	244.3495	11818.47	256.2985	4518.515	30.71417
760	655.9298	3555.724	176.6519	3555.7	175.5247	3555.654	175.5019

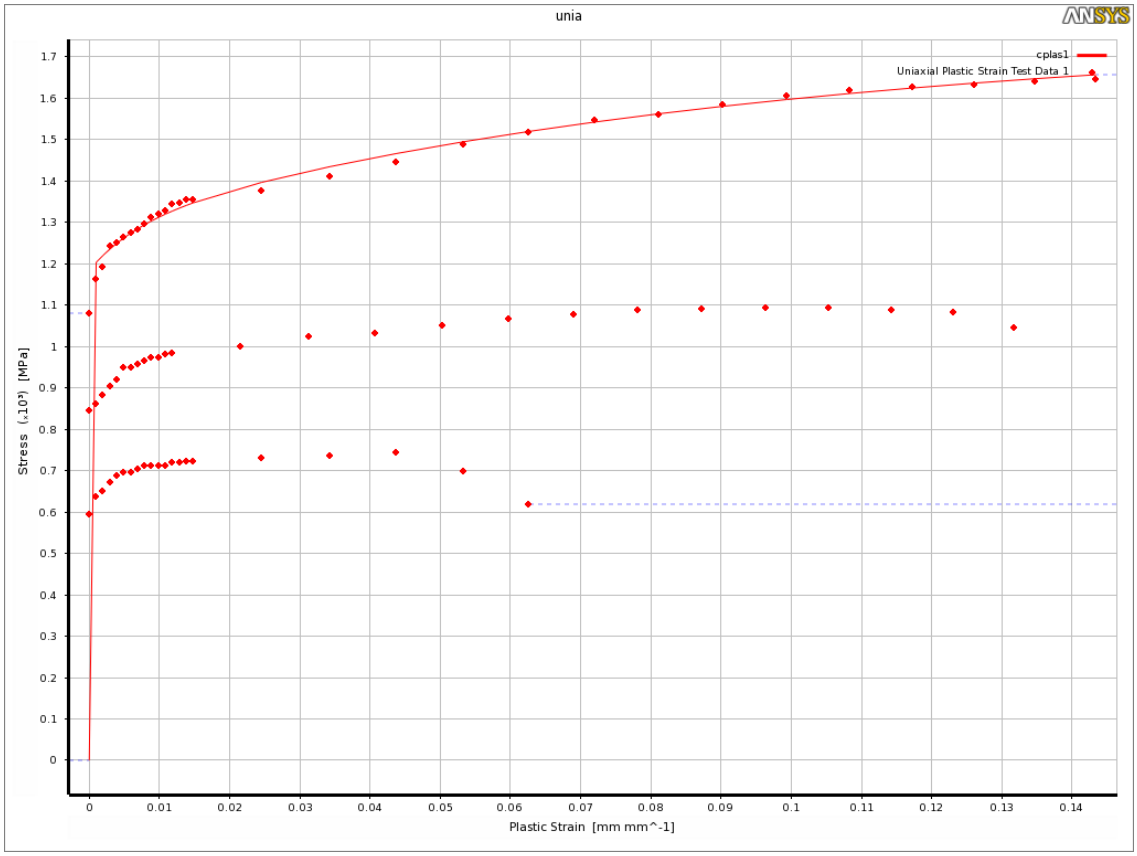

Figure A.1: Comparison of ANSYS 3 term Chaboche non-linear kinematic hardening model at 760°C compared to published data [15]

Since creep effects for the temperature range evaluated are not expected to develop significantly, a model was selected that focused on primary creep. The modified time hardening model in ANSYS was selected for this reason. It has the form:

$$\varepsilon_{cr} = \frac{C_1 \sigma^{C_2} t^{C_3+1} e^{\frac{-C_4}{T}}}{C_3 + 1} \tag{A.1}$$

with the parameters for fitting to published data shown in Table A.2.

Table A.2: ANSYS modified time-harding material model coefficients

Modified time-hardening coefficients	
C1	2.38 x 10^{-20}
C2	7.9599
C3	-0.707010
C4	11796.0

Figure A.2 shows how the modified time-hardening model compares to published

data.

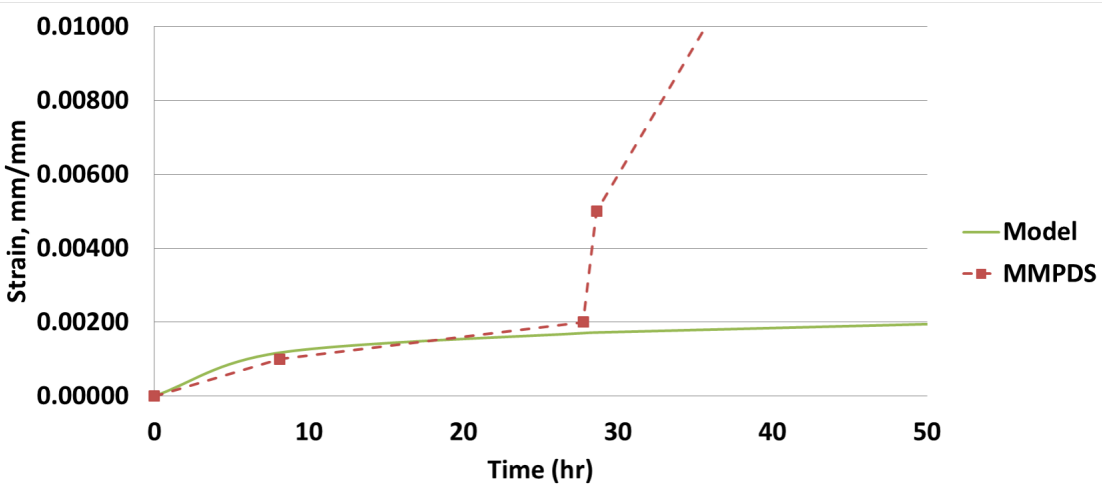

Figure A.2: Comparison of ANSYS modified time-hardening material model to published data [15]

REFERENCES

[1] *Airplane Flying Handbook*. US Department of Transportation, Federal Aviation Administration–Flight Standards Service. FAA-H-8083-3A, 2004.

[2] Reed, R. C., *The superalloys: fundamentals and applications*. Cambridge university press, 2006.

[3] Rosenker, M. V., "Safety recommendation, NTSB report on Los Angeles engine failure, safety recommendation, 60-06 60-64," tech. rep., 2006.

[4] "NTSB issues second update on British Airways engine fire at Las Vegas," October 6 2015. http://www.ntsb.gov/news/press-releases/Pages/PR20151006.aspx.

[5] Harris, J. A. J., "Engine component retirement for cause, volume 1 - executive summay," Tech. Rep. AFWAL-TR-87-4096, Air Force Wright Aeronautical Laboratories, Wright-Patterson AFB, OH, 1987.

[6] Whittle, F., "The first James Clayton lecture: The early history of the whittle jet propulsion gas turbine," *Proceedings of the Institution of Mechanical Engineers*, vol. 152, no. 1, pp. 419–435, 1945.

[7] Smith, C., "Frank Whittle and the jet engine," vol. 83, (Boston, MA, USA), pp. 769 – 774, 1995.

[8] Paulonis, D. F. and Schirra, J. J., "Alloy 718 at Pratt & Whitney–historical perspective and future challenges," *Superalloys 718, 625, 706 and Various Derivatives*, pp. 13–23, 2001.

[9] Radavich, J. F., "The physical metallurgy of cast and wrought alloy 718," in *Conference Proceedings on Superalloy 718–Metallurgy and Applications, The Minerals, Metals & Materials Society, Warrendale, PA* (Loria, E., ed.), pp. 229–240, 1989.

[10] Oblak, J., Paulonis, D., and Duvall, D., "Coherency strengthening in Ni base alloys hardened by DO_{22} γ' precipitates," *Metallurgical Transactions*, vol. 5, no. 1, pp. 143–153, 1974.

[11] Wlodek, S. and Field, R., "The effects of long time exposure on alloy 718," *Superalloys*, vol. 718, pp. 625–706, 1994.

[12] Gessinger, G. H., *Powder Metallurgy of Superalloys: Butterworths Monographs in Materials*. Elsevier, 2013.

[13] Brook, J. and Bridges, P., "Long term stability of Inconel alloy 718 for turbine disc applications," *High temperature alloys for gas turbines and other applications*, pp. 1431–40, 1986.

[14] McClung, R. C., Lee, Y. D., Tschopp, J. A., Srivatsa, S. K., Leverant, G. R., Waldhart, C. J., Jameel, M. A., Enright, M. P., Millwater, H. R., Lehmann, D. J., Huyse, L., Fitch, S. H. K., and Dubke, J. P., "Turbine rotor material design - phase II," tech. rep., DOT/FAA/AR-07/13, 2008.

[15] *Metallic Materials Properties Development and Standardization (MMPDS-08)*. Columbus, OH: Battelle Memorial Institute, 2013.

[16] Andersson, H., Persson, C., and Hansson, T., "Crack growth in IN718 at high temperature," *International journal of fatigue*, vol. 23, no. 9, pp. 817–827, 2001.

[17] "Inconel alloy 718," *Publication No. SMC-045, Special Metals Corporation, Huntington, WV, USA*, 2007.

[18] Pieraggi, B. and Uginet, J., "Fatigue and creep properties in relation with alloy 718 microstructure," in *LORIA E A. Third International Symposium on Superalloys*, vol. 718, pp. 625–706, 1994.

[19] Krueger, D. D., Antolovich, S. D., and Van Stone, R. H., "Effects of grain size and precipitate size on the fatigue crack growth behavior of alloy 718 at 427°C," *Metallurgical transactions A*, vol. 18, no. 8, pp. 1431–1449, 1987.

[20] Pedron, J. and Pineau, A., "The effect of microstructure and environment on the crack growth behaviour of Inconel 718 alloy at 650°C under fatigue, creep and combined loading," *Materials science and engineering*, vol. 56, no. 2, pp. 143–156, 1982.

[21] Nicholas, T., Weerasooriya, T., and Ashbaugh, N. E., "A model for creep/fatigue interactions in alloy 718," in *Fracture mechanics: sixteenth symposium, ASTM STP 868*, pp. 167–180, 1985.

[22] Weerasooriya, T. and Venkataraman, S., "Frequency and environment effects on crack growth in Inconel 718," *Effects of load and thermal histories on mechanical behavior of materials*, 1987.

[23] Weerasooriya, T., "Effect of frequency on fatigue crack growth rate of Inconel 718 at high temperature," tech. rep., Air Force Wright Aeronautical Labs, Wright Patterson AFB, OH, 1987.

[24] Pineau, A., "High temperature fatigue: creep–fatigue–oxidation interactions in relation to microstructure," *Subcritical Crack Growth Due to Fatigue, Corrosion and Creep*, pp. 483–530, 1981.

[25] Ghonem, H. and Zheng, D., "Depth of intergranular oxygen diffusion during environment-dependent fatigue crack growth in alloy 718," *Materials Science and Engineering: A*, vol. 150, no. 2, pp. 151–160, 1992.

[26] Ghonem, H., Nicholas, T., and Pineau, A., "Elevated temperature fatigue crack growth in alloy 718 part I: effects of mechanical variables," *Fatigue & Fracture of Engineering Materials & Structures*, vol. 16, no. 5, pp. 565–576, 1993.

[27] Wei, R. P., Miller, C., Huang, Z., Simmons, G. W., and Harlow, D. G., "Oxygen enhanced crack growth in nickel-based superalloys and materials damage prognosis," *Engineering Fracture Mechanics*, vol. 76, no. 5, pp. 715–727, 2009.

[28] Sadananda, K. and Shahinian, P., "The effect of environment on the creep crack growth behavior several structural alloys," *Materials Science and Engineering*, vol. 43, no. 2, pp. 159–168, 1980.

[29] Floreen, S. and Kane, R., "Effects of environment on high-temperature fatigue crack growth in a superalloy," *Metallurgical Transactions A*, vol. 10, no. 11, pp. 1745–1751, 1979.

[30] Ghonem, H., Zheng, D., Andrieu, E., and Pineau, A., "Experimental observations and quantitative modelling of oxidation-assisted crack growth behavior in alloy 718 at 650°C," in *Annu. Rep. AFOSR-89-0285*, Bolling AFB Washington, DC, 1990.

[31] Zheng, D., Rosenberger, A., and Ghonem, H., "Influence of prestraining on high temperature, low frequency fatigue crack growth in superalloys," *Materials Science and Engineering: A*, vol. 161, no. 1, pp. 13–21, 1993.

[32] Khobaib, M., Ashbaugh, N. E., Hartman, G. A., Weerasooriya, T., and Maxwell, D. C., "Research on mechanical properties for engine life prediction, AFWAL-TR-88-4062," tech. rep., Wright-Patterson AFB, OH, 1988.

[33] Sadananda, K. and Shahinian, P., "Crack growth under creep and fatigue conditions," *Creep–Fatigue–Environment Interactions*, pp. 86–111, 1979.

[34] James, L. A., "The effect of grain size upon the fatigue-crack propagation behavior of alloy 718 under hold-time cycling at elevated temperature," *Engineering Fracture Mechanics*, vol. 25, no. 3, pp. 305–314, 1986.

[35] Diboine, A. and Pineau, A., "Creep crack initiation and growth in Inconel 718 alloy at 650°C," *Fatigue & Fracture of Engineering Materials & Structures*, vol. 10, no. 2, pp. 141–151, 1987.

[36] Ponnelle, S., Brethes, B., and Pineau, A., "High temperature fatigue crack growth rate in Inconel 718: dwell effect annihilations," *European Structural Integrity Society*, vol. 29, pp. 257–266, 2002.

[37] Gustafsson, D., Moverare, J., Johansson, S., Hörnqvist, M., Simonsson, K., Sjöström, S., and Sharifimajda, B., "Fatigue crack growth behaviour of Inconel 718 with high temperature hold times," *Procedia Engineering*, vol. 2, no. 1, pp. 1095–1104, 2010.

[38] Rosenberger, A. Personal Interview. 21 Jan 2016.

[39] Wanhill, R., "Significance of dwell cracking for IN718 turbine discs," *International journal of fatigue*, vol. 24, no. 5, pp. 545–555, 2002.

[40] Ghonem, H., Nicholas, T., and Pineau, A., "Analysis of elevated temperature fatigue crack growth mechanisms in alloy 718," *Creep-fatigue interaction at high temperature*, pp. 1–18, 1991.

[41] Woodford, D. A., "Gas phase embrittlement and time dependent cracking of nickel based superalloys," *Energy Materials*, vol. 1, no. 1, pp. 59–79, 2006.

[42] Atkinson, A., Taylor, R., and Hughes, A., "A quantitative demonstration of the grain boundary diffusion mechanism for the oxidation of metals," *Philosophical Magazine A*, vol. 45, no. 5, pp. 823–833, 1982.

[43] Molins, R., Hochstetter, G., Chassaigne, J., and Andrieu, E., "Oxidation effects on the fatigue crack growth behaviour of alloy 718 at high temperature," *Acta Materialia*, vol. 45, no. 2, pp. 663–674, 1997.

[44] Andrieu, E., Molins, R., Ghonem, H., and Pineau, A., "Intergranular crack tip oxidation mechanism in a nickel-based superalloy," *Materials Science and Engineering: A*, vol. 154, no. 1, pp. 21–28, 1992.

[45] Pfaendtner, J. and McMahon Jr, C., "Oxygen-induced intergranular cracking of a Ni-base alloy at elevated temperaturesan example of dynamic embrittlement," *Acta Materialia*, vol. 49, no. 16, pp. 3369–3377, 2001.

[46] Pang, X., Dwyer, D., Gao, M., Valerio, P., and Wei, R., "Surface enrichment and grain boundary segregation of niobium in Inconel 718 single-and poly-crystals," *Scripta metallurgica et materialia*, vol. 31, no. 3, pp. 345–350, 1994.

[47] Miller, C., Simmons, G., and Wei, R., "Mechanism for oxygen enhanced crack growth in Inconel 718," *Scripta materialia*, vol. 44, no. 10, pp. 2405–2410, 2001.

[48] Viskari, L., Johansson, S., and Stiller, K., "Oxygen influenced intergranular crack propagation: analysing microstructure and chemistry in the crack tip region," *Materials at High Temperatures*, vol. 28, no. 4, pp. 336–341, 2011.

[49] Antolovich, S. D. and Saxena, A., "Thermomechanical fatigue: mechanisms and practical life analysis.," *Materials Park, OH: ASM International.*, pp. 738–748, 2002.

[50] Pineau, A. and Antolovich, S. D., "High temperature fatigue of nickel-base superalloys–a review with special emphasis on deformation modes and oxidation," *Engineering Failure Analysis*, vol. 16, no. 8, pp. 2668–2697, 2009.

[51] Moverare, J. J. and Gustafsson, D., "Hold-time effect on the thermomechanical fatigue crack growth behaviour of Inconel 718," *Materials Science and Engineering: A*, vol. 528, no. 29, pp. 8660–8670, 2011.

[52] Heil, M. L., "Crack growth in alloy 718 under thermal-mechanical cycling," tech. rep., DTIC Document, 1986.

[53] Jacobsson, L., Persson, C., and Melin, S., "Thermo-mechanical fatigue crack propagation experiments in Inconel 718," *International Journal of Fatigue*, vol. 31, no. 8, pp. 1318–1326, 2009.

[54] Nicholas, T., Heil, M. L., and Haritos, G. K., "Predicting crack growth under thermo-mechanical cycling," *International Journal of Fracture*, vol. 41, no. 3, pp. 157–176, 1989.

[55] Xiao, L., Chen, D., and Chaturvedi, M., "Effect of boron and carbon on thermomechanical fatigue of IN 718 superalloy: Part I. deformation behavior," *Materials Science and Engineering: A*, vol. 437, no. 2, pp. 157–171, 2006.

[56] Liu, X., Ma, L., Chang, K., and Barbero, E., "Fatigue crack propagation of Ni-base superalloys," *Acta Metallurgica Sinica*, vol. 18, no. 1, pp. 55–64, 2005.

[57] Gustafsson, D., Moverare, J., Simonsson, K., Johansson, S., Hörnqvist, M., Månsson, T., and Sjöström, S., "Fatigue crack growth behaviour of Inconel 718–the concept of a damaged zone caused by high temperature hold times," *Procedia Engineering*, vol. 10, pp. 2821–2826, 2011.

[58] Barker, V. M., Johnson, W. S., Adair, B. S., Antolovich, S. D., and Staroselsky, A., "Load and temperature interaction modeling of fatigue crack growth in a Ni-base superalloy," *International Journal of Fatigue*, vol. 52, pp. 95–105, 2013.

[59] Lundström, E., Simonsson, K., Månsson, T., and Gustafsson, D., "Modelling of fatigue crack growth in Inconel 718 under hold time conditions-application to a flight spectrum," *Advanced Materials Research*, vol. 891, pp. 759–764, 2014.

[60] Storgärds, E. and Simonsson, K., "Crack length evaluation for cyclic and sustained loading at high temperature using potential drop," *Experimental Mechanics*, vol. 55, no. 3, pp. 559–568, 2015.

[61] Hörnqvist, M., Månsson, T., and Gustafsson, D., "High temperature fatigue crack growth in alloy 718–effect of tensile hold times," *Procedia Engineering*, vol. 10, pp. 147–152, 2011.

[62] Zhao, L., Tong, J., and Hardy, M., "Prediction of crack growth in a nickel-based superalloy under fatigue-oxidation conditions," *Engineering fracture mechanics*, vol. 77, no. 6, pp. 925–938, 2010.

[63] Newman, J. J., "A crack opening stress equation for fatigue crack growth," *International Journal of fracture*, vol. 24, no. 4, pp. R131–R135, 1984.

[64] Storgärds, E., Simonsson, K., Sjöström, S., and Moverare, J., "Thermomechanical fatigue crack growth modeling in a Ni-based superalloy subjected to sustained load," *Journal of Engineering for Gas Turbines and Power*, vol. 138, no. 1, p. 012503, 2016.

[65] Larsen, J. M., Rosenberger, A. H., Hartman, G. A., Russ, S. M., and John, R., "The role of spectrum loading in damage-tolerance life-management of fracture critical turbine engine components," Tech. Rep. ADP014134, Air Force Research Lab Wright-Patterson AFB, OH Materials and Manufacturing Directorate, 2003.

[66] Johnson, W., "Multi-parameter yield zone model for predicting spectrum crack growth," *ASTM STP*, vol. 748, pp. 85–102, 1981.

[67] Barker, V. M., "Thermo-mechanical fatigue crack growth modeling of a nickel-based superalloy," Master's thesis, Georgia Institute of Technology, 2011.

[68] Gallagher, J. and Hughes, T., "Influence of yield strength on overload affected fatigue crack growth behavior in 4340 steel," tech. rep., AFFDL-TR-74-27, 1974.

[69] Adair, B., Johnson, W., Antolovich, S., and Staroselsky, A., "Identification of fatigue crack growth mechanisms in IN100 superalloy as a function of temperature and frequency," *Fatigue & Fracture of Engineering Materials & Structures*, vol. 36, no. 3, pp. 217–227, 2013.

[70] Forman, R., Hickman, J., and Shivaskumar, V., "Stress intensity factors for circumferential through cracks in hollow cylinders subjected to combined tension and bending loads," *Engineering fracture mechanics*, vol. 21, no. 3, pp. 563–571, 1985.

[71] ASTM E647-13ae1, *Standard Test Method for Measurement of Fatigue Crack Growth Rates*. ASTM International, West Conshohocken, PA, 2013. www.astm.org.

[72] Adair, B. S., "Thermo-mechanical fatigue crack growth of a polycrystalline superalloy," Master's thesis, Georgia Institute of Technology, Atlanta, GA, 2011.

[73] Woodworth, B., "Development of a thermo-mechanical fatigue test apparatus with crack growth monitoring capability," tech. rep., Georgia Institute of Technology, 2009. p. 110.

[74] Johnson, H., "Calibrating the electric potential method for studying slow crack growth (calibration of electric potential technique to study slow or steady crack growth in high strength materials)," *Materials Research and Standards*, vol. 5, pp. 442–445, 1965.

[75] Fournier, L., Delafosse, D., and Magnin, T., "Oxidation induced intergranular cracking and portevin–le chatelier effect in nickel base superalloy 718," *Materials Science and Engineering: A*, vol. 316, no. 1, pp. 166–173, 2001.

[76] Chang, K. M., "Time-dependent mechanisms of fatigue crack propagation in high-strength superalloys," tech. rep., GE-CRD Report 89CRD116, June 1989.

[77] Sadananda, K. and Shahinian, P., "Effect of environment on high temperature crack growth behavior of several nickel-base alloys," *Corrosion of Nickel-Base Alloys*, pp. 101–115, 1984.

[78] Balsone, S. J., Nicholas, T., and Khobaib, M., "Effects of stress and stress history on the magnitude of the environmental attack in Rene 80," in *Environmentally Assisted Cracking, Science and Engineering* (Lisagor, W. B., Croofer, T. W., and Leis, B. N., eds.), Special Technical Publication 1049, p. 303, ASTM International, 1990.

[79] Coffin Jr, L., "Cyclic-strain-induced oxidation of high-temperature alloys," tech. rep., General Electric Co. Research Lab., Schenectady, NY, 1962.

[80] Mills, W., "The effect of heat treatment on the room temperature and elevated temperature fracture toughness response of alloy 718," *Journal of Engineering Materials and Technology*, vol. 102, no. 1, pp. 118–126, 1980.

[81] Clavel, M. and Pineau, A., "Fatigue behaviour of two nickel-base alloys i: Experimental results on low cycle fatigue, fatigue crack propagation and substructures," *Materials Science and Engineering*, vol. 55, no. 2, pp. 157–171, 1982.